Interruption of retinoid metabolism exerts a major impact on the development of obesity and metabolic disorders.

By

Di Yang

A dissertation submitted in partial satisfaction of the requirements for the degree of

Doctor of Philosophy

In

Metabolic Biology

In the

Graduate Division

of the

University of California, Berkeley

Committee in Charge

Professor Joseph L Napoli, Chair

Professor Andreas Stahl

Professor James Olzmann

Professor Richard M. Harland

Summer 2017

Abstract

Dysfunction of retinoid metabolism affects development of obesity and metabolic disorders.

By

Di Yang

Doctor of Philosophy in Metabolic Biology

University of California, Berkeley

Professor Joseph L. Napoli. Chair

All-*trans*-retinoic acid (atRA) controls adiposity by affecting adipogenesis, lipolysis, fatty acid oxidation and non-shivering thermogenesis. The availability of atRA is controlled precisely by biosynthesis as well as degradation. Multiple retinol dehydrogenases (Rdh) catalyze the first, regulated and rate-limiting step of atRA biosynthesis—conversion of retinol into retinal. Enzymes involved in this process are, but not limited to, Rdh10, Rdh1, Dhrs9 and Rdhe2. Increasing evidence suggests each enzyme may support different biological functions. RDH10Rdh10, the most highly expressed retinol dehydrogenase in both stem cells and many adult tissues, has been reported as a key atRA synthesizing enzyme during embryogenesis. However, the role of RDH10Rdh10 in adult tissues, especially in the context of metabolic disorders has not been defined. Our data suggests that a heterozygous hypomorphic RDH10Rdh10 mutation (HYPO) in mouse embryonic fibroblasts (MEF) decreases the amount of atRA synthesized and leads to increased adipogenesis. This phenotype can be reversed by atRA supplementation in adipocyte induction medium of MEF. HYPO MEF demonstrates an impaired response to retinol compared to WT when treated with graded amounts of retinol as a result of reduced atRA synthesis efficiency. *Rdh10*$^{+/-}$ mice fed a high-fat diet display an adiposity phenotype along with metabolic disorders such as glucose intolerance, hyperinsulimia, insulin resistance, liver steatosis (males only) and bone marrow adipocyte proliferation (females only). More interestingly, even though both male and female *Rdh10*$^{+/-}$ fed HFD have increased body weight, they demonstrate different phenotypes in different organs. *Rdh10*$^{+/-}$ males have increased liver steatosis compared to WT, while no significant differences were detected in females. Female *Rdh10*$^{+/-}$ mice have increased numbers of bone marrow adipocytes compared to WT, whether fed a HFD or a low-fat diet (LFD). RA supplementation with 5 mg-90 day release pellets (~56 µg/day) by subcutaneous implantation reversed the obesity phenotype in males. Taken together, these data indicate that Rdh10 is an important atRA generating enzyme that controls adipose tissue development and function.

The second step of atRA biosynthesis converts retinaldehyde into atRA by retinaldehyde dehydrogenases such as RALDH1, RALDH2 and RALDH3. RALDH1, the most highly-expressed retinaldehyde dehydrogenase in MEF and adipose tissue, affects adipogenesis and adiposity in an opposite way as RDH10. RALDH1 KO mice are resistant to diet induced obesity (DIO) and Pparγ-induced osteoporosis. A hypothesis by the Plutzky group claims that resistance to DIO of RALDH1 KO was the result of accumulation of retinaldehyde in tissues (Ziouzenkova et al., 2007a). However, tissue retinaldehyde measurements done by our group by a specific and sensitive LC/MS/MS assay showed no differences in retinaldehyde levels in 6-7 week old mice, with significant differences in body weight at that age. Retinaldehyde levels were lower in 26-week-old HFD fed Raldh1 KO mice compared to WT, i.e. after the phenotype was established, which indicated it was the result rather than the cause of the phenotype. Also, treating Raldh1 KO MEFs with RAR or PPARβ/δ antagonists or agonists did not change the phenotype, further suggesting resistance to DIO of Raldh1 KO mice is independent of retinoid function. Further study is needed to elucidate the mechanism by which Raldh1 KO mice resist DIO.

This dissertation is dedicated to my dad and mom for their unconditional love and support.

List of Figures

Acknowledgements

First I want to express my greatest appreciation to my advisor Prof. Joseph L Napoli for his motivation, continuous support, guidance and patience over my years in graduate school. His immense knowledge and constructive ideas helped me to find the right direction for my research as well as this dissertation. I could hardly have imagined having a better mentor for my graduate studies.

I would like to thank the rest of my dissertation committee: Prof. Andreas Stahl, Prof. James Olzmann and Prof. Richard M Harland, for the encouragement, support, and insightful comments they provided.

I would also want to thank Dr. Marta Vuckovic, a post-doc researcher in the lab. I really appreciate the guidance she provided when I first joined the lab. I also want to thank her for all the constructive comments as well as mental support during my graduate studies.

I would like to thank Dr. Charles Krois, Dr. Hong Sik Yoo and Dr. Yinghua Deng for their insightful discussions whenever problems arise, as well as their help with experiments.

I also want to thank all the intelligent undergraduate researchers, rotating students and summer interns I worked with over the years. They all contributed a great deal to my dissertation. Myeongcheol (Mitch) Kim, Carolyn P.Smullin, Emily Devericks, Christabel Pui-See, Anh Hoang Nguyen, Milena Tintcheva, Candice Gibson and Pete Zushin.

I also want to thank everyone from the department, especially Hanzhi Luo, Jiehan Li Tianyi Tang and Yuhui (Dawn) Wang, for their support and encouragement.

Last I want to thank my mom Lifen Yang, my dad Fei Yang and my fiancé Steve M Huang, for their unconditional love and support. I would not have gotten here without them.

Chapter 1. atRA generated by Rdh10 affects adipogenesis and osteoblast differentiation in vitro.

Introduction

All-trans-retinoic acid (atRA), the most physiologically active metabolite of vitamin A, plays key roles in embryogenesis, cell growth and differentiation by regulating the expression of target genes. atRA regulates gene expression through nuclear hormone receptors RARα/β/γ or PPARβ/δ. About 500 genes are regulated by retinoic acid receptors (Balmer and Blomhoff, 2002). However, a separate non-canonical pathway also responds to atRA, activating extracellular signal 1/2 (ERK1/2) without binding to nuclear receptors (Persaud et al., 2013). Regulation of atRA synthesis and degradation affects its availability and retinoid action. Vitamin A (retinol) is converted in atRA in a two-step process (Napoli, 2012a). The first step converts retinol into retinal by retinol dehydrogenases (Rdh). Enzymes involved in this step are: RDH1, RDH10, DHRS9 and RDHE2. The second step involves conversion of retinal into atRA by three retinaldehyde dehydrogenases RALDH1, RALDH2 and RALDH3. Even though multiple RDHs and RALDHs catalyze the same reactions, their functions are not redundant. The spatial and temporal-specific expression of different isoforms of RDHs and RALDHs suggest that there are discrete pools of atRA to serve specific vitamin A-dependent functions. Furthermore, these discrete atRA pools are generated by different combinations of specific RDH and RALDH isoforms (Jiang and Napoli, 2012, 2013). This hypothesis is supported by the observation of different phenotypes in different retinol or retinaldehyde dehydrogenase knockout mice. For example, Rdh1 KO mice show no developmental defects, but are prone to diet-induced-obesity (DIO), related to disrupted brown adipose function (Zhang et al., 2007; Napoli lab, unpublished data). Raldh1 KO mice show no developmental problems but are resistant to DIO as well as Pparγ induced bone marrow fat development (Nallamshetty et al., 2014a; Ziouzenkova et al., 2007a). Raldh2 KO mice are embryonic lethal, embryos die before e10.5 with hindbrain and spinal cord defects (Duester, 2008). Amongst RDH, RDH10 is the primary retinol dehydrogenase that makes RA during early embryogenesis and organ differentiation. The expression of RDH10 is around 10-20 fold higher than the other RDHs during embryogenesis. The RDH10 mutation is embryonic lethal in mice, with morphological defects in limbs, optic vesicles and caudal pharyngeal arches, and lack of brain development (Balmer and Blomhoff, 2002; Rhinn et al., 2011). Our lab showed that Rdh10 colocalizes with with lipid droplets during lipid droplet synthesis (Jiang and Napoli, 2013), indicating a potential function of lipid droplets as “hormone” generating organelles.. As RDH10 is critical in early development; it is possible that it might be an atRA-generating enzyme that determines cell fate choice.

White adipose tissue (WAT) is the major energy storage reserve of the body and it is also an active endocrine organ, secreting hormones and cytokines that regulate body metabolism (Otto and Lane, 2005). WAT begins to develop during late gestation, when

precursor cells undergo morphological and functional conversion from spindly fibroblasts into round, lipid-containing fat cells (Cristancho and Lazar, 2011). To study the mechanism by which precursor cells differentiate into fat cells, In vitro cell models have provided important insights, for example, showing that mesenchymal stem cells (MSC) are multipotent stem cells that can differentiate into different cell types. MSC can be found in many adult tissues such as adipose (ASC), bone marrow (BMSC) and cardiac (CSC). These cells have important functions in maintaining tissue homeostasis and repair (Williams and Hare, 2011). The differentiation of mesenchymal stem cells (MSC) into adipocytes has two phases. The first phase, also known as the commitment or cell fate determination phase, involves conversion of multipotent cells into pre-adipocytes. Pre-adipocytes are fibroblast-like cells that have lost the ability to differentiate into other cell types. The second phase, known as terminal differentiation or maturation, displays lipid droplet accumulation, as pre-adipocytes acquire the shape and appearance of adipocytes (Cristancho and Lazar, 2011). During early adipogenesis, according to Lazar, atRA inhibits adipogenesis by inhibiting C/EBPβ mediated transcription (Schwarz et al., 1997a) in 3T3L1 cells; while Berry and Noy (Berry et al., 2012) demonstrated that atRA upregulates pre-adipocyte genes such as *Pref-1* to block adipogenesis in both NIH3T3L1 and 10T1/2 cell lines. atRA also was reported to affect functions of mature adipocytes. Berry and Noy (2009a) reported that atRA binds to PPARβ/δ and stimulates lipolysis in mature adipocyte cultures, while Mercader et al. (2010) reported that atRA induced browning of white adipocytes in cultured cells by upregulating the UCP1 gene; Mercader et al. (2007) also showed that acute treatment 3T3L1 adipocytes with atRA increased oxidative metabolism (Mercader et al., 2007). These results suggest the importance of atRA as a promising anti-obesity agent and that more studies are necessary to understand its mechanism of action to provide a basis for its application as an anti-obesity drug.

According to National Institute of Health statistics, osteoporosis is a disease that affects about 53 million Americans, with particularly high prevalence in post-menopausal women. Osteoporosis is characterized by a decrease in bone quality and mineral density resulting from increased osteoclastogenesis, inadequate osteoblastogenesis and possibly increased adipogenesis in bone (Pino et al., 2012). Osteoclasts are specialized cells involved in bone reabsorption, an important function in bone homeostasis. Osteoblasts are specialized cells responsible for production and mineralization of the bone matrix (Hartmann, 2009). Bone marrow stem cell (BMSC) serve as a major reservoir of homeostatic cells in bone marrow, and can differentiate into osteoblasts, osteoclasts and adipocytes to maintain the balance among different cell types (Pittenger et al., 1999). Imbalance of marrow cell differentiation, or increased adipogenesis in bone marrow are major causes of osteoporosis (Akune et al., 2004; Pei and Tontonoz, 2004). Therefore studying the balance between osteoblast and adipocyte production may provide a basis for treating osteoporosis. As white adipocytes and osteoblasts are derived from the same progenitor cells, many transcription factors that inhibit adipocyte development can potentially promote bone development (Stephens, 2012). PPARγ, a key transcription factor in adipogenesis, negatively regulates

osteoblast differentiation in progenitor cells (Patel et al., 2014; Viccica et al., 2010). On the other hand, Runx2, a key transcription regulator for osteoblast differentiation, negatively regulates adipogenesis. Runx2 KO cells show enhanced adipogenesis (Enomoto, 2003; Zhang et al., 2012). Because atRA inhibits adipogenesis in a dose dependent manner, it is reasonable to suggest that atRA may be a positive regulator of osteoblast differentiation. However, the actual situation is more complicated than was predicted. Although some studies showed that treatment of mesenchymal progenitor cells (MPCs) with atRA along or in combination with BMP2 or BMP9 enhances osteoblast differentiation (Sun et al., 2009; Zhang et al., 2010), others found that atRA inhibits osteoblast differentiation (Wang et al., 2008; Yan et al., 2001). The discrepancies between different studies could be a result of using different cell or animal models in different studies, or could be affected by the dose of atRA used or during which differentiation stage atRA was introduced. In the study presented in this thesis, a model with moderate atRA deficiency (Rdh10 HYPO) and a model with severe atRA deficiency (Rdh10 CKO) were used, with the hope that those models will help to partially elucidate the mode of action that atRA on osteoblast differentiation.

Material and Methods.

Animal maintenance. Mice carrying RDH10m366Asp were used (Ashique et al., 2012). Rdh10 m366Asp mutation locates at the substrate-binding pocket of Rdh10, which reduces catalytic activity. *Rdh10^{m366Asp}* mutants are embryonic lethal, so heterozygous mutant mice were used as breeders. We also used Rdh10 floxed mice with loxP-flanked exon 2, which we commissioned the UC Davis Mouse Biology Program to create for us. We backcrossed the founders to C57>10 times, and were crossed with mice expressing CMV Cre (obtained from Jackson lab, B6.C-Tg(CMV-cre)1Cgn/J, stock number 006054) to generate Rdh10 knock out mice. Homozygous Rdh10 KO are embryonic lethal, so heterozygous KO mice were used as breeders. Mice carrying mutated Rdh10 were fed an AIN93G diet containing 4 IU/g vitamin A with 9% fat or the same diet with 50% fat (HFD). All animal experiments were performed in accordance with the National Institutes of Health's Guide for the Care and Use of Laboratory Animals, and all protocols were approved by University of California, Berkeley Animal Care and Use Committee

Mouse embryonic fibroblast isolation and differentiation. MEF were isolated from e13.5-e14 embryos and cultured in UV-irradiated growth medium containing Dulbecco's modified Eagle's medium (DMEM; Gibco BRL), 10% bovine calf serum (BCS; ATCC 30-2030), and 100 U/ml penicillin/streptomycin (Gibco BRL). Embryos were separated from maternal tissue and yolk sacs, heads and internal organs were removed, and bodies were minced, digested with 2 ml 0.25% trypsin/1 mM EDTA for 15 min at 37°C, re-suspended in 8 ml growth medium and centrifuged 5 min at 1,000 x *g.* Cells (8 x 10^3 cells/cm^2) were cultured in 6-well plates at 37ºC in high-glucose Dulbecco's modified

Eagle's medium (DMEM; Gibco BRL) supplemented with 10% (vol/vol) BCS and 100 U/ml penicillin/streptomycin. Adipogenic differentiation was induced two days after reaching confluence, designated dd0. The medium was replaced with differentiation induction medium containing 0.5 mM methylisobutylxanthine (IBMX), 1 µM dexamethasone (DEX), 0.85 µM insulin, 100 nM roglitazone, and 10% (vol/vol) UV-irradiated BCS. After 3 days, the medium was switched to growth medium with 0.85 µM insulin and 100 nM rosiglitizone until harvesting. The medium was renewed every other day. To induce osteoblastic differentiation, the medium was replaced on dd0 with osteogenic differentiation induction medium containing DMEM + 10% BCS, 10 mM β-glycerol phosphate and 100 µg/ml ascorbic acid. The medium was refreshed every three days.

UV-irradiation of medium. 50ml DMEM growth medium with 10% BCS was poured into 15cm glass dishes. The glass dish is placed under UV light for 1hr (with ice bag on top to avoid over heating).

RDH10 CRISPR KO cell line generation. MEF Immortalized by introducing SV40 T antigen and series passages was used to generate Rdh10 CKO lines. A LentiCRISPRv2 (with guide RNA targeting exon 3 inserted, original Addgene plasmid number #52961) (Ran et al., 2013) vector was introduced into immortalized MEF cells by lentivirus to generate *Rdh10* CRISPR KO cells lines. Puromycin was used as a selection marker. Surviving cells were plated into 96 well plates (one cell per well). When clones were formed, the genomic DNA was extracted and sequenced. Clones into which random mutations were introduced are used as KO lines (confirmed by sequencing). Clones that contain the plasmid but no mutations (confirmed by sequencing) are used as WT controls. A total of 5 different guide RNAs were tested to generate clones. 1 out of 5 successfully knocked out *Rdh10*. Guide RNA sequence, targeting exon 3.
Forward 5’ CACCGCCCGGAAAGGAACACCCCGC
Reverse 5’ CGCGGGGTGTTCCTTTCCGGGCAAA

Oil Red O quantification for cells—Oil red O staining was done with cells (dd7) washed twice with phosphate-buffered saline (PBS) and fixed with 10% formalin in PBS for 1 hour. Cells were washed three times with water and stained with Oil red O (6 parts of 0.6% Oil red O dye in isopropanol and 4 parts of water) for 30 min. Excess stain was removed by washing with water 5 times. Stained cells were dried. Spectrophotometric quantification of the stain was performed by dissolving the stained oil droplets in 100% isopropanol for 10 min. Optical density was then measured at 510 nm.

RNA isolation- Cultured cells were harvested in 1 ml Trizol. Cells were allowed to lyse for 3 min and then 200 µL chloroform were added. Tubes were inverted by hand vigorously for 15 sec and then incubated at room temperature for 3 min. Centrifuge at 12,000 x g for 15 min at 4 °C. The top aqueous layer was transferred into a new 1.5 ml tube without taking any DNA. Add 0.5 ml isopropanol for every 1 ml Trizol. Invert by

hand several times to mix. Incubate samples at RT for 10 min. Centrifuge at 12,000 x g for 5 min at 4 °C. Discard supernatant. Add 1 mL 75% ethanol for every 1 mL Trizol, vortex. Centrifuge at 12,000 x g for 5 min at 4 °C. Remove most of the ethanol and air dry tubes for 10 min. Add 20-30 µL of RNAse/DNAse-free H_2O and dissolve by pipetting up and down. Store RNA at -80 °C.

Gene Expression. One µg total RNA was used for reverse transcription (Iscript 170-8891 BioRad). RT-qPCR was performed with a Bio-RAD CFX Connect Real-Time Detection System. Gene expression was normalized to the geometric means of *Gusb* and *Tbp*. qPCR Primers were from Life Technologies or Integrated DNA technologies. *Acadm* (Mm01323360_g1), *Aldh1a1* (Mm00657317_m1), *Aldh1a2* (Mm00501306_m1), *Aldh1a3* (Mm00474049_m1), *Cpt1b* (Mm00487191_g1), *Cyp26A1* (Mm00514486_m1), *Cyp26B1* (Mm00558507_m1), *Dhrs3* (Mm00488080_m1), *Dhrs9* (Mm00615706_m1), *Fabp4* (Mm00445878_m1), *Fabp5* (Mm00783731_s1), *Gusb* (Mm01197698_m1), *Hif1a* (Mm01198376_m1), *Hmgcs2* (Mm00550050_m1), *Hnf4a* (Mm00433959_m1), *Ppara* (Mm00440939_m1), *Pparg* (Mm00440940_m1), *Rarb* (Mm01319677_m1), *RdhE2* (Mm00725380_m1), *Rdh1* (Mm00650636_m1), *Rdh10* (Mm00467150_m1), *Saa1* (Mm00656927_g1), *Tbp* (Mm01277042_m1), *Saa3* (Mm00441203_m1), *Tnfa* (Mm00443258_m1), *Zfp423* (Mm00677660_m1), *Pparg2* (Mm.PT.58.12797903).

Rescue experiment. MEF were induced to adipogenic differentiation with 500 nM atRA (refreshed daily) or 100 nM TTNPB (RAR agonist, T3757 Sigma) or 100 nM GW0742 (PPARδ agonist, G3295 Sigma) (refreshed every two days). Adipogenesis was assessed on dd7 by gene expression and oil red O assay.

atRA biosynthesis and quantification. MEF were incubated 2 hr with 250 nM retinol under subdued light. Cells were washed twice with ice cold DPBS and collected with 1X reporter lysis buffer (E397A, Promega), flash frozen. atRA in tissues and cells was quantified by LC/MS/MS as described (Kane et al., 2005, 2008a).

Alkaline phosphate staining- Alkaline phosphate activity staining was done with osteoblast cell culture (dd7) by an alkaline phosphatase kit from Sigma-Aldrich (Catalog number: 86R-1KT). The medium was removed and then the cells were gently rinsed with PBS. Fix the cells with citrate-acetone-formaldehyde fixative (to 20 ml citrate solution, add 65 ml acetone and 8 ml 37% formaldehyde) for 30 sec and then rinse gently in deionized water for 45 sec (do not allow plate to dry). To prepare the staining solution, measure 45 ml deionized water and adjust temperature to 18-26 °C. Add 1 ml sodium nitrite solution to 1 ml FRV-Alkaline Solution, mix gently and allow to stand for 2 min. Add this solution to the deionized water prepared in previous step, then add 1 ml Naphthol AS-BI Alkaline Solution and mix thoroughly. Add the mixture to cell culture plate and incubate at room temperature for 15 min, make sure to avoid direct light. After the incubation, remove the staining mixture and rinse the wells in deionized water for 2 min. Co-stain with hematoxylin for 2 min. Rinse slides thoroughly in tap water and air dry.

Alizarin red staining- Dissolve 2 g Alizarin Red S (C. I. 58005) in 100 ml distilled water, mix, and adjust pH to 4.1-4.3 with HCL or NH_4OH to prepare the Alizarin Red S staining solution. Filter the dark-brown solution and store it in the dark. Take the cells from the incubator and carefully aspirate the medium. Carefully wash cells with Dulbecco's PBS, w/o Ca++/ Mg++ (Cat. No. C-40232). Carefully aspirate the PBS and transfer the flask to a fume hood. Add enough neutral buffered formalin (10%) to cover the cellular monolayer. After at least 30 min. carefully aspirate the formalin and wash the cells with distilled water. Carefully aspirate the distilled water and add enough Alizarin Red S staining solution to cover the cellular monolayer. Incubate at room temperature in the dark for 45 min. Carefully aspirate the Alizarin Red S staining solution and wash the cell monolayer four times with 1 ml distilled water. Carefully aspirate the Washing Buffer and add PBS. (Protocol adapted from PromoCell, Osteogenic Differentiation and Analysis of MSC)

Statistical analyses. Data are expressed as means ± SD, unless noted otherwise. Statistical significance was determined by two-tailed, unpaired student t tests for comparison of two groups or two-way ANOVA for comparison of two variables.

Results

atRA biosynthesis decreases during adipogenesis.

In undifferentiated WT MEF (dd0), *Rdh10* is the most highly expressed *Rdh*. Expression of *Rdh10* was ~20 fold higher compared to *Dhrs9*, and neither *RdhE2* nor *Rdh1* was detected (Fig. 1A). During the adipogenesis process, expression of both Rdh (*Rdh10* and *Dhrs9*) decreased. From dd0 to dd7 a 60% reduction was detected for *Rdh10*, while a 70% reduction was detected for *Dhrs9*. Among the three *Raldh*, *Raldh1* was the most highly expressed in MEF. Expression of *Raldh1* peaks at dd4, which is ~14-fold higher compared to dd0. Both *Raldh2* and *Raldh3* levels were relatively stable during adipogenesis (Fig.1B). Expression of *Dhrs3*, a gene that encodes a reductase converting retinal to retinol, went up by 4-fold from dd0 to dd7 (Fig.1C). *Cyp26b1*, an atRA response gene that also catabolizes atRA to maintain homeostasis, went down by 50%. atRA biosynthesis during adipogenesis was also measured. 250nM retinol was added to the cell culture and incubated for 2 hr (avoid light) before collected for retinoids extraction. From dd0 to dd1, a 40% reduction was detected, then the atRA was further decreased by 20% from dd1 to dd7 (Fig.1D). These data provide evidence to support the hypothesis that a decrease in atRA allowed initiation of adipogenesis. Down-regulation of atRA biosynthesis and up regulation of reductases is important to lower atRA. However, *Raldh1* expression was increased during adipogenesis. One possible explanation would be Raldh1 has other important functions that are involved in controlling adipogenesis, such as acting as a transcription factor. We later demonstrate that Raldh1 does not generate atRA to affect adiposity.

atRA inhibits adipogenesis in a dose dependent manner

WT MEF was treated with graded concentrations of atRA throughout the adipogenic differentiation process and collected on dd7 for gene expression and oil red O staining. Expression of Fabp4 and Pparg go down in a dose-dependent manner and 1 μM atRA almost brought the expression of both genes to base line (Fig.2A). Data generated from oil red O staining also supports the gene expression data (Fig.2B). *Rarβ*, an atRA response gene that could be used as an atRA level indicator, went up 25 fold when MEF were treated with 1 μM atRA compared to control (Fig.2C). These data taken together shows that atRA inhibits adipogenesis in a dose dependent manner. More importantly, even the lowest dose, 1nM atRA, causes a 40%-50% decrease of adipocyte markers and lipid content in differentiated MEF.

Rdh10 generates atRA in pre-adipocytes that regulates adipogenesis

Among the various Rdh, *Rdh10* is the most highly expressed in primary undifferentiated MEF (Fig. 3A). Expression of *Rdh10* was ~20 fold higher compared to Dhrs9, while neither Rdh1 nor Rdhe2 were detected in this model. Expression of *Rdh10* mRNA was 50% lower in differentiated MEF compared to undifferentiated MEF (Fig. 3B). The decrease in the amount of atRA synthesized correlated well to the decrease of *Rdh10* expression. These data suggest one potential important function of Rdh10 could be generating atRA to inhibit adipogenesis. In other words, down-regulation of Rdh10 signaling is necessary to induce adipogenesis. To test this hypothesis, we first utilized a mouse model harboring a mutated Rdh10 protein, $Rdh10^{m366Asp}$, to mimic low Rdh10 activity required to initiate adipogenesis. *Rdh10* m366Asp is a single nucleotide mutation at the substrate binding pocket that reduces substrate binding affinity, thus reducing enzymatic activity (Ashique et al., 2012). The benefit of this model is that while catalytic activity is reduced, *Rdh10* expression is not altered, which helps to exclude possible scenarios, such as the phenotype could be caused by some none-retinoid-related functions of this protein.

All MEFs used in this study were isolated from mice fed a vitamin A-sufficient diet (4 IU/g). Under these conditions, homozygous embryos die before MEF can be collected (dd13.5-dd14). For this reason, MEF isolated from hypomorphic heterozygous Rdh10 mutant (HYPO) embryos were used. To verify whether MEF isolated from Rdh10 HYPO embryos is an appropriate model, in vitro atRA biosynthesis assay were performed with 250 nM retinol added to the culture. There was a 40% reduction of atRA synthesized in HYPO MEF compared to WT MEF (Fig.4A). There was no compensation from other retinoid metabolizing genes (supplementary data) when Rdh10 was mutated. Then the HYPO and WT MEF were induced to differentiation with adipogenic cocktail and collected on dd7 for oil red O neutral lipid quantification as well as marker gene expression. The number of oil red O positive cells was ~40% higher in HYPO MEFs compared to WT (Fig.4B and 4C), while expression of adipogenic markers (*Pparg* and *aP2*) was ~2 to 3 fold higher in HYPO (Fig. 4D). This was further supported by completely knocking out Rdh10 with CRISPR CAS9 in immortalized MEF. Expression of

Rdh10 was barely detected in Rdh10 CRISPR KO MEF (CKO) (Fig. 9A). The amount of atRA synthesized in CKO was ~70% lower compared to WT when incubated with 250nM retinol for two hr. The amount of retinol in cells was similar in both CKO and WT (Fig.9B). When induced to become adipocytes, there was a dramatic increase of oil red O positive cells in the CKO culture compared to WT (Fig. 10A and 10B). Both *Pparg* and *aP2* level were~3 fold higher in CKO (Fig. 10C). These findings were further supported by a third model, *Rdh10*$^{+/-}$ MEF. Rdh10$^{+/-}$ MEF were obtained from Rdh10 heterozygous total knockout mice (C57 background). These cells were induced to adipogenic differentiation with adipogenic cocktail and 100nM retinol and oleate. On dd7, *Rdh10*$^{+/-}$ MEF showed a noticeable two fold increase of lipid containing cells compared to WT (Fig.17A and 17B). However, *Pparg* expression was not altered in *Rdh10*$^{+/-}$, while *aP2* and *Fabp5* expression went up ~2-fold. *Pref-1* expression was ~40% lower in *Rdh10*$^{+/-}$ (Fig.17C).Taken together, these data support the hypothesis that Rdh10 is an important atRA generating enzyme in MEF and reduced *Rdh10* expression mimics a low atRA condition that allows the cells to become more sensitive to adipogenic induction signals.

RA inhibit the upregulation of adipocyte markers, thus inhibit adipogenesis.

To understand whether it is the atRA generated from Rdh10 that's primarily responsible for the phenotype or the other unknown functions of Rdh10, a retinol dose response was conducted. Graded concentrations of retinol were added to the cell culture in addition to adipogenic induction medium. When treated with same amount of retinol, expression of atRA response genes (*Cyp26a1*, *Cyp26b1* and *Rarb*) (Fig. 5A-5C) was higher in the HYPO MEF compared to WT, which indicates more atRA was generated in WT MEF. atRA generated by Rdh10 directly affects adipogenesis, which is supported by the expression of adipogenic marker genes Pparg and aP2. The IC_{50} for HYPO is higher than WT (Pparg, HYPO IC_{50} = 915, WT IC_{50} = 453; aP2, HYPO IC_{50}=703, WT IC_{50}=65) (Fig. 6C and 6D), meaning more substrate (retinol) is needed to reduce the adipogenesis effect by half. However, when total lipids were used as measurement (oil red O stain quantification), HYPO IC_{50} is slightly higher than WT IC_{50} (Fig.6B), which could be explained by the fact that total lipid quantification is a result of adipogenesis and de novo lipogenesis, so it may be possible that both adipogenesis and de novo lipogenesis are affected. The difference would be smaller compared to measuring adipogenic genes. These taken together these data suggest that retinol is less potent in inducing atRA response genes in HYPO compared to WT, further supporting the hypothesis that the atRA synthesized by Rdh10 is key to regulate adipogenesis.

RAR agonist, but not PPARd agonist rescues the adipogenesis phenotype.

To test whether the phenotype was a result of reduced endogenous atRA biosynthesis, 500nM atRA was added to the induction medium during adipogenic differentiation. On differentiation day 7 (dd7) lipid droplets formation were measured by oil red O staining and quantification, expression of adipogenic marker genes. *Pparg* and *aP2* were measured by quantitative PCR. atRA treatment decreased the number of oil

red O positive cells in both WT and HYPO MEF (Fig.7A). This is also supported by the expression of *Pparg* and *aP2*(Fig. 8A and 8B). These data indicate, HYPO MEF are sensitive to atRA treatment and the adipogenesis phenotype was rescued when 500nM atRA was added to the induction medium. Because it was reported that atRA works though two different receptors to regulate gene expression, RAR and PPARβ/δ, we next tested which receptor was primarily responsible for the phenotype. 100nM RAR pan-agonist (TTNPB) and PPARβ/δ agonist (GW0742) was added to the induction medium. On dd7, cells were collected for oil red O assay and gene expression. RAR pan-agonist (TTNPB) but not PPARβ/δ agonist (GW) treatment reduced the amount of lipid droplets formation in the CKO (Fig. 11A and 11B). RAR agonist also brought the CKO Pparg and aP2 expression level down to WT level (Fig.12A and 12B). To sum up, in vitro, atRA or RAR pan-agonist, but not PPARβ/δ agonist rescues the phenotype.

atRA generated by Rdh10 possibly regulates early transcription factor for adipogenesis

According to previous hypothesis, reduction of Rdh10 decreases endogenous atRA, thus causing cells to be more sensitive to adipogenic induction signal. A reasonable experiment to do is to compare the Rdh10 KO MEF to the WT MEF before adipogenesis induction to see whether they have genetic differences. CKO and WT MEF were cultured in growth medium. Two days after reaching confluence, cells were collected for gene expression assay. A panel of early genes that may affect adipogenesis were assayed. *Bmp4*, *Bmp2*, *Klf2*, *Zfp521* and *Ebf1* were decreased in CKO. *Fabp5*, *Crabp2*, *Pparg* and *Pref1* were increased in CKO (Fig.13). However, when rescued with TTNPB (treated from dd-2 to dd0), only *Pref1* expression was rescued. *Pref1* was reported to be expressed in pre-adipocytes and its expression decreases in mature adipocytes. One important function of *Pref-1* is to keep the cells at a pre-adipocyte stage while inhibiting the differentiation from pre-adipocytes to adipocytes. In this model, it's possible that Rdh10 CKO has more *Pref-1* positive pre-adipocytes to begin with, and adding TTNPB would suppress the commitment from progenitor cells to pre-adipocytes. To verify the findings from the Rdh10 CKO, I next tested this theory with the $Rdh10^{+/-}$ MEF. WT MEF from 5 different embryos and $Rdh10^{+/-}$ MEF from 7 different embryos were used in this study. According to Figure 18, expression of *Bmp2*, *Bmp4*, *Zfp521*, *Zfp423* and *Smad3* was significantly lower in Rdh10+/- compared to WT. However, no difference was detected in Pref1 as CKO. When a rescue experiment was performed by treating the cells from dd-2 to dd0 with 100nM TTNPB, only *Bmp* and *Zfp423* levels went up. It is likely that atRA generated from Rdh10 affects a network of genes that regulates adipogenesis as a whole. In this case, RNAseq or microarray could be a better solution to understand the mechanism how adipogenesis is affected by Rdh10.

Expression of retinoid metabolizing gene during osteoblast differentiation.

Raldh1 is the most highly expressed Raldh in MEF, which is ~20 fold higher than *Raldh2* and *Raldh3*. Expression of *Raldh1* goes up ~5 fold from dd0 to dd4, suggesting some role of Raldh1 in the osteoblast differentiation process (Fig.21A). *Raldh1* KO mice

are protected from osteoporosis (Nallamshetty et al., 2014a). Expression of *Raldh2*/*3* keeps relatively stable during the process. Both *Rdh10* and *Dhrs9* goes down during osteoblast differentiation (Fig. 21B), while *Dhrs3* expression doesn't change (Fig.21C). Overall, the pattern of retinoid gene expression during osteoblast differentiation is different from that during adipogenesis, suggesting differential regulation of retinoid metabolism during different developmental processes.

The effect of atRA on osteoblast differentiation may be dose and time dependent.

Rdh10 HYPO showed a decrease in alkaline phosphate activity and calcium deposits when induced into osteoblasts in vitro (Fig.22A). A ~70% decrease in ALP positive cells and a 55% decrease in alizarin red positive areas were detected (Fig. 22B). Expression of osteoblast markers *Smad3* and *Opn* showed ~20% decrease in HYPO osteoblasts while no difference was detected in *Runx2* (Fig. 22C). What makes it more interesting was that adipocytes were found in the osteoblast culture, as shown in Fig.22A, oil red O staining. An increase of oil red O positive cells were noticed in HYPO culture. When assayed for adipocyte markers, we found a 40% increase of *Pparg* and a 50% increase of *aP2* in the HYPO culture. This result suggests that a partial Rdh10 knock down potentiates adipogenesis, while down regulating osteoblast differentiation.

However, when Rdh10 CKO MEF were used for osteoblast differentiation assay, we noticed a completely opposite result. WT immortalized MEFs don't differentiate when treated with osteoblast induction medium, while CKO MEF showed dramatic differentiation, as evident by alizarin staining for calcium deposits (Fig.23 A). Expression of *Alp* and *Opn* was ~10 fold and 5 fold higher in CKO, respectively, while Runx2 expression was not changed (Fig.23B). Even though the osteoblast phenotype was completely different from that of HYPO MEF, the increased adipogenesis phenotype was the same. A noticeable increase of oil red o staining was observed in osteoblast culture in CKO (Fig. 23A), while expression of Pparg was up ~2-fold (Fig. 23 B). Given the discrepancy shown above, one possible explanation could be that the effect of atRA on osteoblast differentiation is dose dependent and temporal. To test this hypothesis, the next thing is to add different doses of atRA to the culture at different differentiation periods. The first experiment was done with WT MEF, with 10nM, 200nM, 600nM and 1μM atRA added to the differentiation medium during the entire period of osteoblast differentiation (dd0 to collection on dd14). It's worth noting that starting from 200nM atRA, ALP activity was inhibited by ~90% (dd7). On dd21, even 10nM atRA almost completely abolished calcium deposition (Fig.24A). On dd14 when samples were collected for gene expression, even the lowest atRA concentration decreased the expression of *Runx2* and *Sox9* by 50% and 80% respectively, while no further decreases were detected even with a very high atRA concentration. However, a dose dependent increase of *Smad3* was detected (Fig 23B).

The next experiment was to test whether atRA would have a different effect when added early. Fig.25A to C show gene expression from cells treated with graded amounts of atRA from dd0 to collection day (dd4). Treatment of atRA was effective as

shown by an increase of atRA response gene *Cyp26b1*. One µM atRA increased *Alp* expression by ~4-fold, while lower concentrations didn't show much difference. Smad3 expression has only a modest increase at 1µM atRA. *Runx2* expression didn't change with atRA treatment (Fig.25B). Response of *Opn* was more complicated. Only lower atRA concentration increase *Opn* expression, 10 M and 100nM atRA increase *Opn* expression by 3-fold, while 1µM atRA dramatically inhibits *Opn* expression. Similar results with *Opn* were observed when cells were treated with atRA from dd0 to dd4 but collected on dd14 (Fig.25D). *Runx2* was decreased in a dose-dependent manner. Alp expression peaks at 10nM atRA treatment. It could be possible that atRA promotes osteoblast commitment only during early differentiation, but may have a different role during late differentiation (maturation stage). It seems that a low dose of at RA (10nM) would promote osteoblast formation but high doses inhibit osteoblast differentiation.

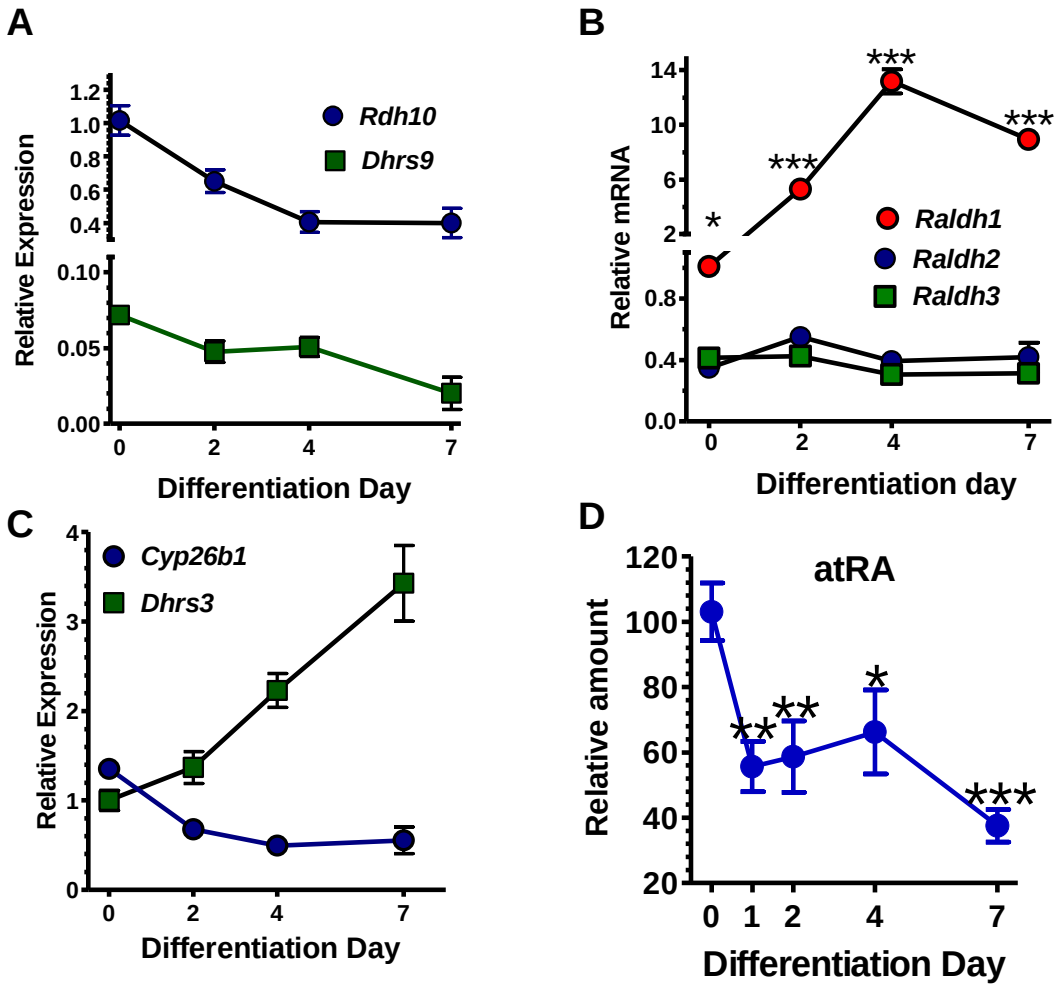

Figure 1. Retinoic Acid Metabolism during adipogenesis.

(A) *Rdh* mRNA expression in WT MEF normalized to *Rdh10* on dd0. *p<0.05 vs. dd0.
(B) *Raldh* mRNA expression during MEF differentiation into white adipocytes, normalized to *Raldh1* on dd0. One-way ANOVA: differentiation effect on *Raldh1* mRNA (p<0.0001). Dunnett's multiple comparison: *p<0.05; ***p<0.001 vs dd0.
(C) *Dhrs3* and *Cyp26B1* mRNA expression in WT MEF. *Dhrs3* and *Cyp26B1* were normalized to *Dhrs3* on dd0. One-way ANOVA: differentiation effect on both *Dhrs3* and *Cyp26B1* for both WT and KO, p<0.02. Dunnett's multiple comparison: significant differences between dd0 and dd4, and dd0 and dd7 for each gene and genotype, p<0.05.
(D) atRA biosynthesis during adipogenesis. WT MEF was treated 2 hr with 250 nM retinol during differentiation. atRA was measured by LC/MS/MS. Combined data from two individual experiments: n = 6-11 biological replicates.

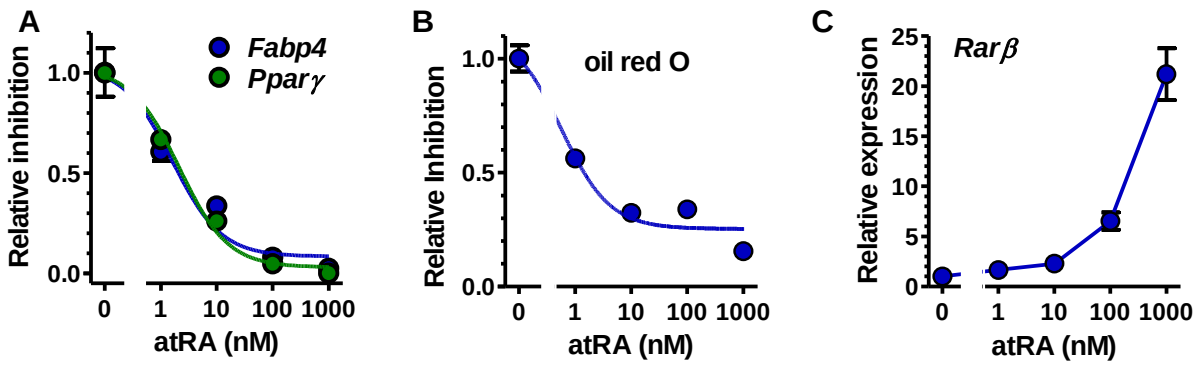

Figure2. atRA inhibits adipogenesis in a dose dependent manner.

(A) *Fabp4* and *Pparg* mRNA expression at the end of dd7 in WT MEF. MEF were treated with increasing doses of atRA from dd0 through dd7. Media were refreshed every 24 hr with add atRA to foster continued atRA presence. Values were normalized to values of 1 for untreated cells.
(B) MEFs from WT as treated in A were stained with oil red O at the end of dd7.
(C) Effects of graded doses of atRA on *Rarβ* mRNA in WT (blue) and KO (red) MEF at the end of dd7. Two-way ANOVA: gene $p>0.49$; dose $p<0.0001$.

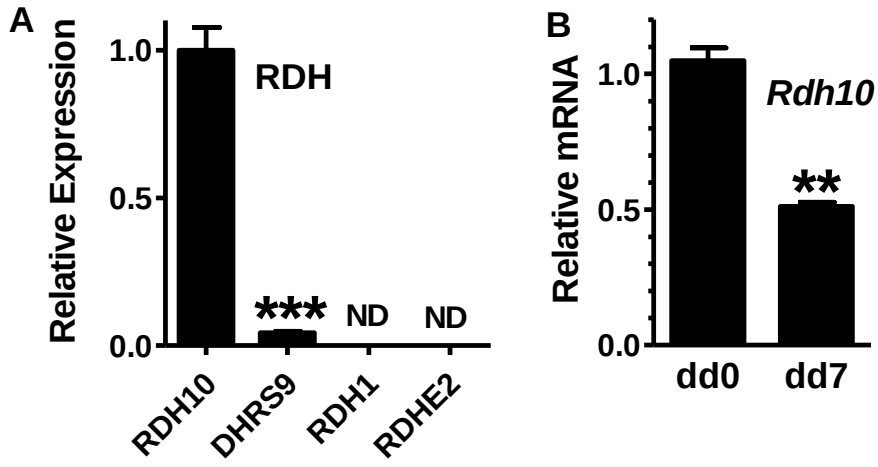

Figure 3. *Rdh10* is the most highly expressed RDH in MEF and its expression level goes down after adipogenic differentiation.

(A) Relative expression of retinol dehydrogenase in undifferentiated WT MEFs. n=5 (biological replicates). ND: not detected. ***p<0.001 by student t test.
(B) *Rdh10* mRNA before (dd0) and after (dd7) adipogenic differentiation: n = 4 biological replicates each dd. Representative data from two independent experiments. **p<0.01 by student t test.

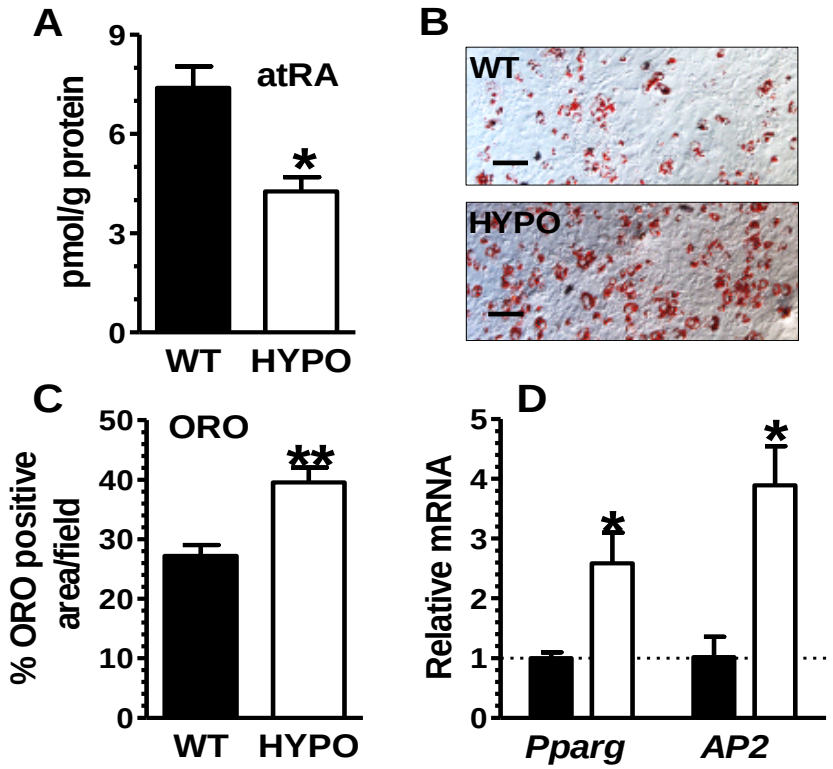

Figure 4. Reduction of Rdh10 activity reduces the amount of atRA produced, thus increasing adipogenic potential of MEF.

Black bars= WT; white bars=HYPO.

(A) atRA biosynthesis during adipogenesis. WT MEF were treated 2 hr with 250 nM retinol during differentiation. atRA was measured by LC/MS/MS. Combined data from two individual experiments: n = 6-11 biological replicates.
(B) atRA biosynthesis in WT and Rdh10 HYPO mutant MEF (dd0). Cells were treated 2 hr with 250 nM retinol: n = 6 biological replicates each group. Representative data from 3 independent experiments.
(C)Representative images of oil red O staining of differentiated WT and Rdh10 HYPO mutant MEF. Representative data from 3 independent experiments.
Quantification of data in E. Oil red O positive cell numbers were counted by two individuals independently.
(D) Expression of adipogenic markers on dd7: n = 3 biological replicates each group. Representative data from 3 experiments.

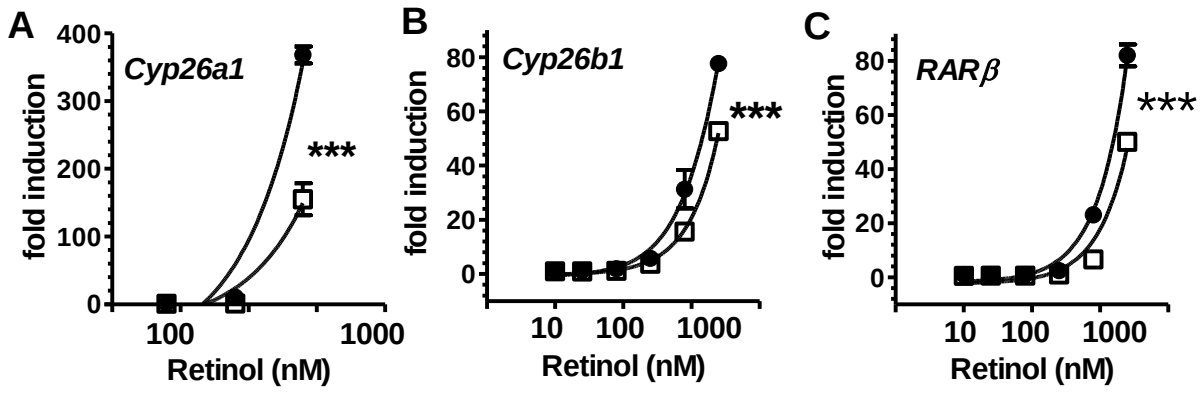

Figure 5. HYPO MEF produce less atRA when treated with the same amount of retinol.

Black circle= WT; white square=HYPO.

(A-C). Rdh10 HYPO and WT MEFs treated with graded amount of retinol every 24 hours during differentiation. Cells were collected for qPCR assay on dd7. Figures showing expression of atRA response genes, *Cyp26a1*, *Cyp26b1* and *Rarβ*. Representative figure of two independent experiments. Data are shown as means ± SEM (n = 2): *p<0.05, **p<0.01, ***p<0.001 by two-way ANOVA.

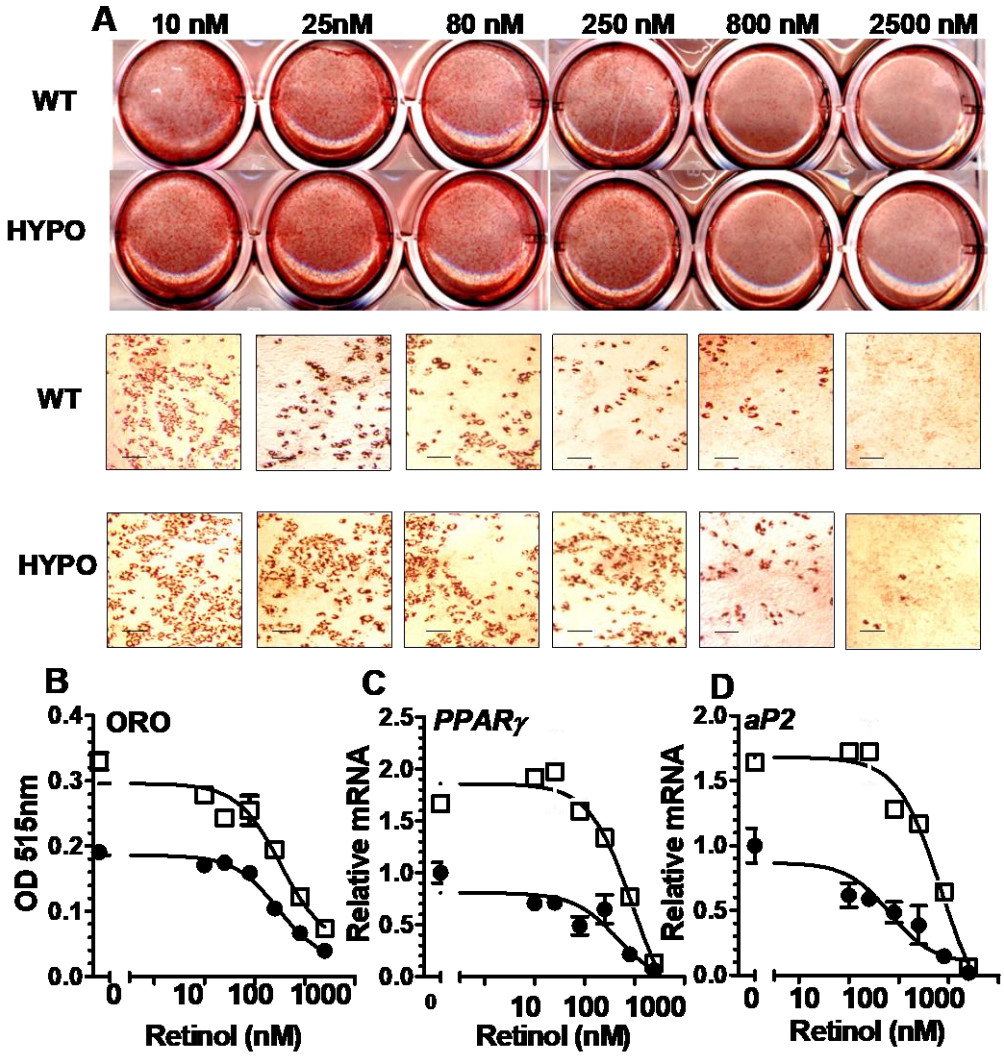

Figure 6. HYPO MEF are less sensitive to retinol inhibition of adipogenesis.

Black circle= WT; white square=HYPO.

(A)Representative oil red o pictures of Rdh10 mutant (+/-) and WT MEFs treated with graded amount of retinol (10nM, 25nM, 80nM, 250nM, 800nM and 2500nM) every 24 hours during differentiation and stained on dd7.
(B)Dose response curve of oil red O stain quantification by isopropanol extraction.(n=3)
(C and D). Rdh10 HYPO and WT MEFs treated with graded amount of retinol every 24 hours during differentiation. Cells were collected for qPCR assay on dd7. Figures showing expression of adipogenic marker *Pparγ* and *Ap2*. Representative figure of two independent experiments. Data are shown as means ± SEM (n = 2): *p<0.05, **p<0.01, ***p<0.001 by two-way ANOVA.

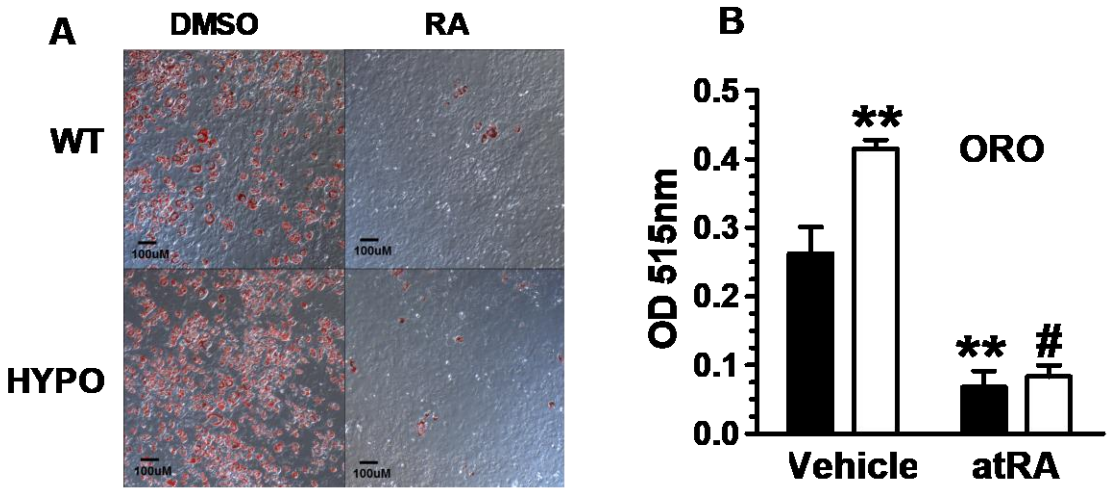

Figure 7. atRA rescues the adipogenesis phenotype.

Black bars= WT; white bars=HYPO.

(A)Oil Red O staining of differentiated WT vs HYPO, treated by DMSO (vehicle) or 500 nM atRA (refreshed every 24 hr): n = 4 biological replicates each group representative result of two independent experiments
(B)Quantification of images in A by extracting oil red o with isopropanol and measuring absorbance at 515nM. n=4 biological replicates.

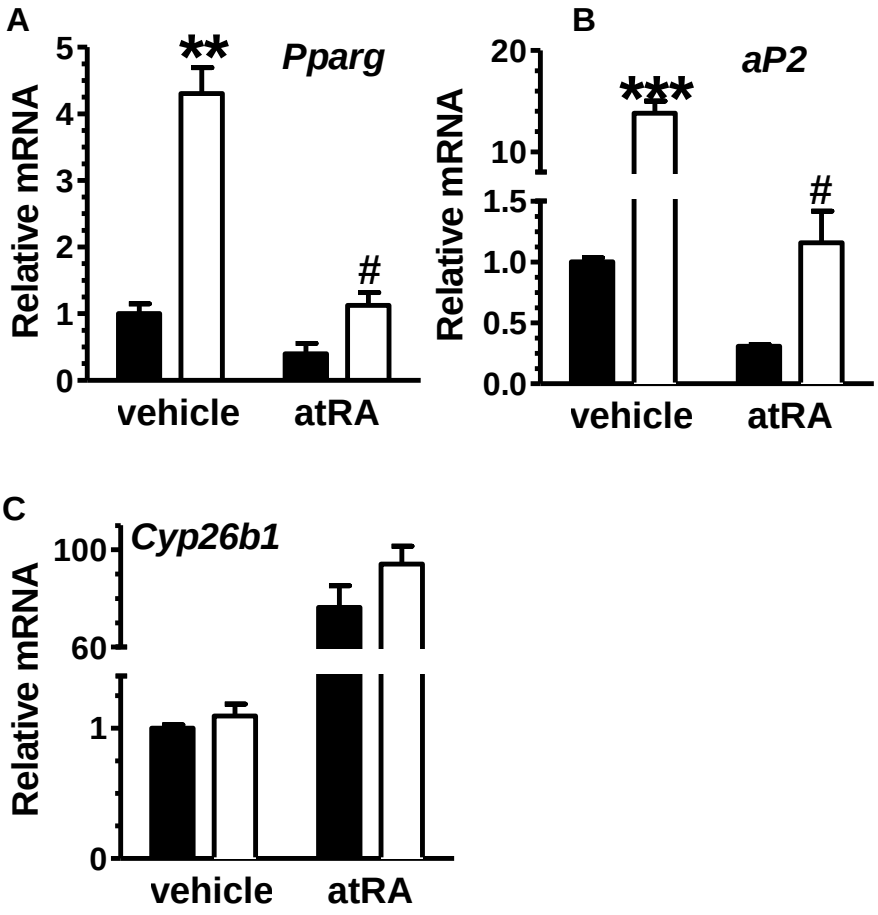

Figure 8. atRA treatment inhibits expression of adipogenic genes while increasing Cyp26b1 gene expression.

Black bars= WT; white bars=HYPO.

(A-C) Expression of adipogenic marker genes (*Pparg* and *Ap2*) differentiated MEFs treated with DMSO or 500nM atRA (refreshed every 24 hr): n = 2-3 biological replicates each group, representative result of two independent experiments.

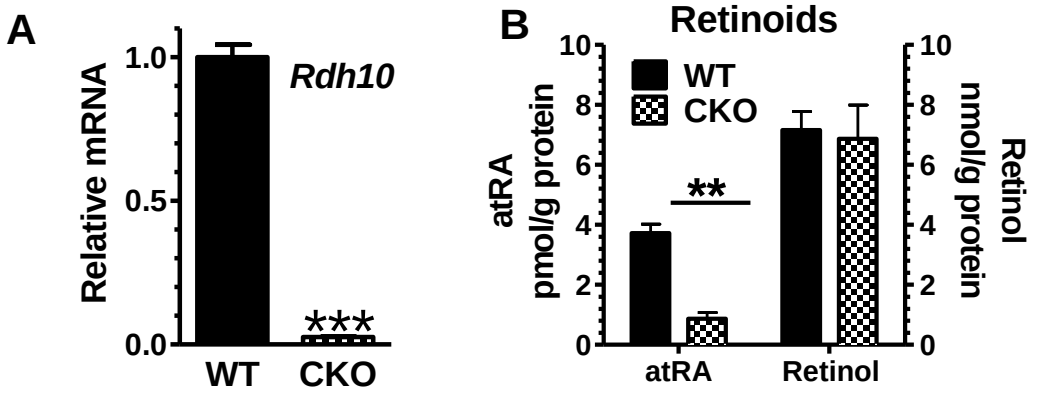

Figure 9. A CRISPR Rdh10 KO abolishes Rdh10 expression and decreases the amount of atRA synthesized.

Black bars= WT; white bars with pattern =CKO.

(A) *Rdh10* mRNA in WT and CRISPR CKO (dd0) immortalized MEF: n = 3 each group. (B) Quantification of atRA and retinol by LC/MS and HPLC. Cells treated with 250nM retinol and incubated for 2 hours before collected for extraction.

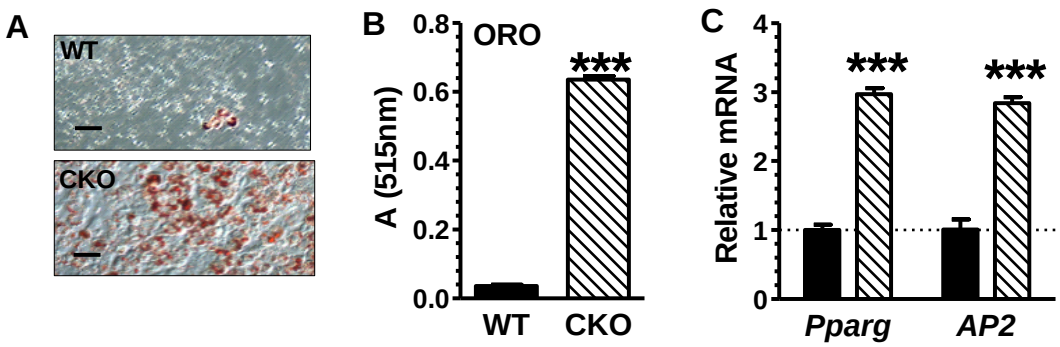

Figure 10. RDH10 CRISPR KO has increased adipogenesis.

Black bars= WT; white bars with pattern =CKO.

(A) Representative oil red O images of differentiated WT and CKO MEF (dd7).
(B) Quantification of data in B. Representative data from two independent experiments, n=3 for each experiment.
(C)Expression of adipogenic markers on dd7 in WT and CKO MEF: n=3 each group. Representative data from two experiments.

A-C. Means ± SE, two tailed, unpaired students t tests:. *p<0.05, **p<0.01, ***p<0.001.

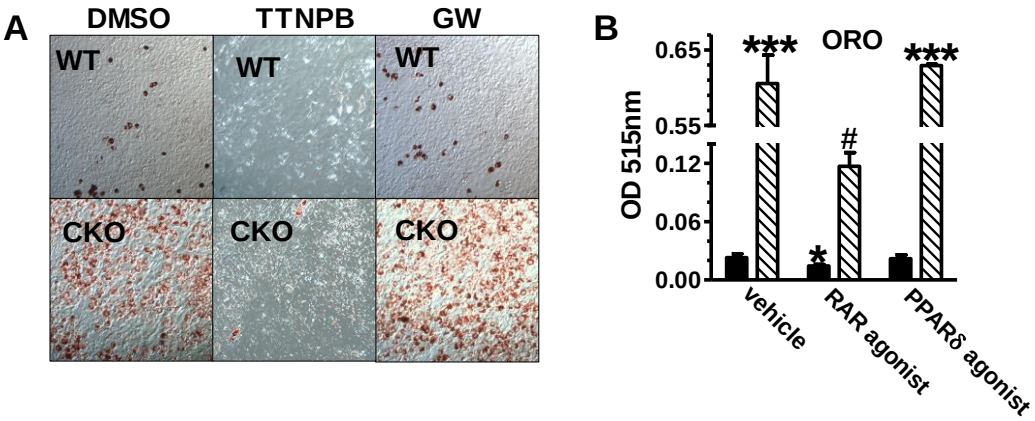

Figure 11. RAR agonist, but not PPARδ agonist rescues the Rdh10 CKO adipogenesis phenotype.

Black bars= WT; white bars with pattern =CKO.

(A)Oil red O images of differentiated WT vs CKO on dd7, treated with DMSO (vehicle), 100 nM TTNPB (RAR agonist) or 100 nM GW0742 (PPARδ agonist) for 7 days. Representative result of two independent experiments. n=3 for each experiment.

(B)Quantification of images in E by extracting oil red O with isopropanol and measuring absorbance at 515 nm.

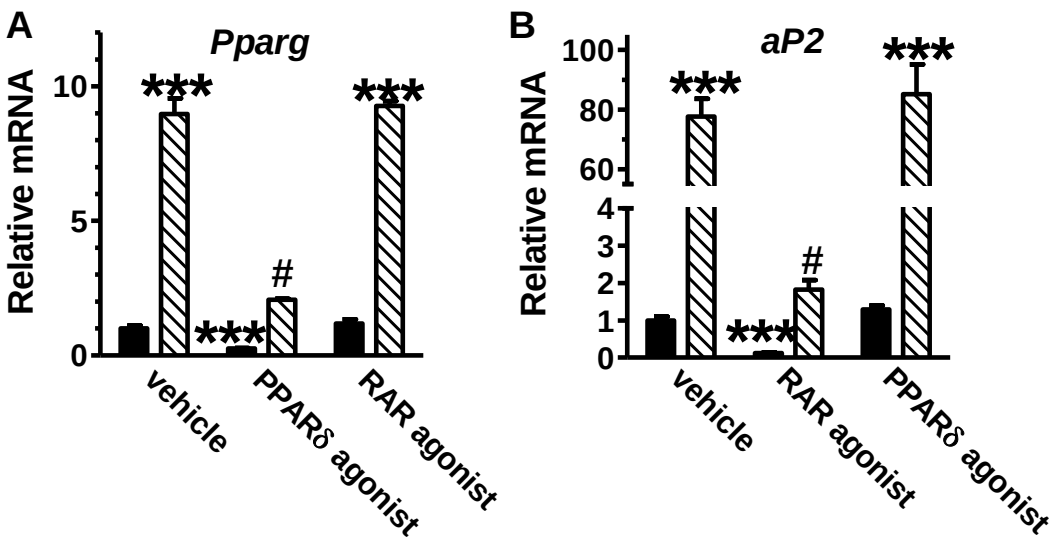

Figure 12. RAR agonist, but not PPARδ agonist inhibits adipogenic marker gene expression.

Black bars= WT; white bars with pattern =CKO.

(A-B) Expression of *Pparg* and *Ap2* in samples from fig.9. Representative result from two independent experiments. n=3 for each experiment. Data were analyzed by unpaired, two-tailed student's t test: *p<0.05, **p<0.01, ***p<0.001. #p<0.05 compared to CKO control.

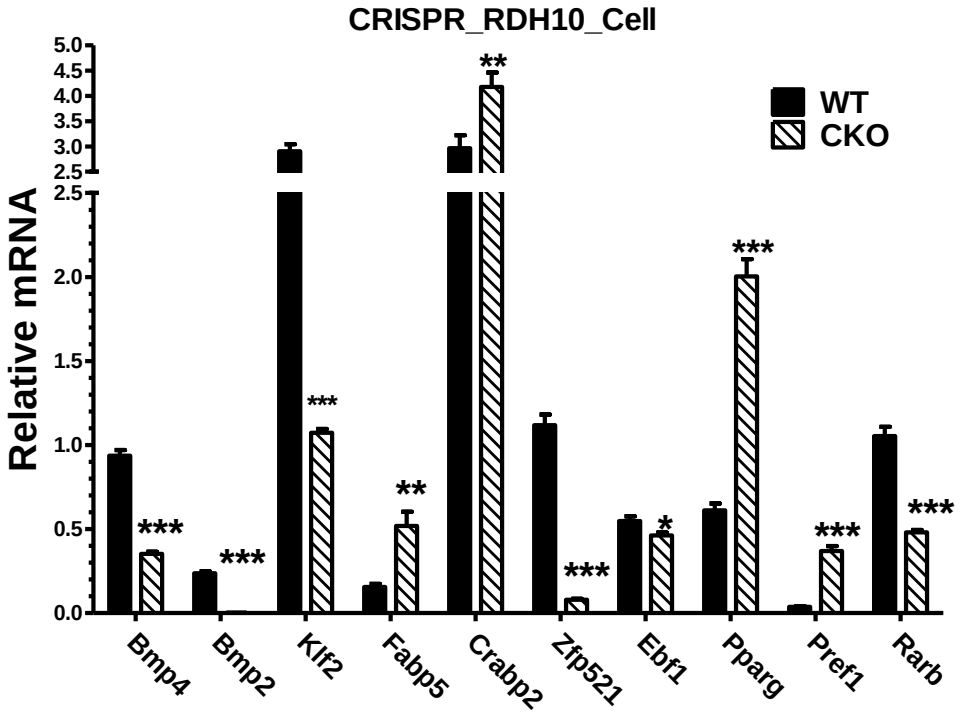

Figure 13. Early gene expression in dd0 WT vs dd0 CKO

Black bars= WT; white bars with pattern =CKO.

WT and CKO MEF cultured in growth medium, collected on dd0 for gene expression measurement. n=6 for each genotype. Data were analyzed by unpaired, two-tailed student's t test: *p<0.05, **p<0.01, ***p<0.001.

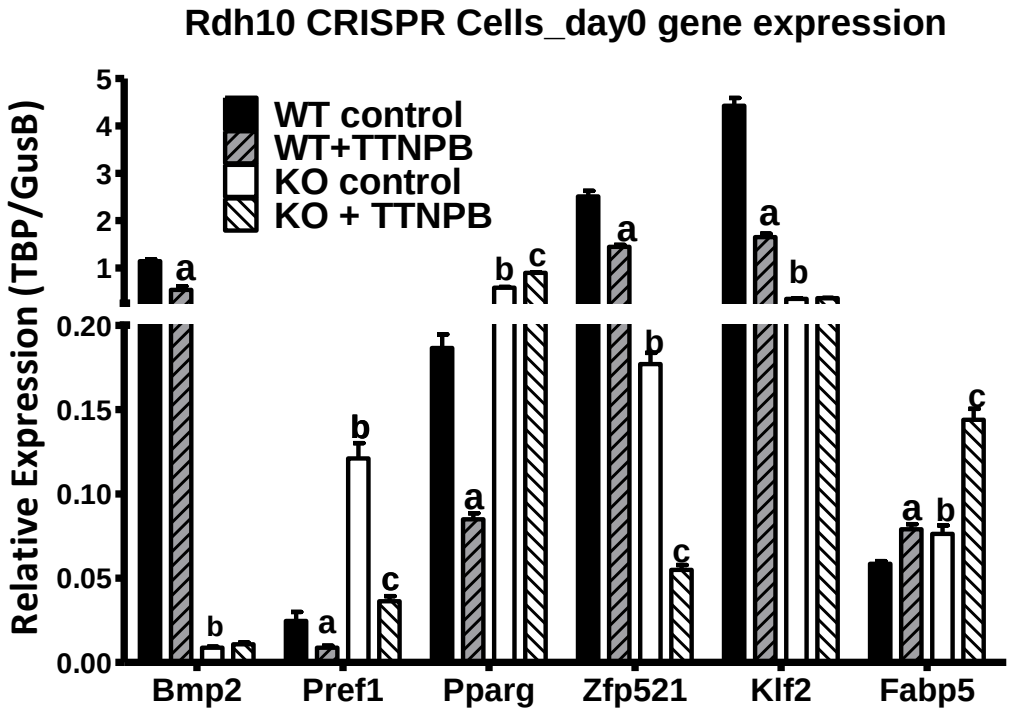

Figure 14. TTNPB did not rescue most early gene expression other than Pref-1.

MEF was treated with 100nM TTNPB from dd-2 to dd0, and collected for gene expression on dd0, n=3 each group. a= WT +TTNPB significant different from WT control. b=KO control significant from WT control. c= KO+TTNPB significant different from KO control.

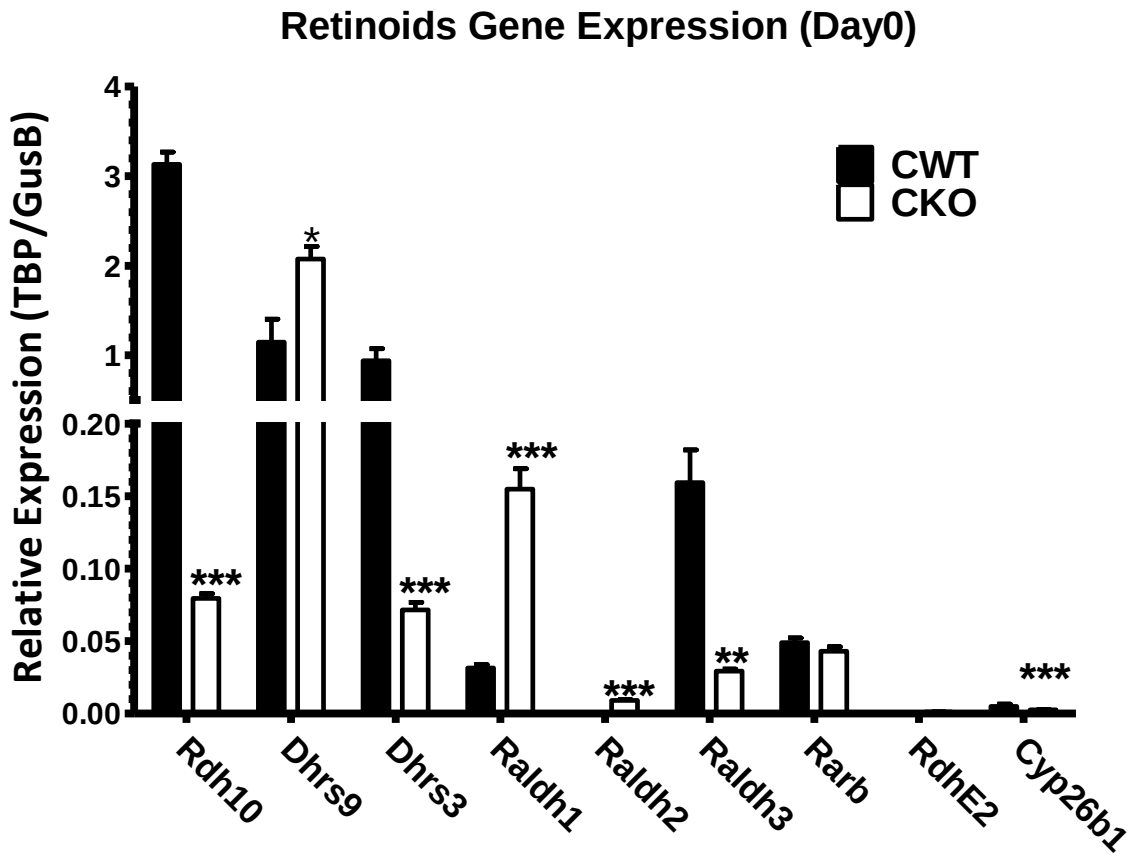

Figure 15. Expression of retinoid metabolizing genes on dd0, CKO vs WT.

Black bars= WT; white bars with pattern =CKO.

WT and CKO MEF was cultured in growth medium and collected on dd0 for gene expression measurement. n=3 for each genotype. Data were analyzed by unpaired, two-tailed student's t test: *p<0.05, **p<0.01, ***p<0.001.

Compensation from Dhrs9, Raldh1, Raldh2 and RdhE2 was observed.

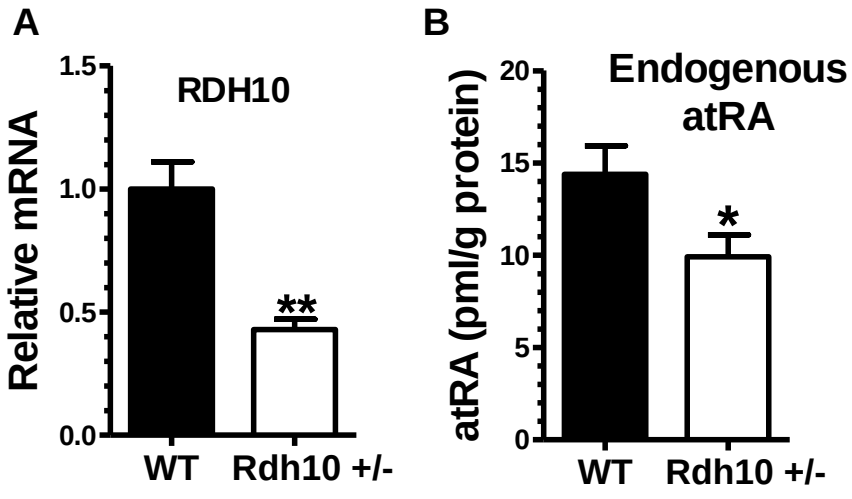

Figure 16. *Rdh10* $^{+/-}$ mice have decreased *Rdh10* expression and reduced atRA biosynthesis.

(A)MEF was cultured in growth medium. On dd0, cells were collected for Rdh10 expression. n=3-5 biological replicates.

(B)MEF was cultured in 10cm plate with growth medium. On dd0, cells were collected for endogenous atRA analysis. n=6-7 biological replicates.

Data were analyzed by unpaired, two-tailed student's t test: *p<0.05, **p<0.01, ***p<0.001.

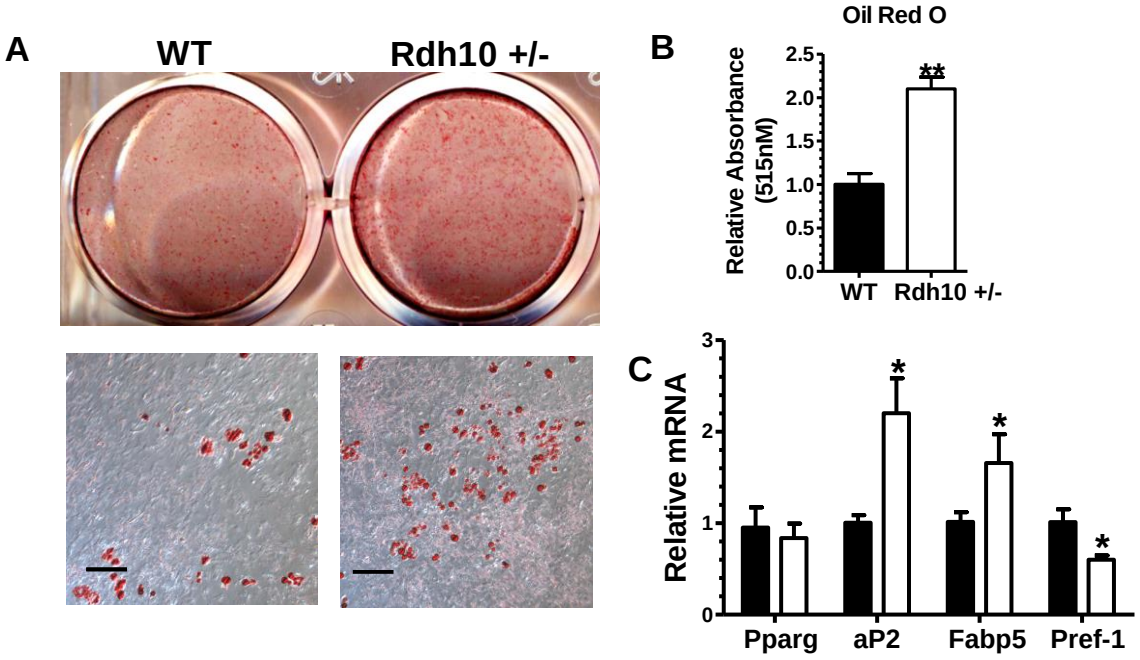

Figure 17. *Rdh10* $^{+/-}$ mice have increased adipogenesis.

(A) MEF were differentiated in adipogenic induction medium with additional 100nM retinol and oleate acid. Representative pictures of oil red O stained MEF (dd7).

(B)Oil red O quantification of pictures in A. n=4.

(C)Expression of adipocyte marker genes on dd7. n=4

Data were analyzed by unpaired, two-tailed student's t test: *p<0.05, **p<0.01, ***p<0.001.

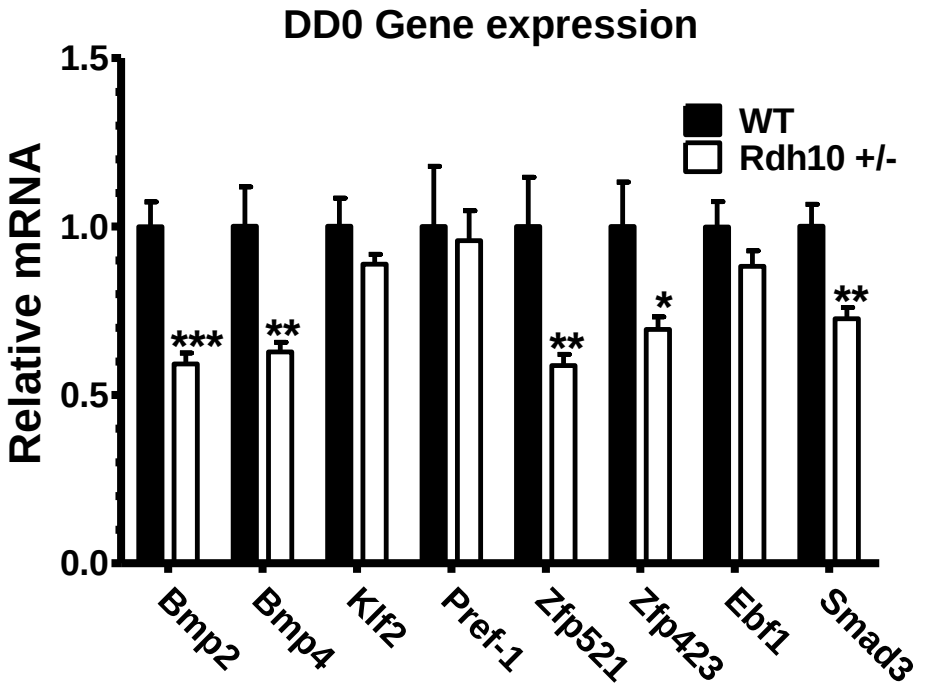

Figure 18. Expression of early adipogenesis genes.

WT MEF collected from 5 different embryos and Rdh10+/- MEF collected from 7 different embryos were used in this study. Cells were cultured in growth medium and collected on dd0. Data were analyzed by unpaired, two-tailed student's t test: *p<0.05, **p<0.01, ***p<0.001.

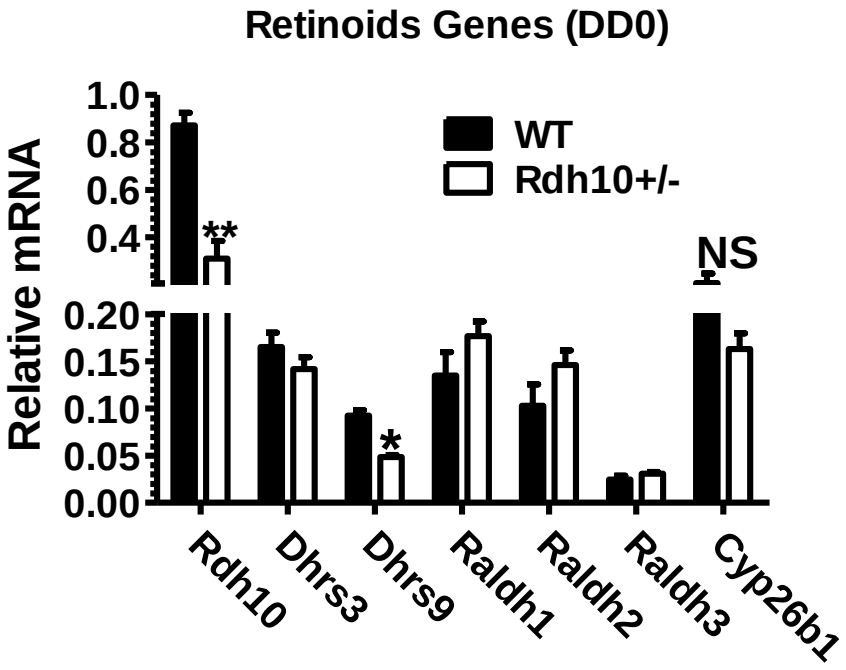

Figure 19. Expression of retinoid metabolizing genes.

WT MEF collected from 5 different embryos and *Rdh10*$^{+/-}$ MEF collected from 7 different embryos were used in this study. Cells were cultured in growth medium and collected on dd0. *p<0.05 by two tailed student t test.

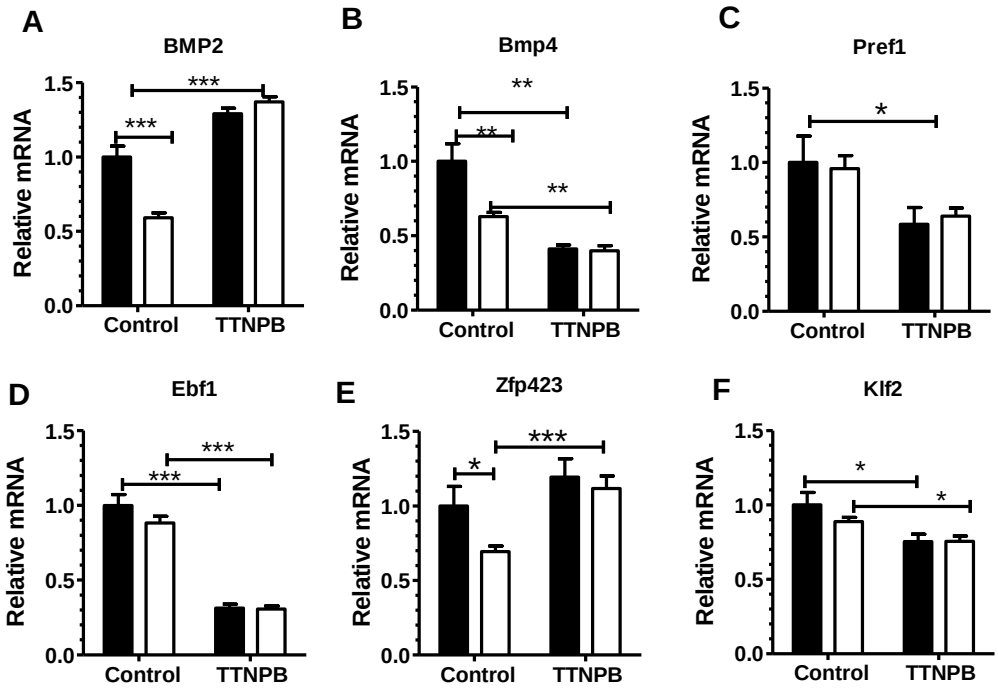

Figure 20. TTNPB treatment rescues BMP2 expression in *Rdh10$^{+/-}$*.

Black bar= WT. White bar=*Rdh10*$^{+/-}$

(A-F)MEF were treated with 100nM TTNPB from dd-2 to dd0, then collected on dd0 for gene expression. n=4 -7 . *p<0.05, **p<0.01, ***p<0.001 by student t test.

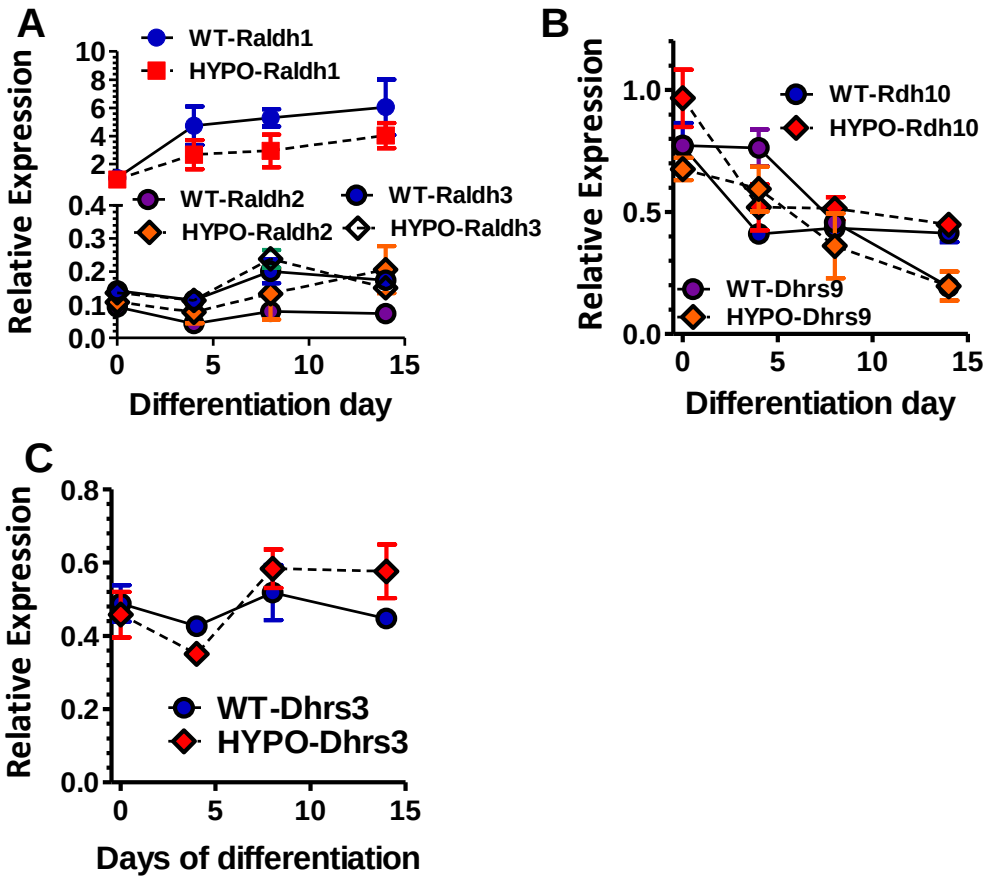

Figure 21. Expression of retinoid metabolizing genes during osteoblast differentiation.

(A)Expression of Raldh1, Raldh2 and Raldh3 during osteoblast differentiation in both WT and HYPO. n=3 (biological replicates). No compensation from *Raldh1*, *Raldh2* nor *Raldh3* in HYPO.
(B)Expression of *Rdh10* and *Dhrs9* during osteoblast differentiation in both WT and HYPO. n=3 (biological replicates). No compensation from *Rdh10* or *Dhrs9* in HYPO.
(C)Expression of *Dhrs3* during osteoblast differentiation in both WT and HYPO. n=3 (biological replicates).

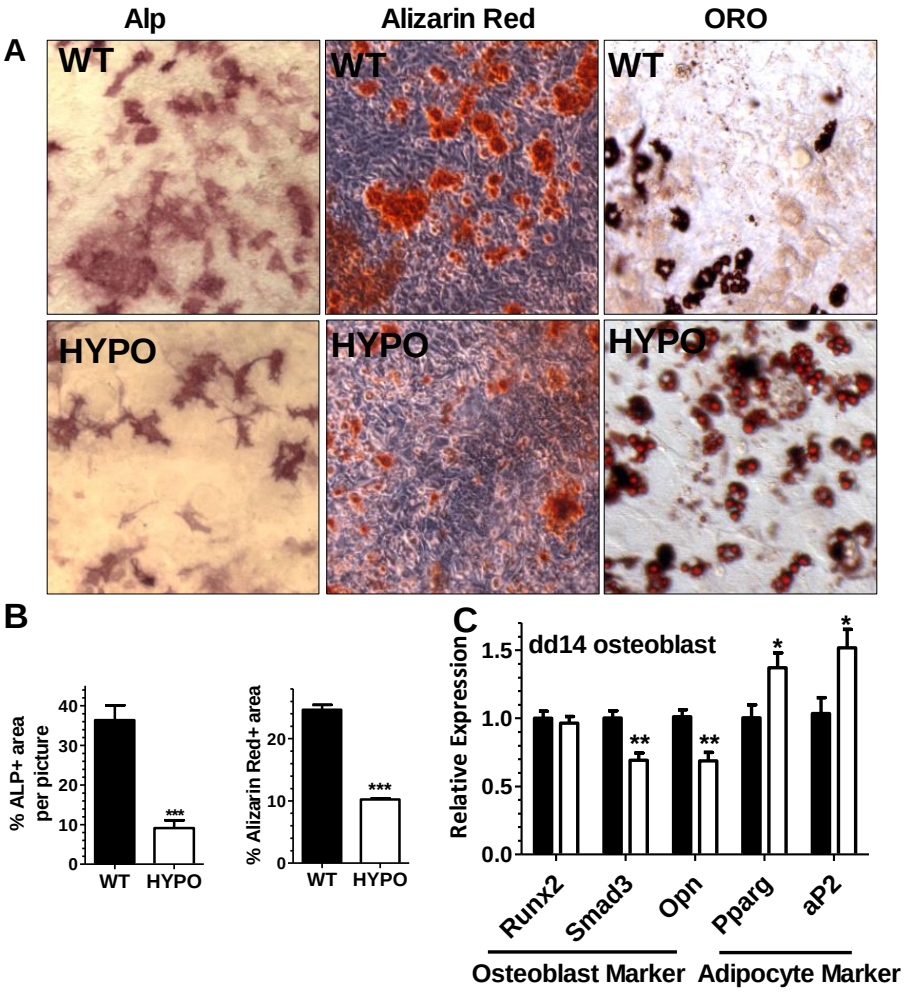

Figure 22. Partial loss of *Rdh10* decreased osteoblast differentiation but increased adipocyte formation in primary cell culture.

Black bar= WT. White bar=CKO

(A)Representative pictures of alkaline phosphate activity stain, alizarin staining for calcium deposits and oil red o staining (from left to right). Each staining performed at least two times with n=3 to 4, getting consistent results.
(B)Quantification of staining in A. n=3-4
(C)Expression of osteoblast and adipocyte marker in dd14 osteoblast culture. n=6-7 (biological replicates), combined results of two independent experiments.

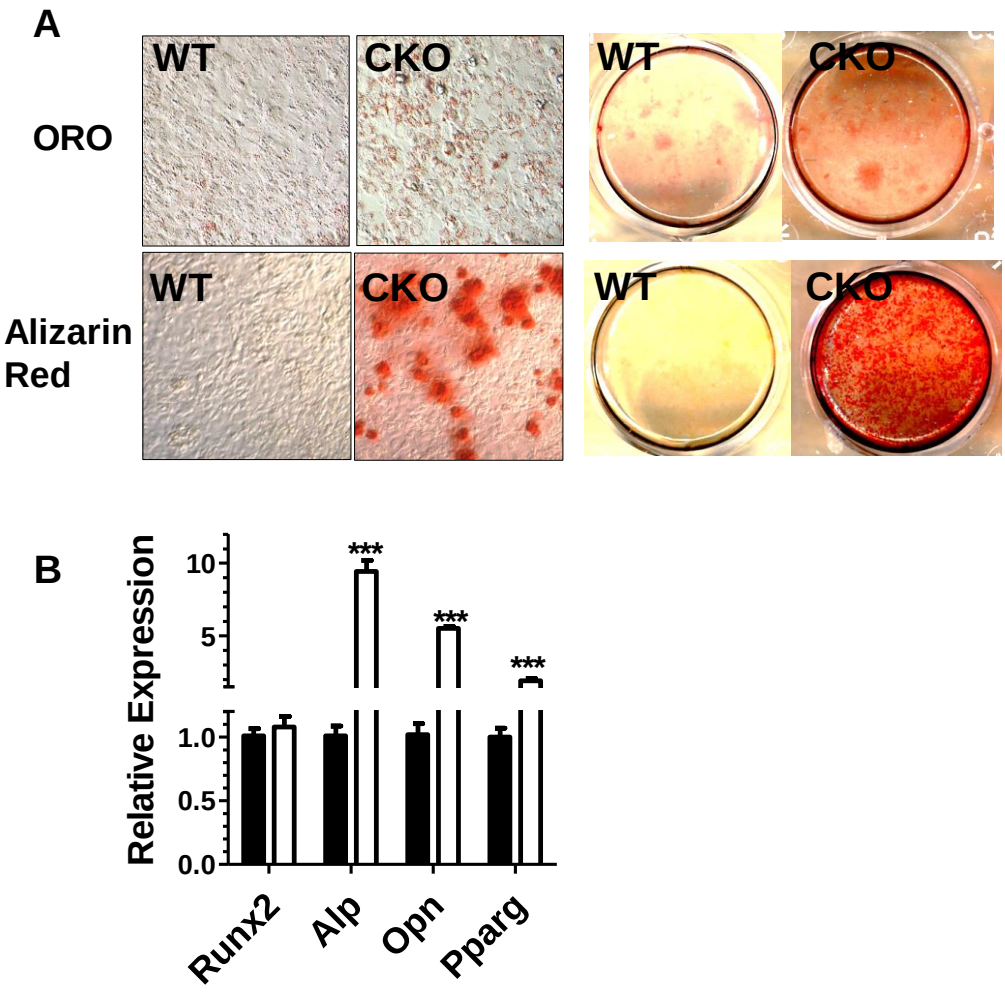

Figure 23. Complete loss of *Rdh10* increased osteoblast differentiation and increased adipocyte formation in osteoblast in vitro culture.

Black bar= WT. White bar=CKO

(A)Oil red O and alizarin red stain of Rdh10 CRISPR KO immortalized MEFs. n=3
(B)Expression of osteoblast and adipocyte marker genes in dd14 osteoblast culture (Rdh10 CRISPOR KO immortalized MEFs) n=3. More osteoblast differentiation in CKO MEFs, not consistent with HYPO result. The only consistency is increased oil red o and increased PPARg, meaning increased adipocyte formation in osteoblast culture.

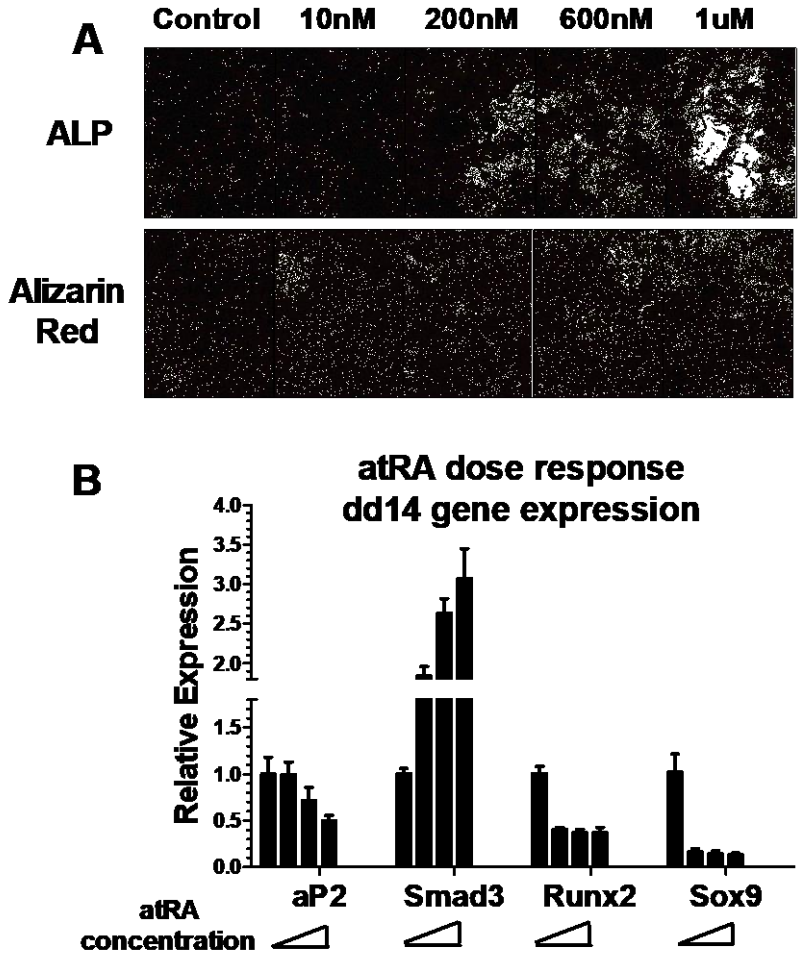

Figure 24. Retinoic acid dose response curve (osteoblast differentiation)

WT MEFs treated with osteoblast induction medium and atRA during the entire process (refreshed every 24hours). A. top: alkaline phosphate activity staining on dd7 ; bottom alizarin red staining for calcium on dd21. B. Expression of osteoblast and adipocyte markers on dd14. There is a clear trend that atRA inhibits osteoblast differentiation if treated throughout the entire differentiation process.

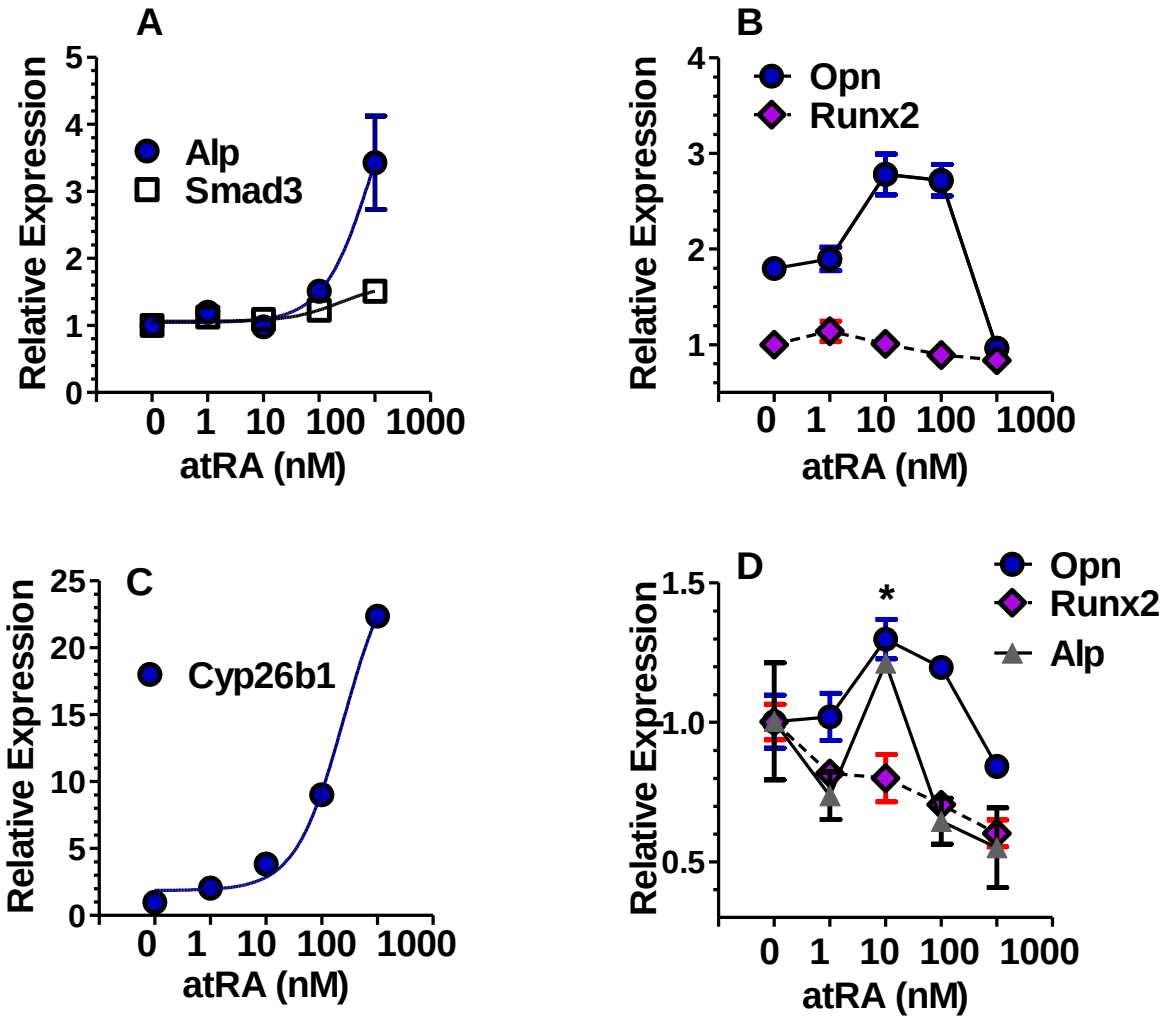

Figure 25. Retinoic acid dose response curve (osteoblast differentiation) when atRA were only added during early differentiation.

(A-C)WT MEFs treated with osteoblast induction medium and atRA during the early differentiation period (from dd0 to dd4), cells collected on dd4 for gene expression. It seems Alp (Alkaline phosphate gene) and Smad3 expression goes up with atRA concentration. Opn expression goes up when treated with low RA dose (10nM and 100nM) but inhibited by high RA (1uM). Runx2 level doesn't change much. (D)WT MEFs treated with osteoblast induction medium and atRA during the early differentiation period (from dd0 to dd4), cells collected on dd14 for gene expression. This experiment atRA only exist during early commitment stage (dd0 to dd4), then from dd5-dd14, no RA in the medium. It seems low dose of RA (10nM) would promote osteoblast formation but high does inhibit the differentiation.

Discussion

One of the advantages of this study is that primary cells were used instead of established cell lines. The primary cells isolated from adult tissues have privilege over established cell lines for biological research, as they mimic in vivo condition better than the cell lines, even though they are more difficult to obtain. Established cell lines, such as 3T3L1, 10T1/2 cells are widely used to study adipogenesis. However, these cell lines are immortalized and passaged in vitro for many years. The chances for mutations and DNA damage are quite high. This causes problems in biological research. For example, some results obtained from established cell lines cannot be repeated in in vivo models. To avoid this problem, primary mouse embryonic fibroblasts (MEF) was used as major in vitro model for this study. MEF are similar but not identical to MSC, in that MEFs share some common cell surface markers as MSC, can differentiate into different cell types in vitro like the MSC, but are easier to obtain and have higher growth rate in culture (Saeed et al., 2012). The primary model used in this study is Rdh10 HYPO MEF. This is a single nucleotide mutation at the substrate binding pocket. In other words, the mutated Rdh10 has lower substrate affinity thus lower enzymatic activity. Even though the enzymatic activity of Rdh10 was altered, protein structure and expression levels were not changed. The advantage of this model over the knockouts is that it focuses on studying the ability of Rdh10 to generate atRA, but not the other potential function that Rdh10 may have.

After adipogenesis induction, atRA biosynthesis is decreased by more than 50%. The net atRA amount in the cells is regulated by the atRA synthesis as well as degradation enzymes. Among the Rdh, Rdh10 is the most highly expressed in MEF. Expression of Rdh10 is ~20-fold higher than Dhrs9, while RdhE2 and Rdh1 were not detected in MEF. More importantly, Rdh10 expression goes down during differentiation and tracks with the decrease in atRA. Among the Raldh, Raldh1 is the most highly expressed but it was reported in another study I did (see chapter 3) that the effect of Raldh1 on adipogenesis is independent of retinoid action. The expression of both Raldh2 and Raldh3 doesn't change much during differentiation. On the other hand, expression of Dhrs3, a retinal reductase, goes up during adipogenesis. So it's likely that upon adipogenic induction, Rdh10 and Dhrs3 collaborate to decrease cellular atRA to initiate the process. As the amount of atRA present in the cell potentially serve as cell fate signals. We hypothesize that high level of atRA help to maintain cells at multipotent stage, and/or inhibit adipogenic differentiation. Work done by the Noy group supported this hypothesis in that they reported atRA induced Pref-1 expression in pre-adipocytes to inhibit adipogenesis (Berry et al., 2012). atRA serves as 'gate-keeper' for cell fate determination. In other words, to trigger differentiation, atRA generating enzymes, or primarily Rdh10, need to be down-regulated so that cellular atRA decreases and alleviates the inhibitory effect of atRA on adipogenesis. The fact that Rdh10 mutant MEF has increased adipogenesis over WT, also supports the hypothesis that atRA levels need to be lowered before the onset of adipogenesis. Furthermore, dosing cells

with atRA or more specifically TTNPB, a pan RAR agonist, showed that atRA generated by Rdh10 binds to RARs to inhibit adipogenesis.Rdh10. However, since RAR binds to more than 500 genes, it is likely that the increased adipogenesis in Rdh10 mutant MEF is a cumulative effect of changes of several genes, not one single gene. This hypothesis can be further tested with RNAseq or microarray.

The effect of Rdh10 on osteoblast differentiation is more complicated than adipogenesis. Results from previous studies were inconclusive, even some studies showed opposite results against each other. This situation could be caused by the dose of atRA used, the cell culture model, and the stage of differentiation when atRA was introduced. In this study, I used a model with a modest decrease of Rdh10 activity as well as a Rdh10 total knockout model to study the effect on osteoblast differentiation. It seems that a model with a moderate decrease of atRA has decreased osteoblast differentiation, and yet a model with an almost total decrease of atRA faced increased osteoblast differentiation. Also results from the atRA dosing experiment also showed that even with 200nM atRA, if treated throughout the entire differentiation, atRA completely abolishes osteoblast differentiation. However, if only treated from dd0 to dd4, and collected on dd4, atRA seems to stimulate the expression of alkaline phosphate. So it is likely that during early osteoblast commitment, atRA is needed to stimulate osteoblast early gene, however, during the maturation stage, atRA is no longer needed and excess atRA can inhibit maturation and keep cells at a pre-osteoblast stage. The fact that Rdh10 CKO and Rdh10mut MEF have different phenotypes could be explained by ‘hormesis’, a ‘U’ shaped dose response curve. The hormesis effect of vitamins and minerals has been previously discussed, and it was proposed that it could be a result of hermetic stress response (Hayes, 2008). If this hypothesis is true, it’s likely that very low atRA or normal atRA level would facilitate osteoblast differentiation, while atRA deficiency inhibits osteoblast differentiation.

Chapter 2. Rdh10 dependent retinoids metabolism affects progression of metabolic diseases in rodents.

Introduction

Obesity is a growing problem in modern society, especially in western countries where ~33% of adults are obese and ~67% of adults are overweight (Korner and Aronne, 2003). Two major types of adipose tissue exist in the human body, namely white and brown adipose. White adipocytes, as the major TAG storage site, are large, lipid laden cells that contain only one huge lipid droplet. Brown adipose tissue (BAT), however, is considered 'good fat', as BAT mainly functions as a site for energy expenditure. BAT contains multiple small lipid droplets and is rich in mitochondria: it is an important organ involved in non-shivering thermogenesis. Obesity is caused by the expansion of white adipose tissue, mainly the result of hypertrophy or hyperplasia. It is becoming more and more accepted that instead of being an inert fat storage site, white adipose is an endocrine organ that secretes a variety of hormones and cytokines that affect whole body metabolism, such as leptin, adiponectin and inflammatory cytokines (TNFα, lL-6, IL-8 etc) (Trayhurn and Wood, 2004). In other words, dysfunction of white adipose tissue could lead to metabolic disorders, such as diabetes and liver steatosis. Retinoids and their generating enzymes contribute to the development and metabolic regulation in adipose tissue, such as adipocyte differentiation, lipogenesis, adaptive thermogenesis, lipolysis and fatty acid oxidation (Bonet et al., 2012a). Several studies show that genetic manipulation of retinoid-metabolizing enzymes alters adiposity in mice. For example, although Rdh1 and Raldh1 both contribute to adipose function, knocking down Rdh1 or Raldh1 leads to opposite phenotypes (Zhang et al., 2007a; Ziouzenkova et al., 2007a). The contradictory results from different studies that describe the role of all-*trans*-retinoic acid (atRA) in adipogenesis and adipose function indicate the need for further research in this area.

White adipose tissue (WAT) is a multiple depot organ. The function and characteristics of the adipocytes are depot specific. Mouse WAT includes several subcutaneous and visceral depots. Mouse visceral depots are named depending on their location, the fat depot surrounding the reproductive system is named epididymal fat in males, parameterial fat in females; the depot surround the kidney is named perirenal fat and the depot along the intestine is named mesenteric fat Johnson and Hirsch, 1972). The inguinal subcutaneous adipose depot is the major subcutaneous depots that's found right beneath the skin and surrounds the legs. Subcutaneous WAT contains both white adipocytes and beige adipocytes. Upon stimulation, such as cold or epinephrine treatment, beige adipocytes take on the morphology of brown adipocytes and become capable of heat generation (Harms and Seale, 2013). Compared to subcutaneous WAT, expansion of visceral WAT is more directly correlated with diabetes, cardiovascular disorders and metabolic disorders (Bergman et al., 2006; Björntorp, 1990). HFD feeding increases WAT expansion, both by hyperplasia and

hypertrophy. During hypertrophy, more pre-adipocytes are recruited and undergo terminal differentiation into adipocytes. Hyperplasia, on the other hand, is the enlargement of existing adipocyte cell sizes. One or both of these processes trigger angiogenesis to provide oxygen to the expanded tissue (Cao, 2007). However, when the adipose expansion rate exceeds the angiogenesis rate, hypoxia cold occur and lead to dysfunction of existing adipocytes (Lawler et al., 2016; Trayhurn, 2013). Hypoxia could cause a series of adverse effects, such as inflammatory response, oxidative stress, inhibition of adiponectin expression (Andrei et al., 2017). When macrophages are recruited to adipose tissue, they cause adipocyte apoptosis and lead to adipose tissue dysfunction. Persistent inflammation in adipose tissue also causes fibrosis and tissue damage (Lawler et al., 2016). Dysfunctional adipocytes show an increased free fatty acid (FFA) secretion rate, so that more FFA gets secreted into circulation and stored elsewhere. This process is called ectopic fat deposition.

Ectopic fat deposition describes the condition of excess fat being stored in tissues such as liver, muscle and pancreas. This is one of the primary causes of metabolic syndrome (Cali and Caprio, 2009). Metabolic syndrome is a general term that includes multiple metabolic diseases, such as insulin resistance, diabetes, dyslipidemia, elevated blood pressure, hyperglycemia (Alberti et al., 2005). It is one of the major causes for diseases such as cardiovascular disease and non-alcoholic fatty liver diseases. Non-alcoholic fatty liver diseases (NAFLD) are defined as excess TAG stored in the liver. Dysregulation of one or several pathways could explain the cause of NAFLD. FFA from adipose could get into the liver via portal vein and get esterified and stored in the liver as TAG. Liver fatty acid oxidation, VLDL incorporation, and LDL secretion could affect liver fat storage (Auguet et al., 2014). atRA dosing in mice increases liver fatty acid oxidation, thus preventing NAFLD (Amengual et al., 2010). However, studies on atRA effects on metabolic disorders such as NAFLD are still at an early stage and more research is needed for its final application to therapeutic purposes.

Material and Methods

Animal maintaince. Rdh10 floxed mice with loxP-flanked exon 2 were obtained from UC Davis Mouse Biology Program (backcrossed to C57>10 times) were crossed with mice expressing CMV Cre (obtained from Jackson lab, B6.C-Tg(CMV-cre)1Cgn/J, stock number 006054) . Mice were fed an AIN93G diet containing 4 IU/g vitamin A with 9% fat or the same diet with 50% fat (HFD). Bodyweight and food weight was measured on the same day every week until euthanasia. Body composition measurements were performed with an EchoMRI-100V whole body magnetic resonance analyzer. All animal experiments were performed in accordance with the National Institutes of Health's Guide for the Care and Use of Laboratory Animals, and all protocols were approved by University of California, Berkeley Animal Care and Use Committee.

Energy expenditure and activity. A Columbus Instruments Comprehensive Lab Animal Monitoring System (CLAMS) was used to measure energy expenditure (O^2 consumption and CO^2 production) and physical activity of individual mice.

GTT/ITT. Mice were fasted 16 hr before GTT and 4 hr before ITT. Mice were then placed in individual cages without food or water. Either glucose (1.5 g/kg body weight) or insulin (0.5 IU/kg body weight) was injected (time 0). Glucose in blood from tail tips was measured with a glucometer.

Tissue Collection. Four-month-old mice were fasted 16 hr and anesthetized with isoflourane. Liver and WAT was collected, placed into embedding cassettes, and stored in 10% neutral-buffered formalin at 4°C overnight. Additional liver tissue was embedded in Tisue-Tek® O.C.T Compound (#4583) in cryomolds, snap-frozen in liquid nitrogen and stored at -80°C. For gene expression and other analyses, tissues were snap-frozen in liquid nitrogen, and stored at -80°C.

atRA quantification. 100 mg liver or adipose tissue was used for atRA extraction. atRA in tissues was quantified by LC/MS/MS as described (Kane et al., 2005, 2008a).

Serum measurements. Whole blood was centrifuged 15 min at 3000 x g at 4°C to separate serum. Serum was stored at -80° C and sent to the UC-Davis metabolic core for quantification of insulin and leptin. Serum NEFA was quantified with an EnzyChrom Free Fatty Acid Assay Kit (EFFA-100).

TAG assay. Measurements were made in homogenized livers using a Triglyceride Colorimetric Assay Kit (Cayman Chemical Company #10010303). Values were normalized to liver wet weight.

RNA isolation (adipose and liver). Liver and adipose tissue were harvested in 1 ml TRI reagent (#T9424, Sigma-Aldrich). Liver and adipose RNA was extracted with RNeasy Fibrous Tissue Mini Kit following supplier protocol (#74704, Qiagen).

Gene Expression. One µg total RNA was used for reverse transcription (Iscript 170-8891 BioRad). RT-qPCR was performed with a Bio-RAD CFX Connect Real-Time Detection System. Gene expression was normalized to the geometric means of *Gusb* and *Tbp*. qPCR Primers were from Life Technologies or Integrated DNA technologies. *Acadm* (Mm01323360_g1), *Aldh1a1* (Mm00657317_m1), *Aldh1a2* (Mm00501306_m1), *Aldh1a3* (Mm00474049_m1), *Cpt1b* (Mm00487191_g1), *Cyp26A1* (Mm00514486_m1), *Cyp26B1* (Mm00558507_m1), *Dhrs3* (Mm00488080_m1), *Dhrs9* (Mm00615706_m1), *Fabp4* (Mm00445878_m1), *Fabp5* (Mm00783731_s1), *Gusb* (Mm01197698_m1), *Hif1a* (Mm01198376_m1), *Hmgcs2* (Mm00550050_m1), *Hnf4a* (Mm00433959_m1), *Ppara* (Mm00440939_m1), *Pparg* (Mm00440940_m1), *Rarb* (Mm01319677_m1), *RdhE2* (Mm00725380_m1), *Rdh1* (Mm00650636_m1), *Rdh10* (Mm00467150_m1), *Saa1*

(Mm00656927_g1), *Tbp* (Mm01277042_m1), *Saa3* (Mm00441203_m1), *Tnfa* (Mm00443258_m1), *Zfp423* (Mm00677660_m1). *Pparg2* (Mm.PT.58.12797903)

Bone marrow extraction and RNA isolation. Marrow cells were prepared as described with modification based on a protocol published by Kelly NH et.al (Kelly et al., 2014). Both femurs were collected from mice as soon as the mice were euthanized. Make sure to clean up the bone and no muscle was left before place the bone in the centrifuge. Then cut one end of the bone to expose the marrow. Place the bone into a 0.2 ml tube with a small hole at the bottom so the bone marrow can flow through but the bone will still stay in the tube after centrifuge. Place the 0.2 ml tube into a 1.5 ml tube (collection tube). Place the whole thing on a centrifuge and spin at 13,000 x rpm, 5 min, 4 °C. After centrifuging, the bone marrow will be at the bottom of the collection tube. Flash freeze with liquid nitrogen and store at -80°C. RNA from bone marrow was extracted using Zymo Research Direct-zol™ RNA MiniPrep kit following instructions provided by the kit.

Paraffin embedding.

Bone: Excised femur were individually transferred to WheatonTM 20 mL PET Liquid Scintillation Vials and fixed using strong Bouin's solution for 24 hr on a rotating plate at 4°C with the ratio of solution to bone at a minimum of 50:1. The bones were rinsed with 20% EtOH two times for 1 hr each, then decalcified in 10% EDTA solution on rotating plate at 4°C with daily solution changes with fresh EDTA solution for one week. Femur bones were then cut at center of diaphysis into proximal and distal halves, using an industrial razor blade, and inserted into two separate vials. Graded series of 20%, 50%, 70%, 95%, 100% EtOH were used to dehydrate the halved bones for 4 hr minimum in each step on the rotating plate at RT. Graded series of xylene (Fischer Scientific L.L.C.) were used to replace ⅓, ½, and ⅔ of the 100% EtOH for 4 hr minimum in each step until bones were suspended in mostly xylene with vial cap on at RT under the fume hood. Pellets of FisherfinestTM Histoplast Paraffin Wax were added to mostly xylene solution to the point of saturation. Graded series of molten paraffin were used to replace ⅓, ½, and ⅔ of the xylene/paraffin-pellet solution for 4 hr minimum in each step until bones were suspended in mostly molten paraffin with cap on at 58°C. Vials containing mostly of molten paraffin solution were left in oven with cap off to evaporate xylene residues. Vial solutions were replaced with fresh molten paraffin solutions daily for five additional days. Each vial containing molten paraffin and halved femur bone was then transferred to aluminium dish (Agar Scientific Ltd.) to be embedded in frontal (coronal) plane at RT overnight. Strong Bouin's solutions were made from 25 mL formalin, 75 mL picric acid (1.3%), and 5 mL glacial acetic acid. 10% EDTA solutions were made with EDTA disodium salt (Fisher Scientific, MW 372.24) and DIH2O with the pH adjusted to 7.2-7.4 using 10 N NaOH. EtOH (VWR® 200 Proof) was diluted with DIH_2O to make various concentrations EtOH solutions. All solutions were prepared the day before tissue collection. Embedded distal and proximal femur bone in solidified paraffin was liberated from the aluminium dish. For this research, only distal femurs were sectioned longitudinally at 10 μm at frontal (coronal) plane using the Leica RM2255 Motorized

Microtome, using disposable Leica 818 Microtome Blade. No further experiments were conducted on the proximal femur bones. The first 50 sections after cutting into the bone were discarded. The next 100 sections were collected by capturing the ribbons onto Premiere® Charged Microscope slides using water bath at 40-42°C. The rest of the paraffin block and sections were discarded. Captured section on slides were left in a 58°C oven overnight to evaporate water residues.

White adipose and liver: Tissues collected from mice were fixed with 10% neutral buffered formalin for a week. The fixed tissues were dehydrated with graded series of ethanol, 70%, 80%, 95% and 100%, 1.5 hr each. Then the dehydrated tissues were incubated in 3 changes of 100% xylenes, 2 hr each. After that, the tissues were transferred into 58°C melted paraffin for two hr, then another change of fresh melted paraffin and incubated overnight.

Oil red O staining for liver. Fresh tissue embedded in OCT in cryostat molds and snap-frozen in liquid nitrogen were sectioned at 12 µm using a Leica cryotome. Ribbons of 3-5 sections were placed on charged slides and allowed to fix to the slides for 10 min at RT before storing in -20°C overnight. Frozen slides were allowed to equilibrate at RT for 10 min. Slides were fixed by submersion in ice-cold 10% neutral-buffered formalin for 10 min. Slides were submerged in Oil Red O (Sigma-Aldrich®) for 5 min. Slides were counterstained in Harris Modified Hematoxylin solution (Sigma-Aldrich®) for 15 sec and rinsed in running tap water for 10 min. Sections were applied with aqueous mounting medium (Shurmount®) then covered with FisherbrandTM Superslip Cover Slips and left under the fume hood to set overnight at RT. Slides were imaged within 24 hr to avoid interference from ORO precipitation.

H and E staining- Formalin-fixed, paraffin-embedded tissue (FFPET) were sectioned at 8 µm using a Leica microtome. Ribbons of 3-5 sections were placed on charged slides and allowed to dry overnight. Sectioned slides were de-paraffinized two times with xylene for 10 min each and then hydrated in 100% EtOH, 95% EtOH, 80% EtOH, 70% EtOH in a graded series for 2 min in each step. Slides were stained in Harris Modified Hematoxylin solution (Sigma-Aldrich®) for 10 min and then rinsed in running tap water for 10 min. Slides were dehydrated in 30% EtOH, 50% EtOH, 80% EtOH, 95% EtOH in a graded series for 2 min in each step. Slides were stained in Eosin Y solution (Fischer Scientific L.L.C.) for 1 min and transferred to 100% EtOH for 10 sec. Slides were then submerged in a 1:1 solution of xylene/100% EtOH for 1 min and then in 2 rounds of xylene for 5 min each. Sections were applied with Fisher Chemical™ Permount™ then covered with Fisherbrand™ Superslip Cover Slips and left under the fume hood to set overnight at RT.

Immunohistochemistry staining. Fresh tissues embedded in OCT in cryostat molds and snap-frozen in liquid nitrogen were sectioned at 12 µm using a Leica cryotome. Ribbons of 3-5 sections were placed on charged slides and allowed to fix to the slides for 10 min at RT before storing in -20 °C overnight. The following procedure was

adapted from Santa Cruz Biotechnology, Inc. Frozen slides were allowed to equilibrate at RT for 10 min. Slides were fixed by submersion in ice-cold acetone for 10 min. Endogenous peroxidase was blocked by incubating slides in 0.3% H_2O_2 diluted in water for 30 min at RT. Slides were incubated with F4/80 antibody according to protocol (Immunocruz® ABC Staining System). Slides were counterstained in Harris Modified Hematoxylin solution (Sigma-Aldrich®) for 15 seconds and rinsed in running tap water for 10 min. Slides were dehydrated in 30% EtOH, 50% EtOH, 80% EtOH, 95% EtOH, 100% EtOH in a graded series for 2 min in each step. Slides were then submerged in a 1:1 solution of xylene/100% EtOH for 1 min and then in 2 rounds of xylene for 5 min each. Sections were applied with Fisher Chemical™ Permount™ then covered with Fisherbrand™ Superslip Cover Slips and were left under the fume hood to set overnight at RT. Experiments performed according to manufactural protocol (Immunocruz® ABC Staining System, #sc-2019)

Western blot-Fresh liver tissue was collected and snap-frozen in liquid nitrogen. For each sample, 5 mg of liver tissue were used. Total proteins were extracted from whole liver tissue using RIPA buffer (Pierce® Thermo-Scientific®) with proteinase inhibitor (Sigma-Aldrich®) and a tissue lyser set to 20Hz for 30 sec. A tissue sonifier was used for 3 rounds to break up any remaining genomic DNA. Samples were centrifuged at 12000 RPM for 20 min at 4°C and the resulting supernatant was collected. Protein concentration was determined using a Peirce Assay. Samples were diluted in RIPA to a final concentration of 10ug of protein and suspended in Laemmli (BioRad®) sample buffer for SDS-PAGE. Proteins were separated by electrophoresis on a 12% Criterion gel (BioRad®) and trans-blotted onto a nitrocellulose membrane (BioRad®). The membrane was probed with rabbit-anti-mouse MCAD primary antibody after blocking in Odyssey Blocking Buffer in PBS. IgG-HRP conjugated goat-anti-rabbit secondary antibody was applied and immunoreactive bands were visualized by LiCor Odyssey Imager. Signal intensity was quantified using ImageStudioLite software using a β-actin probe as control.

Microscopy. Slides were placed on the mechanical stage of the Zeiss AxioImager M1 and orientated so that the images were acquired using Qimaging iClick/MicroPublisher Color program at 5x, 20x, and 60x magnification objective lens.

atRA dosing. Five mg 90-day-slow-release atRA pellets or placebo (Innovative Research of America) were implanted on the lateral side of the neck between the ear and the shoulder following the manufacturer instructions when mice reached 6 weeks old.

Statistical analyses. Data are expressed as means ± SD, unless noted otherwise. Statistical significance was determined by two-tailed, unpaired student t tests for comparison of two groups or two-way ANOVA for comparison of two variables.

Results

Rdh10$^{+/-}$ mice suffer diet induced obesity and insulin resistance.

To study the function of Rdh10 *in vivo*, we generated transgenic mouse model (C57BL/6 background). Mice carrying loxp sites flanking exon two in *Rdh10* were crossed with mice carrying CMV Cre to generate total body *Rdh10* knockout. Homozygots were not viable thus heterozygots were used in the following studies. *Rdh10* expression was decreased in several endocrine organs, including liver, iWAT and eWAT. (Fig. 26A). atRA level was decreased in *Rdh10* heterozygous knockout (Rdh10$^{+/-}$) liver, iWAT and eWAT in both male and females measured by LC/MS/MS. Around 10-20% decrease of atRA in adipose tissue in *Rdh10*$^{+/-}$, and ~30% decrease in liver was detected (Fig. 26B). Fig. 27A shows representative images of both WT and *Rdh10*$^{+/-}$ male and female mice at 4 months of age fed AIN 4IU diet containing 50% fat. Male *Rdh10*$^{+/-}$ mice fed HFD were ~6 g heavier compared to their WT littermates, while female *Rdh10*$^{+/-}$ mice fed HFD were ~4 g heavier compared to WT at 4 month old (Fig. 27B). The increase of total body weight was primarily caused by the increase of fat pad weight, as evident by the echo MRI data in Fig. 27C. There was no significant difference of lean weight between both genotypes (less than 1 g difference) but there was significant difference in fat mass in both male and females. To test whether the increase of body weight was a result of increased food intake, we measured the amount of food taken each day, but there was no significant difference in average food intake between *Rdh10*$^{+/-}$ and the WT (Fig.27D). To determine whether altered bodyweight and fat weight would alter glucose metabolism, we preformed glucose intolerance and insulin intolerance tests with males fed a HFD. HFD-fed *Rdh10*$^{+/-}$ mice demonstrated impaired glucose tolerance and insulin resistance compared to WT littermates (Fig. 28A and 28B). Serum insulin was also increased in *Rdh10*$^{+/-}$ (Fig. 28C), which was caused by compensation from pancreas to compensate for the decreased systemic insulin sensitivity or by reduced hepatic insulin clearance as a result of insulin resistance in liver. An increase of serum leptin and NEFA also supports the fact that the *Rdh10*$^{+/-}$ has increased fat mass compared to WT (Fig. 28D and 28E). No difference was detected in serum b-hydroxybutarate, adiponectin and glucagon (Fig 29A-C).

Rdh10$^{+/-}$ mice showed no difference in energy expenditure nor activity.

Four-month-old males were placed in metabolic chambers with food and water following manufacture instructions. Mice were acclimated in the chamber for 24 hr before the start of data collection. Data was recorded every 15 min for 24 hr total. VO_2 (oxygen consumption) and VCO_2 (carbon dioxide production) are indicators for energy expenditure, yet no difference was detected in either between genotypes (Fig. 30A and 30B). The respiratory exchange ratio (RER) suggests fuel source. A RER < 0.7 indicates that fat is the predominant fuel source and a RER >1.0 indicates that carbohydrates are the predominant fuel source. Here the RER for both WT and Rdh10$^{+/-}$ mice is ~0.78, suggesting that those mice utilize a mixture of both fat and carbohydrates (Fig.30C). X TOT, Y TOT and Z TOT are indicators for activity. During the light cycle, when mice were less active, no difference was detected between genotypes. During the

dark cycle, when mice are active, *Rdh10*$^{+/-}$ mice seems to be less active compared to the WT mice, as evident by lower X, Y and Z TOT counts. However, the difference was not significant when calculated by two tailed student t test (Fig.30 D to F). Since no difference was detected under fed condition, next question was whether those mice respond differently to fasting. A different group of mice was placed into the chambers with water only for 16 hr. No difference was detected between genotypes in terms of energy expenditure, RER nor activity (Fig.31 A to F). It is worth noting that the RER for the fasting group was ~0.7, meaning that fat was the predominant fuel source during fasting. The *Rdh10*$^{+/-}$ has less Z TOT counts compared to WT, but not statistically significant.

Rdh10$^{+/-}$ mice has increased fat pad and adipocyte cell size.

As previous data suggested, the increase of body weight was primarily caused by fat depot expansion, next step requires a more thorough study into the fat depots. Fig. 32 shows representative images of three white adipose depots, epididymal white adipose (eWAT), inguinal white adipose (iWAT) and perirenal adipose tissue (pWAT). Histological examination of eWAT and iWAT showed an increased number of larger adipocytes in *Rdh10*$^{+/-}$, as well as an increase in average cell size (Fig. 33 A-F). *Rdh10*+/- mice have higher white adipose depot weight compared to WT mice (Fig.34A). Average weight for WT eWAT was ~1.4 g, while *Rdh10*+/- eWAT was ~1.85 g. iWAT weight was ~0.7 g and 1.0 g for WT and *Rdh10*$^{+/-}$, respectively. However, no significant difference was detected in BAT weight. Total cell number was calculated based on cell size as measured in Figure 33 and weights from Figure 34, using the equation: m=v*p*n (p, density, 0.915g/ml) $V = 4/3pr^3$. The *Rdh10*$^{+/-}$ mice seem to have ~5% fewer cells compared to WT, but not significantly different. So both WT and *Rdh10*$^{+/-}$, mice have roughly same cell number in both eWAT and iWAT depot. The *Rdh10*$^{+/-}$, mice have bigger and heavier white adipose depot because they have larger adipocytes, not increased cell number. Figure 34C shows fat pat weight gain during development. From 8-14 weeks, *Rdh10*$^{+/-}$ mice gained significantly more fat compared to WT mice. During week 8-10, *Rdh10*$^{+/-}$, gained 2 g of fat while WT gained ~1 g of fat. However, during week 12-14, *Rdh10*$^{+/-}$ gained only slightly more fat compared to WT. These data suggest that the difference between fat pads could very possibly be determined during early age, or right after puberty. The differences could potentially become smaller when mice age. The over expansion of adipose tissue of *Rdh10*$^{+/-}$ caused adipose hypoxia and inflammation, which was supported by a decrease of good adipocyte markers *Pparg* and *Adiponectin*, and an increase of hypoxia induced genes *Hif1a* and inflammatory markers such as *Saa3* and *Tnfa* (Fig.35). Both hypoxia and inflammation led to white adipose dysfunction, thus the ability of white adipose tissue to store fat is decreased, leading to increased FFA release into the circulation system (Fig.28E).

Loss of _Rdh10_ in bone marrow increases bone marrow adipocyte.

Bone marrow stem cells (BMSC) can give rise to both osteoblasts and adipocytes. Because it has been reported that MEF are similar to BMSC (Saeed et al., 2012), it is

worth investigating whether loss of Rdh10 could cause an increase of bone marrow adipocytes.

Femurs of *Rdh10*$^{+/-}$ males fed a HFD showed a slight increase in adipocyte formation near the growth plate area, although not statistically significant (Fig.36 A and B). This is also supported by a slight increase of adipocyte and osteoblast marker gene expression in bone marrow, yet none of these has statistical significance (Fig.37A and B). Because females are more prone to develop osteoporosis, which includes bone marrow fat accumulation, we assayed femurs collected from females fed a HFD. Here we noticed a 3-fold increase in bone marrow adipocyte numbers (Fig.38A and B). This is also supported by the 2-3 fold increase of adipocyte marker genes in the bone marrow (Fig.39A). It's also worth mentioning that the expression of osteoblast markers also was significantly up regulated in female bone marrow (Fig.39B). Even more interestingly, females fed a LFD also demonstrated a 3-fold increase in bone marrow adipocytes, even when there was no difference in body weight (Fig.38D and E). *Rdh10*$^{+/-}$ females have longer femurs compared to WT (Fig.38C), while there was no significant difference in bone length in males (Fig.36C). WT females fed HFD showed two fold increase of adipocyte number compared WT females fed LFD. What's more interesting is that WT females fed HFD had around 2 fold more adipocytes compared to WT males fed HFD. These data also demonstrated the diet/sex effect on the bone marrow adipocyte formation.

***Rdh10*+/- males on HFD are prone to developing liver steatosis.**

As a core endocrine organ, liver of both males and females fed HFD was also studied. *Rdh10*$^{+/-}$ males fed HFD showed increased fat accumulation in liver, as illustrated by H and E and oil red O staining (Fig. 40B), while no significant difference was found in the expression of inflammation marker F4/80. TAG quantification assay demonstrated that there was ~2-fold increase of TAG in *Rdh10*$^{+/-}$ male liver (Fig.40C). However, livers from females fed a HFD showed a relatively smaller difference between genotypes. According to H and E and oil red O histology images, there was a slight increase of fat droplets in the liver (Fig.41B). However, there was no significant differences when liver TAG was quantified (Fig.41C). Fig.40A and 41A shows representative pictures of liver samples collected from both males and females. *Rdh10*$^{+/-}$ male livers were significantly larger compared to WT liver. Expression of genes related to liver functions such as lipogenesis, fatty acid oxidation was also analyzed (Fig.42). However, no difference was found in most genes except *Acadm*, a gene that encodes the medium-chain acyl-CoA dehydrogenase, an enzyme that functions in fatty acid oxidation. Yet when the Acadm protein (Mcad) was quantified, no difference was found between WT and *Rdh10*$^{+/-}$ (Fig.43 A to 43 D). These data, taken together with the bone phenotype, shed light on the gender differences in terms of metabolic diseases progression, which indicate that sex hormones could possibly interact with retinoids metabolism and affects the phenotype.

Loss of Rdh10 affects pancreatic islet morphology and function.

Pancreas was collected from 4-month-old males fed a HFD after over-night fasting. H and E staining was performed to analyze the morphology of the islets. Figure 44A shows representative pictures of pancreas and islets. On average, Rdh10+/- mice have more small size islets and less large islets compared to WT. Insulin and glucagon remaining in islets was assayed by immune-fluorescence staining. Rdh10+/- islets have less insulin compared to WT, while no difference was detected in glucagon levels (Fig.44 C to E). We showed earlier that Rdh10+/- mice are at least pre-diabetic, with glucose intolerance and insulin resistance. The development of type 2 diabetes involves multiple steps, and eventually β-cell exhaustion and apoptosis. It's likely that the Rdh10+/- mice have started to lose insulin secreting β cells, which is a sign of pre-diabetic stage.

atRA supplementation rescues the phenotype of *Rdh10*$^{+/-}$ mice.

Five mg 90-day-slow-release atRA pellets (from Innovative Research of America) were implanted on the lateral side of the neck between the ear and the shoulder. Placebo was implanted the same way. Two weeks after implantation, body weight was measured each week. As shown on Fig. 45A, total body weight started to differ significantly starting from week 6. By the end of week 9 after pellet implantation, the difference of body weight between the atRA and placebo treated group was ~8 g. EchoMRI data showed the fat pat difference was the main contributor to the differences in body weight (Fig.45B). The lean weight of atRA-treated *Rdh10*$^{+/-}$ mice was slightly higher than KO (no statistically significant), but this could be an indication that atRA suppress fat development while increasing lean mass. atRA pellet treated *Rdh10*$^{+/-}$ mice were also more glucose tolerant and more insulin sensitive compared to those treated with placebo (Fig.46A and B). Fig. 47 showed representative H and E staining images of liver, eWAT and iWAT samples collected from *Rdh10+/-* atRA or placebo treated groups. atRA clearly rescued the liver steatosis phenotype while reducing the size of white depot cell size. These data indicates that atRA supplementation reverses the phenotype of *Rdh10+/-* males fed a HFD, and implies the potential of atRA as a treatment for metabolic disorders.

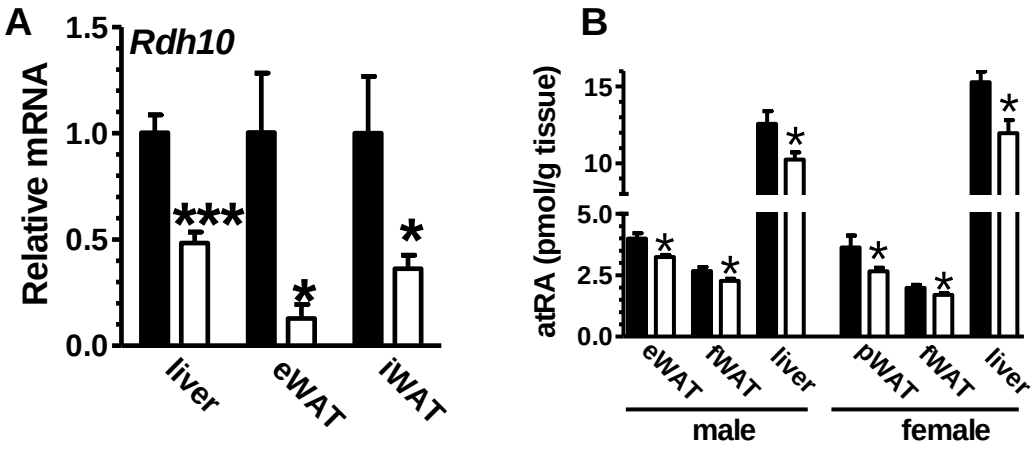

Figure 26. Rdh10$^{+/-}$ mice have decreased tissue atRA.

Mice were 4-month-old males/females fed a HFD, unless stated otherwise.
Black bar: WT; white bar: *Rdh10*$^{+/-}$
(A) *Rdh10* mRNA decreases in liver, eWAT, and iWAT and liver of 4-month-old male *Rdh10*$^{+/-}$ mice: n = 4-7 WT, 3-5 *Rdh10*$^{+/-}$. *p<0.03, ***p=0.008.
(B) Tissue atRA concentrations: n = 7-11 mice/group, *p<0.04.

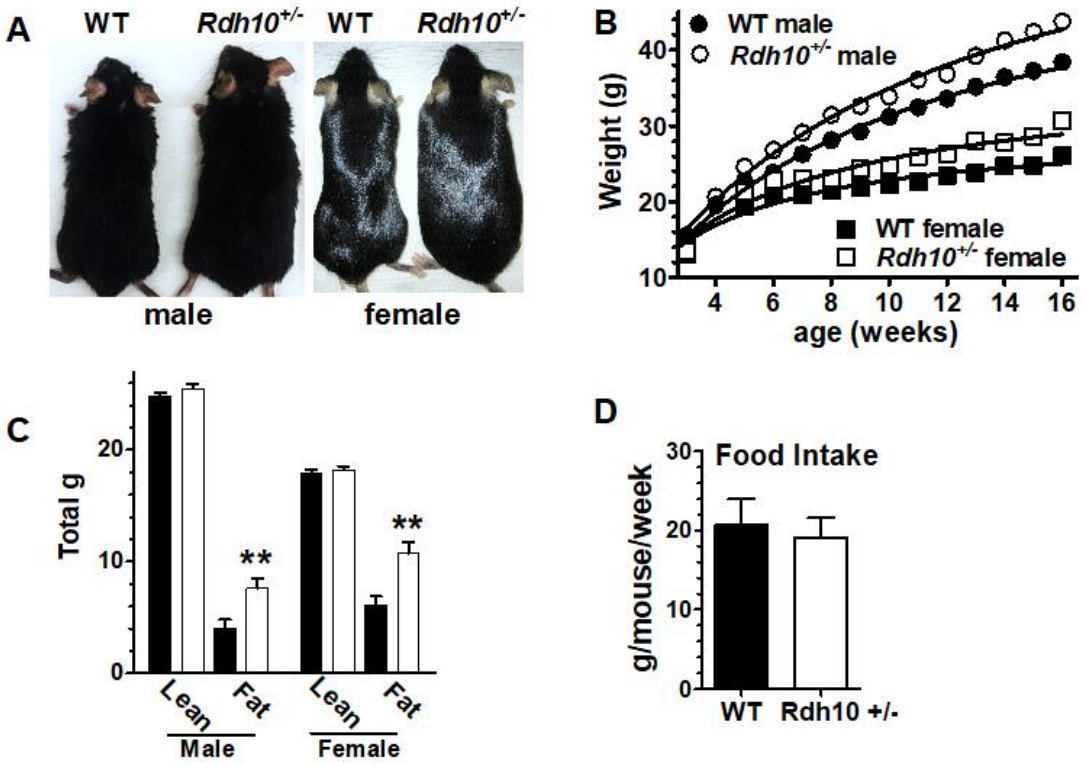

Figure 27. *Rdh10*$^{+/-}$ mice fed a HFD have increased adiposity.

Black bar: WT; white bar: *Rdh10*$^{+/-}$

(A) Representative images of 4-month-old mice fed a HFD.
(B) Body weights of mice fed a HFD. Significant differences with genotype and age by 2-way-ANOVA: males WT n = 30, *Rdh10*$^{+/-}$ n = 33; females WT n = 11, *Rdh10*$^{+/-}$ n = 15; $p<0.0001$ for male and female genotype and age.
(C) Body compositions: **$p<0.009$. Echo MRI of body composition. (Male: n=11 WT, n=12 *Rdh10*$^{+/-}$ Female, 4month old, HFD: n=7 WT, n=10 *Rdh10*$^{+/-}$).
(D) Food intake measurement. Males were fed HFD and separated into single cage for a week. Total food weight was measured at the start and end of the experiment. n=6 WT. n=10 *Rdh10*+/-.

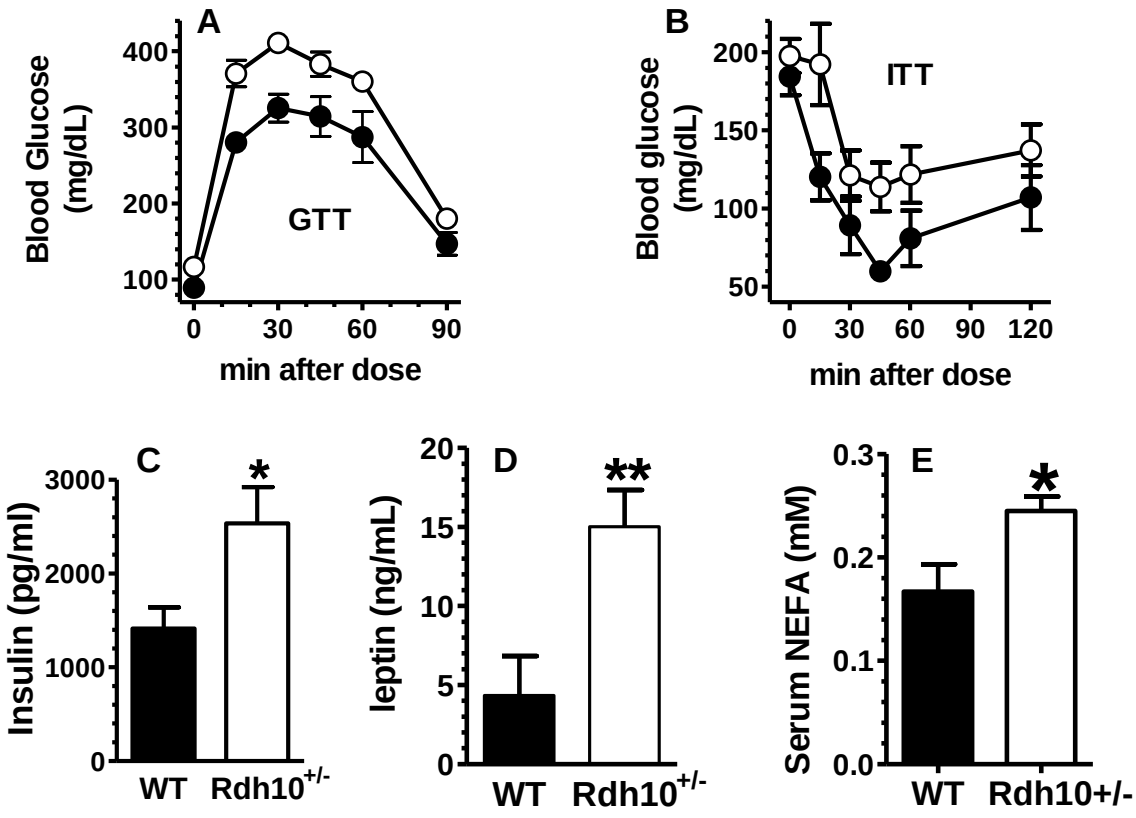

Figure 28. *Rdh10*$^{+/-}$ mice fed a HFD are pro-diabetic.

Black bar: WT; white bar: *Rdh10*$^{+/-}$
(A) Glucose tolerance test: n = 5 WT, 7 *Rdh10*$^{+/-}$. Representative data from three independent experiments. Significant difference for genotype by 2-way ANOVA, p<0.0001.
(B) Insulin tolerance test: n = 6 WT, 10 *Rdh10*$^{+/-}$. Representative data from three independent experiments: Significant difference for genotype by 2-way-ANOVA, p=0.0004.
(C)Serum insulin: n = 3-5 mice/group, *p<0.04.
(D) Serum free fatty acids: n = 5-7 mice/group, *p=0.05.
(E) Serum leptin: n = 5-7 mice/group, **p<0.02.

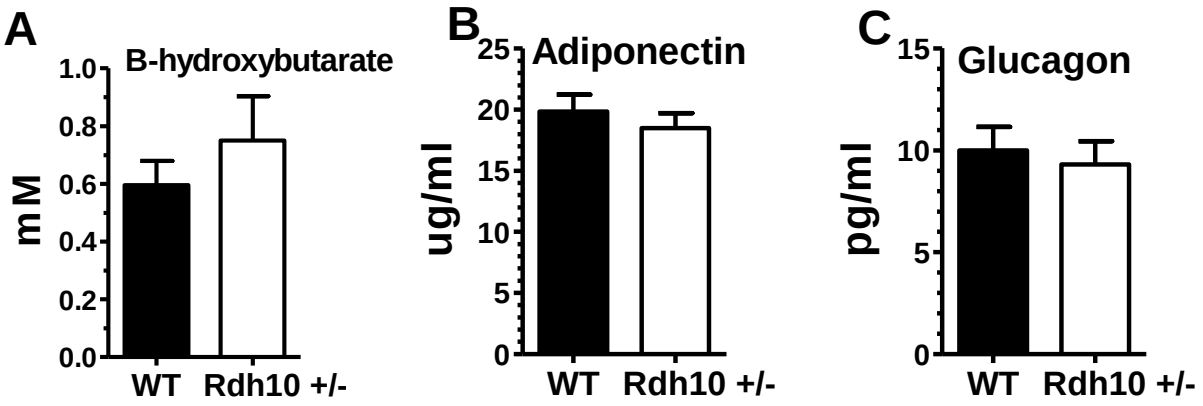

Figure 29. Blood cytokine measurements.

(A-C) Blood cytokines measured from fasted serum. Males, 4month HFD. WT n=5, KO n=3. Representative data from two independent groups.

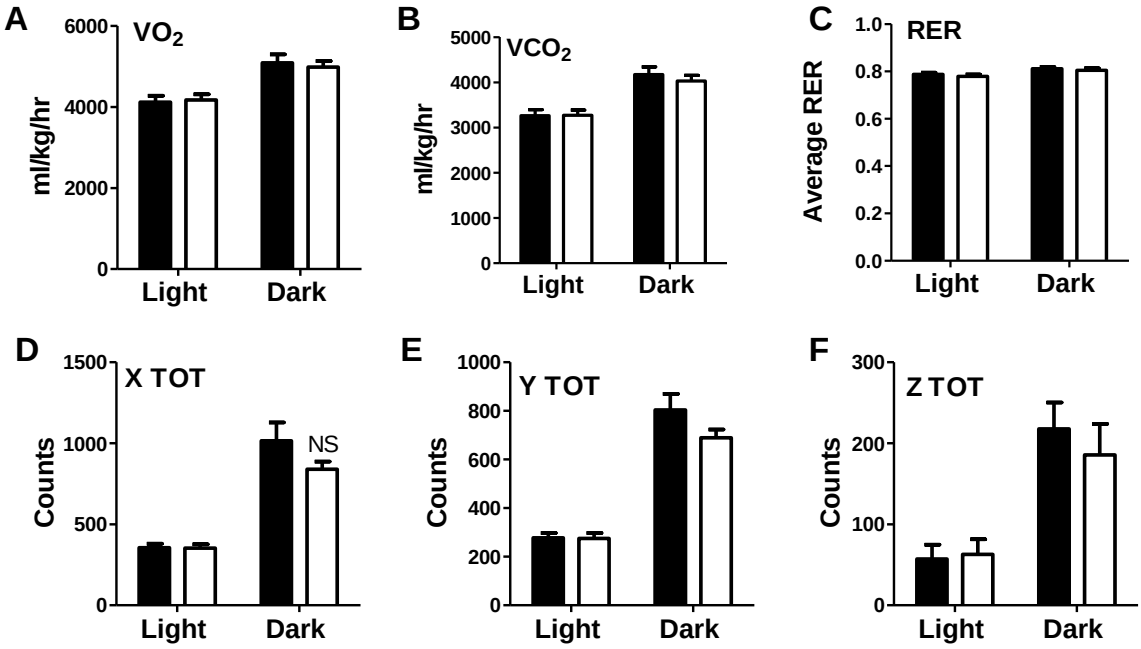

Figure 30. *Rdh10*+/- mice show no difference in energy expenditure nor activity under ad-lib feeding condition.

Black bar: WT; white bar: *Rdh10*$^{+/-}$

(A-B). VO_2 and VCO_2, ad lib feeding. No signification difference between genotype, blue (WT), red (*Rdh10* $^{+/-}$). n=12-14, 4month old males fed HFD (4IU vitamin A)
(C). RER, ad lib feeding. No signification difference between genotype, blue (WT), red (*Rdh10* $^{+/-}$). n=12-14, 4month old males fed HFD (4IU vitamin A)
(D-F). Activity counts. ad lib feeding. No signification difference between genotype, blue (WT), red (*Rdh10* $^{+/-}$). n=12-14, 4month old males fed HFD (4IU vitamin A)

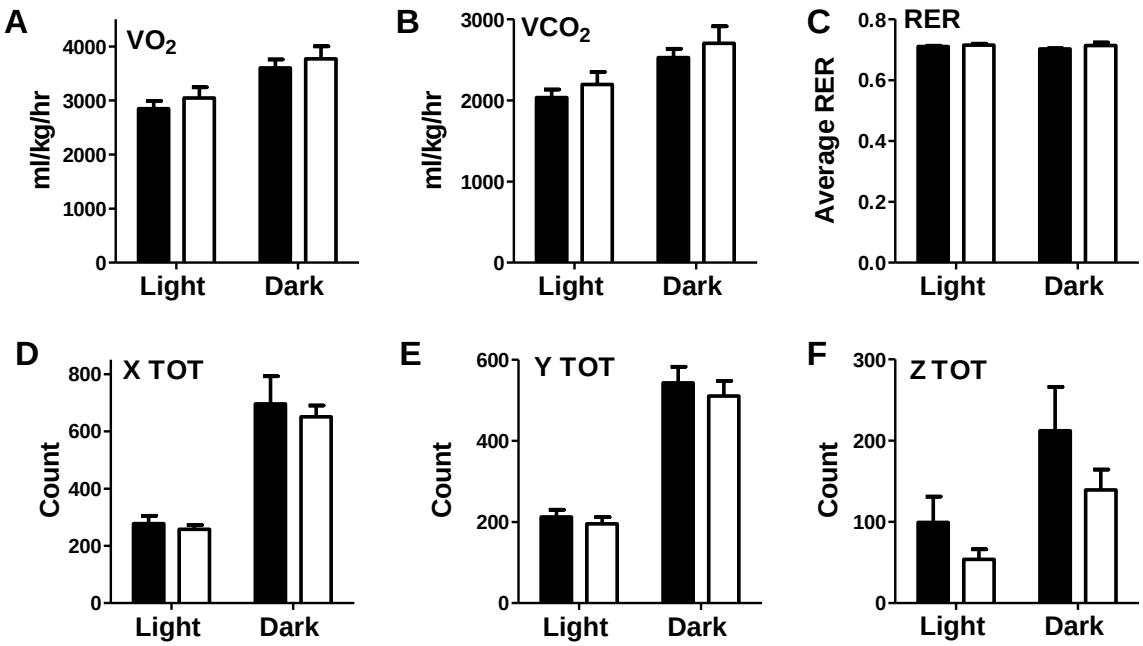

Figure 31. *Rdh10*+/- mice show no differences in energy expenditure nor activity under fasted conditions.

Black bar: WT; white bar: *Rdh10*$^{+/-}$

(A-B). VO2 and VCO2, overnight fasting. No signification difference between genotype, blue (WT), red (*Rdh10* $^{+/-}$). n=8-11, 4month old males fed HFD (4IU vitamin A)
(C). RER, overnight fasting. No signification difference between genotype, blue (WT), red (*Rdh10* $^{+/-}$). n=8-11, 4month old males fed HFD (4IU vitamin A)
(D-F). Activity counts. Overnight-fasting. No signification difference between genotype, blue (WT), red (*Rdh10* $^{+/-}$). n=8-11, 4month old males fed HFD (4IU vitamin A)

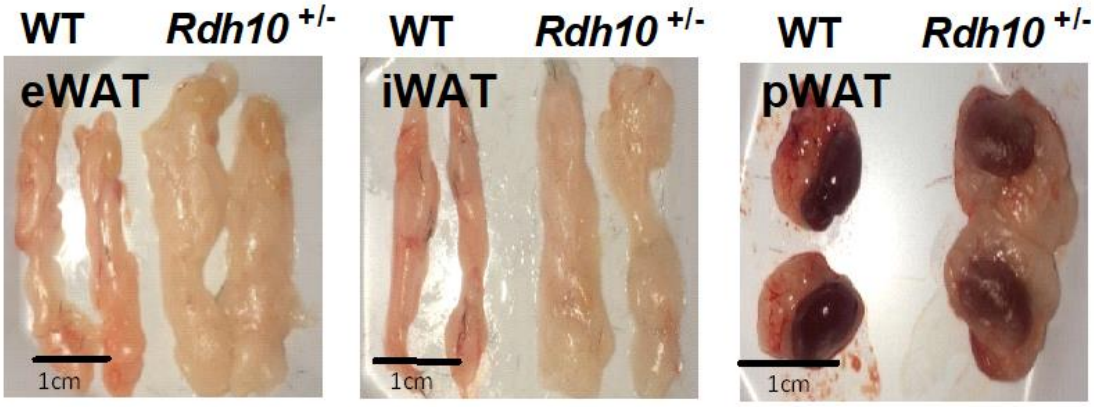

Figure 32. *Rdh10*$^{+/-}$ mice fed a HFD have increased fat pad sizes.

Representative pictures of showing epididymal White Adipose Tissue (eWAT), inguinal white adipose (iWAT) and perirenal adipose tissue (pWAT).

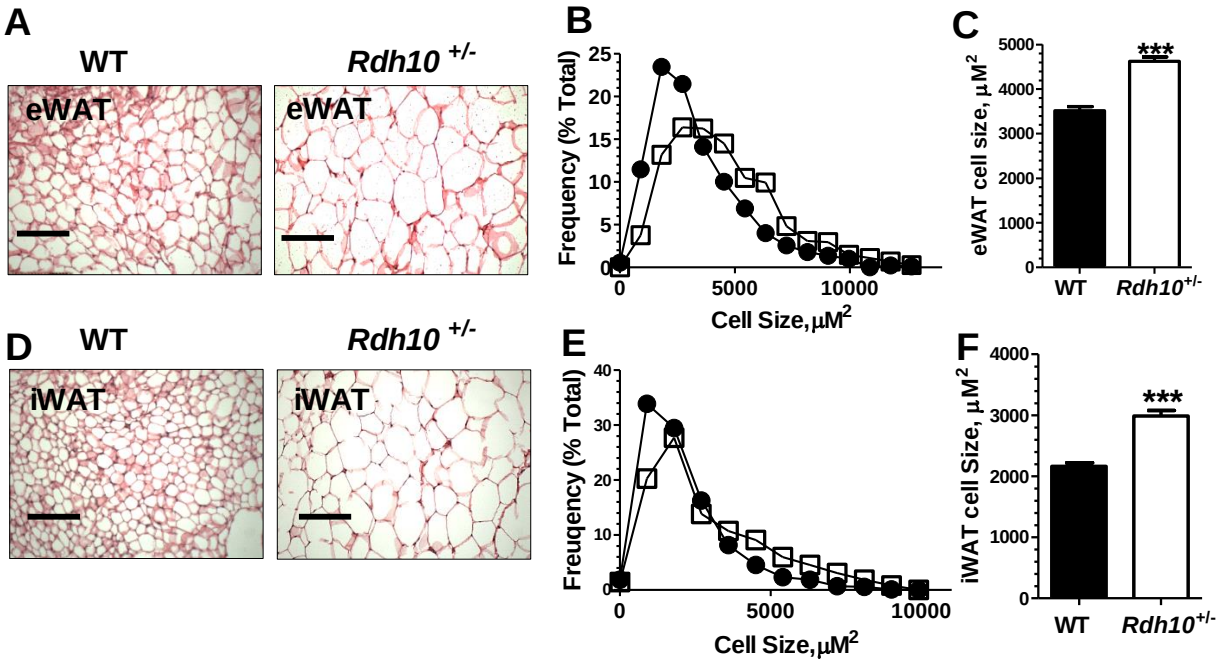

Figure 33. *Rdh10*$^{+/-}$ mice fed a HFD have increased adipose cell sizes.

Black bar: WT; white bar: *Rdh10*$^{+/-}$

(A) Representative pictures of eWAT histology and H and E staining (males, 4-month, HFD, WT n=13, *Rdh10*$^{+/-}$ n=11).
(B) Cell size distribution of eWAT cells (manual blind quantification by two independent individuals).
(C) eWAT average cell size of C.
(D) Representative pictures of iWAT histology and H and E staining (males, 4-month, HFD, WT n=13, *Rdh10*$^{+/-}$ n=11).
(E) iWAT cell size distribution. (manual blind quantification by two independent individuals)
(F) iWAT cells size average of F.
Data presented as mean ± SEM. For all MEF studies, n means biological replicates. Statistics done by two tailed student t test. *p<0.05, **p<0.01, ***p<0.001.

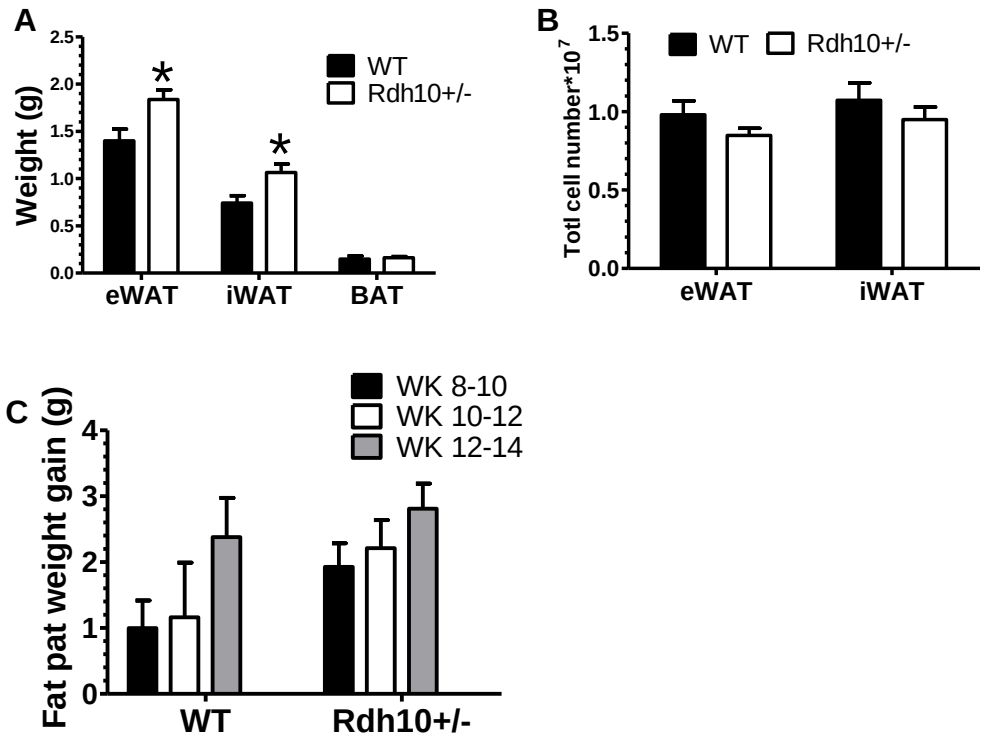

Figure 34. *Rdh10*$^{+/-}$ mice fed a HFD have increased white adipose weight but no differences in cell number

(A) Weight of eWAT, iWAT and BAT. n=36-38.
(B) Total cell number in eWAT and iWAT tissue. Calculated by m=v*p*n (p, density, 0.915g/ml) V = 4/3pr^3 (r calculated from figure 32) n=36-38.
(C) N=12-14 Fat pat net weight gain every two weeks. * 2 way anova- significant difference between genotype"

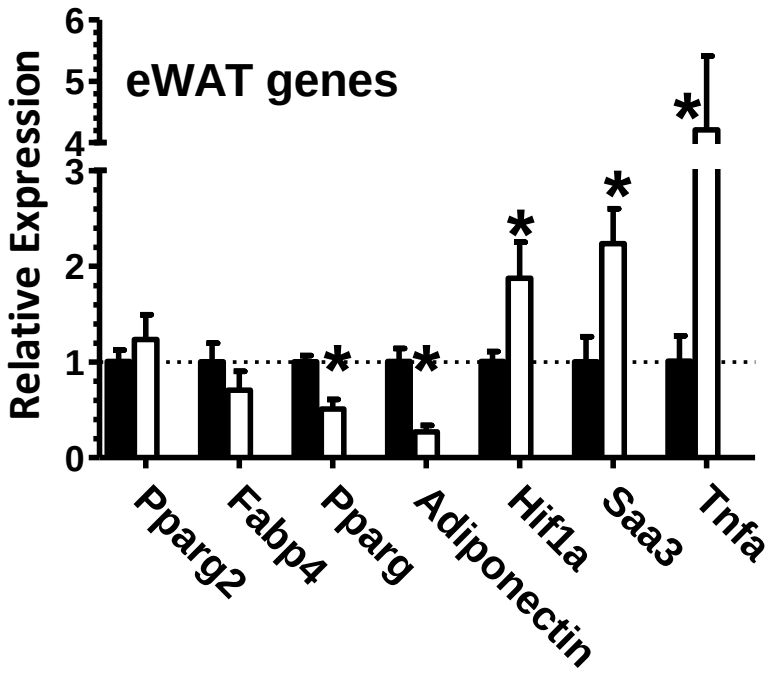

Figure 35. Expression of genes in eWAT.

Black bar: WT; white bar: *Rdh10*$^{+/-}$
Expression of adipocyte differentiation markers (Pparg and Fabp4), adipocyte function markers (adiponectin, Hif1a) and inflammation marker Saa3 and Tnfa. (n=9-11)

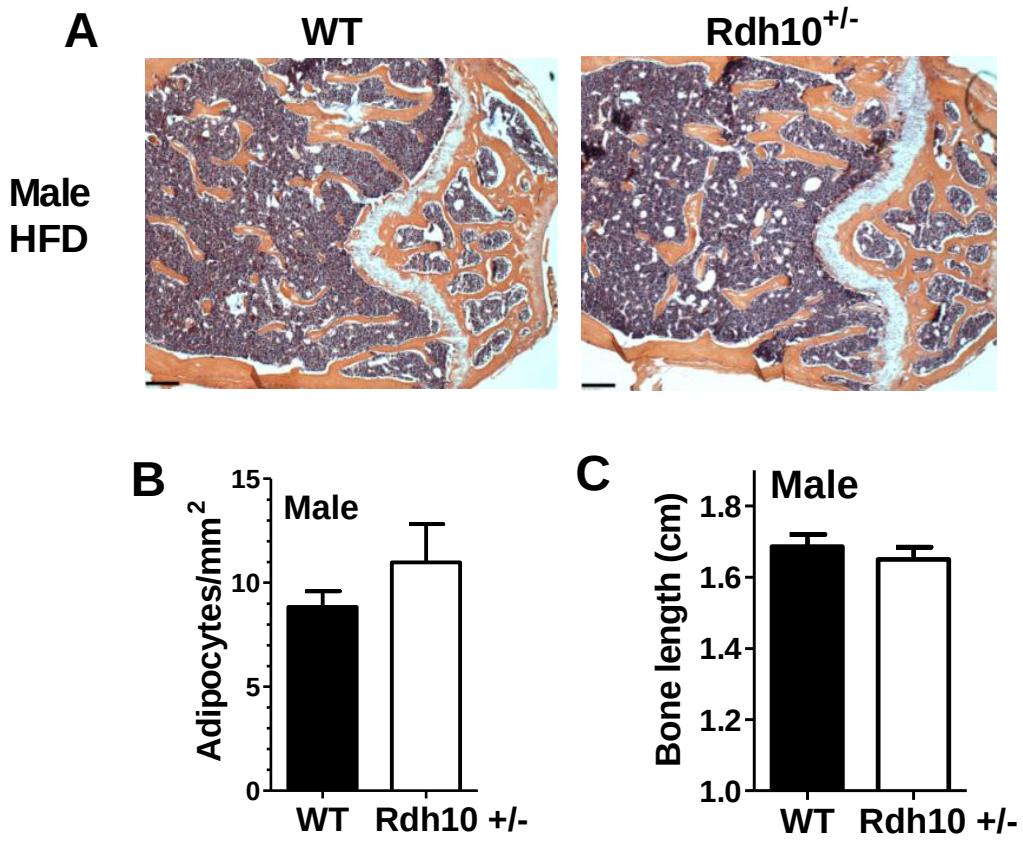

Figure 36. Male femur histology.

Black bar: WT; white bar: *Rdh10*$^{+/-}$
(A)H and E staining of bone marrow , 4 month old, males, HFD, n=5-8.
(B) Quantification of bone images of HFD males in A (image analyzed by two independent individuals)
(C). Femur bone length. 4 month old HFD male. WT: n=7. *Rdh10*+/-: n=10.

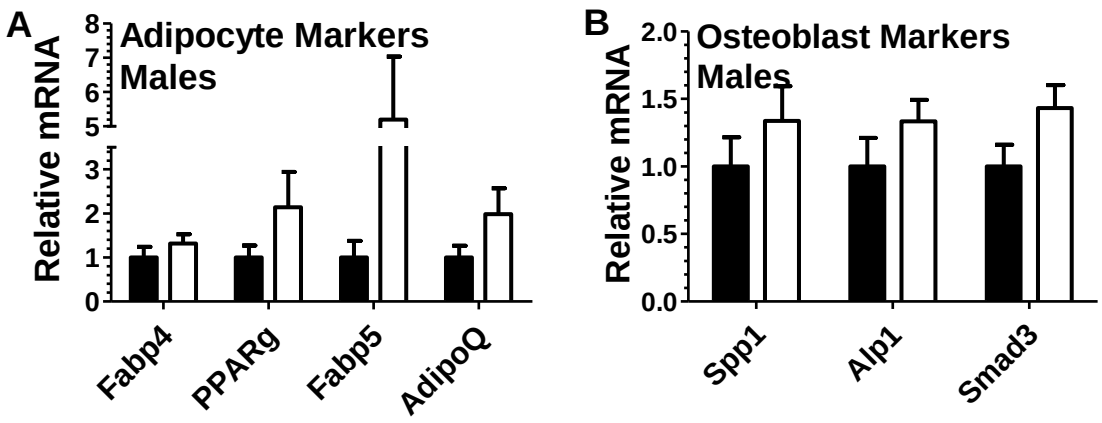

Figure 37. Male bone marrow gene expression

Black bar: WT; white bar: *Rdh10*$^{+/-}$

(A)Expression of adipocyte markers in bone marrows, males HFD. WT: n=7; *Rdh10*$^{+/-}$: n=11.
(B))Expression of osteoblast markers in bone marrows, males HFD. WT: n=7; *Rdh10*$^{+/-}$: n=11.

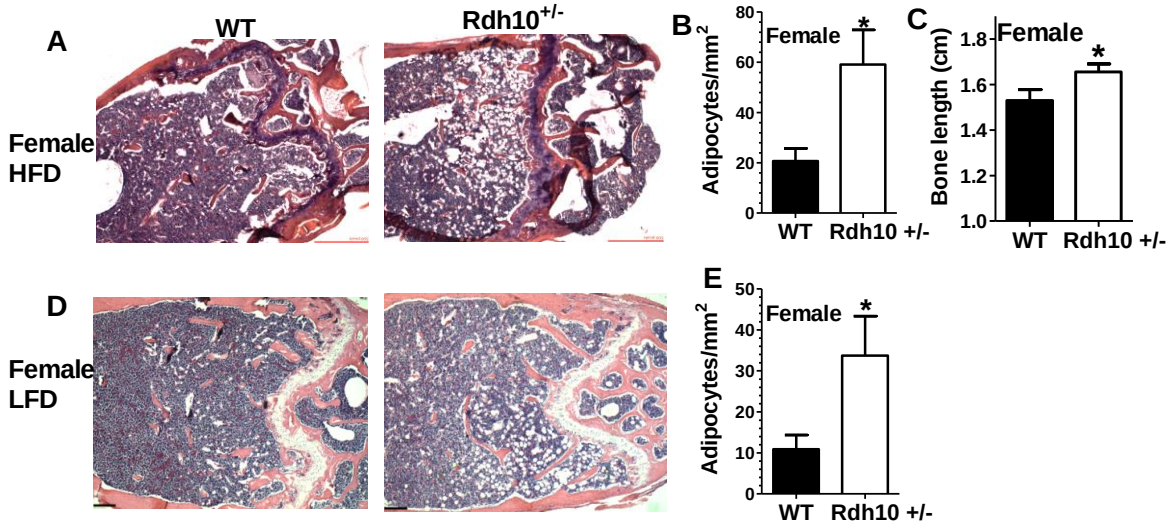

Figure 38. Female femur histology.

Black bar: WT; white bar: *Rdh10*$^{+/-}$

(A)H and E staining of bone marrow. 4 month old females, HFD, n=5-7.
(B) Quantification of bone images of HFD females in A. (image analyzed by two independent individuals)
(C)Femur bone length of 4month old HFD females. WT n=10; *Rdh10*$^{+/-}$ n=10
(D) H and E staining of bone marrow. 4 month old females, LFD, n= 7 both genotypes.
(E) Quantification of bone images of LFD females in D. (image analyzed by two independent individuals)

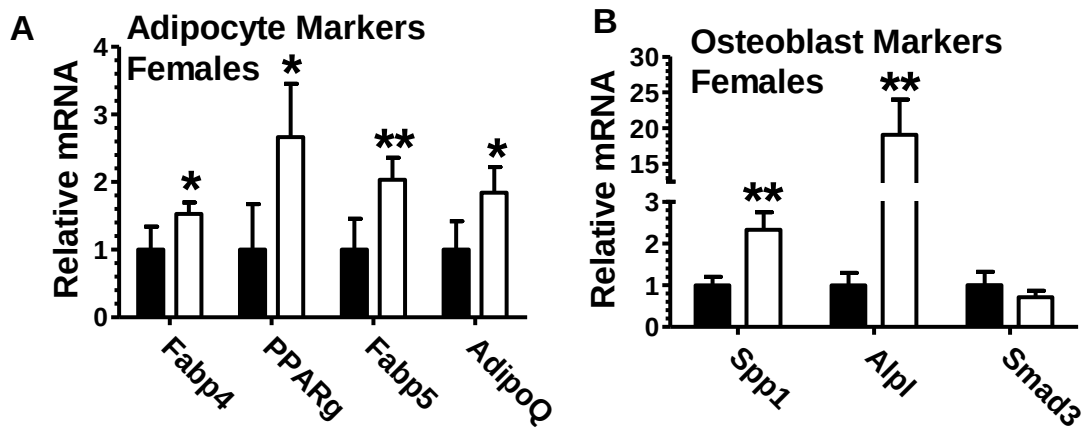

Figure 39. Female bone marrow gene expression

Black bar: WT; white bar: *Rdh10*$^{+/-}$

(A)Expression of adipocyte markers in bone marrows, females HFD. WT: n=13; *Rdh10*$^{+/-}$: n=13
(B))Expression of osteoblast markers in bone marrows, females HFD. WT: n=13; *Rdh10*$^{+/-}$: n=13

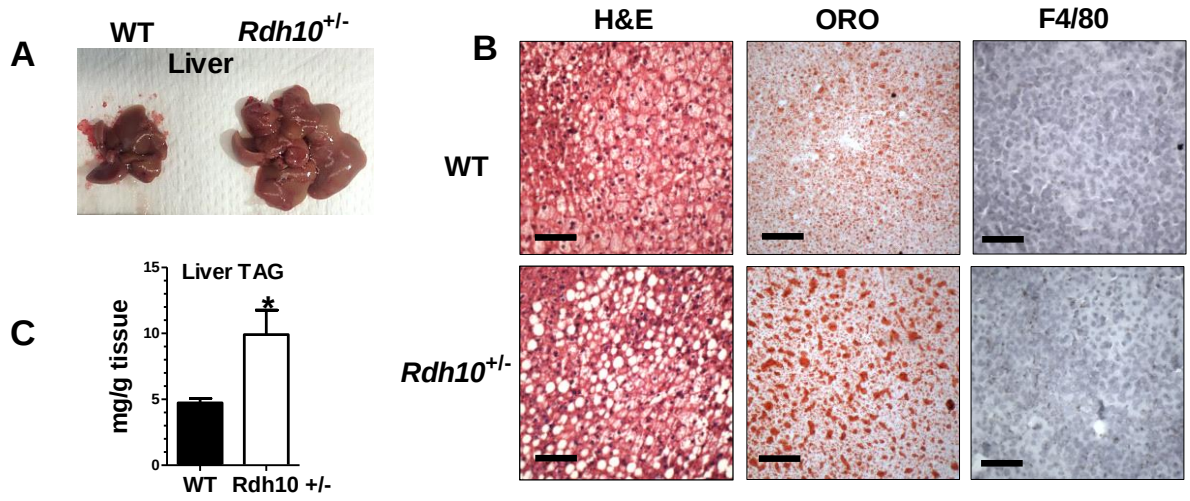

Figure 40. *Rdh10*$^{+/-}$ male fed a HFD are prone to liver steatosis.

A. H and E staining, Oil Red O staining and immunohistochemistry staining of F4/80 (macrophage marker), 4 month old, males, HFD. Representative pictures of 3 independent groups, n=4~6 each group.
B. H and E staining, Oil Red O staining and immunohistochemistry staining of F4/80 (macrophage marker, brown stain), 4 month old, females, HFD. Representative pictures of 3 independent groups, n=4~6 each group.
Liver TAG quantification, males, 4month old, HFD. n=8~12

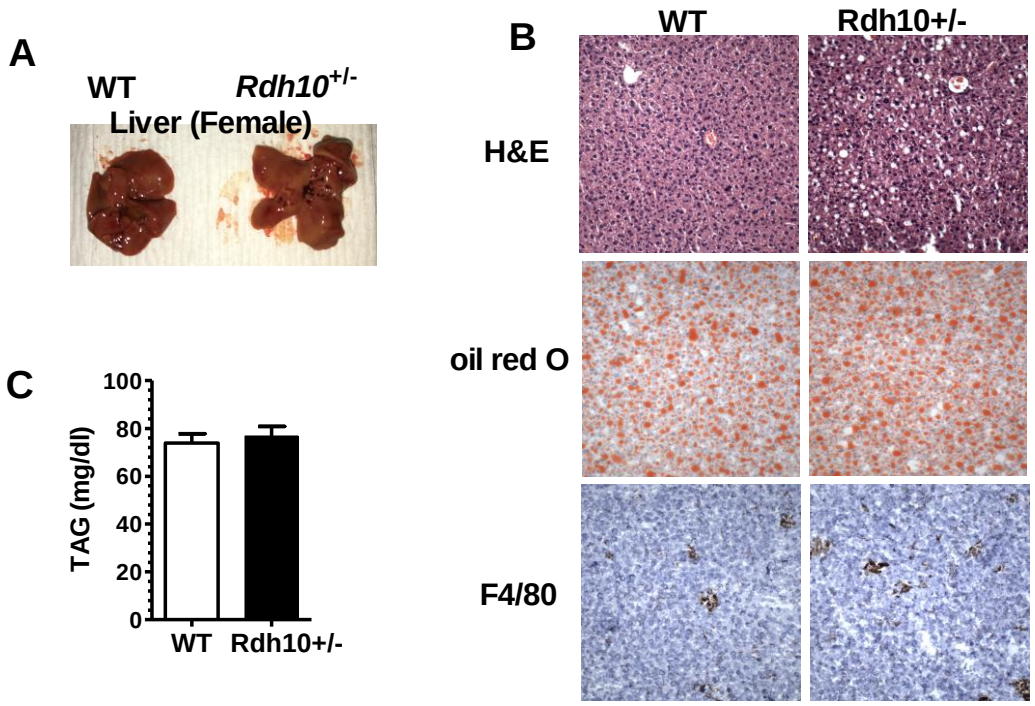

Figure 41. *Rdh10*$^{+/-}$ females fed a HFD showed no significant differences in liver fat accumulation.

(A) Representative pictures of liver from *Rdh10* $^{+/-}$ and WT female mice.
(B) H and E staining, Oil Red O staining and immunohistochemistry staining of F4/80 (macrophage marker, brown color), 4 month old, females, HFD. Representative pictures of 3 independent groups, n=4~6 each group.
(C)Liver TAG quantification, females, 4 month old, HFD. n=6 each group.

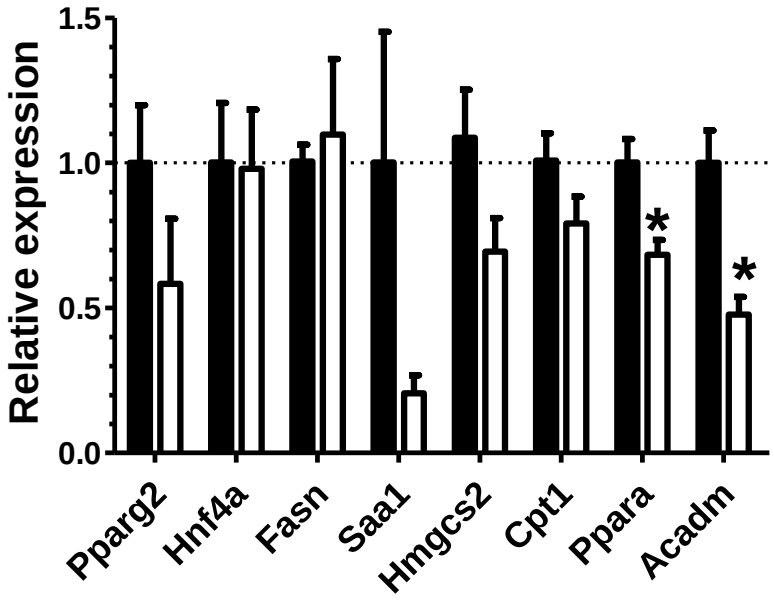

Figure 42. Gene expression of male livers.

Black bar: WT; white bar: *Rdh10*$^{+/-}$

Expression of liver genes, males, 4 month old, liver. Representative result of 2 independent groups, n=6~7 each group.

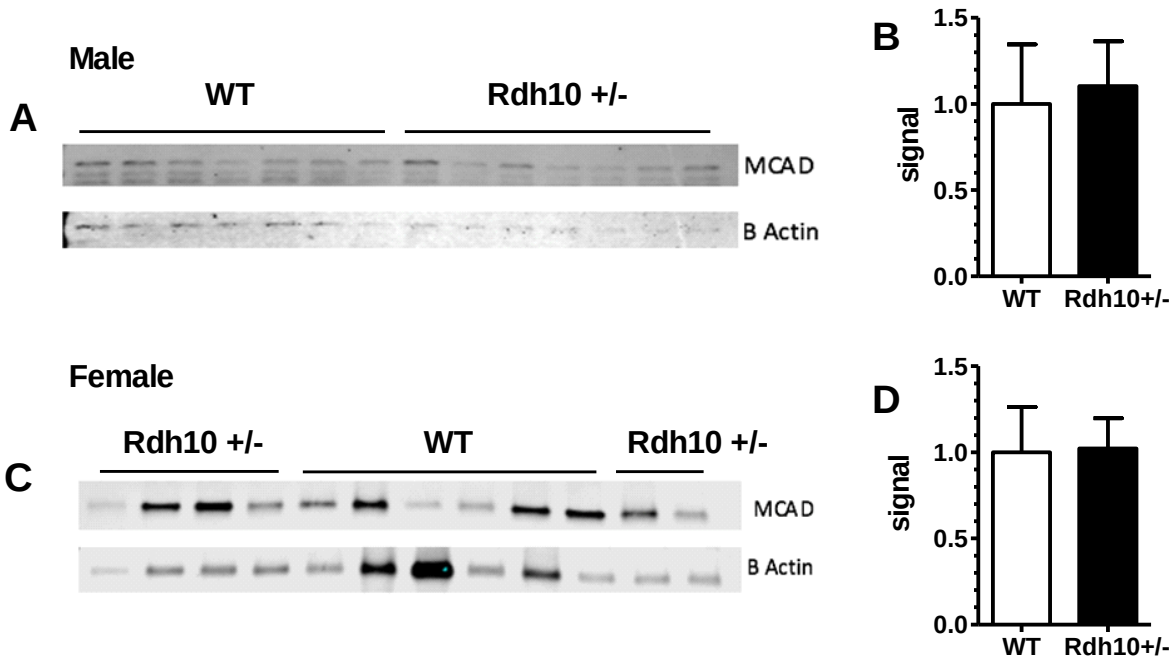

Figure 43. MCAD protein was not changed in both male and female livers.

(A)Western blot of MCAD. Male liver, n=6.
(B)Quantification of bands in A.
(C)Western blot of MCAD. Female liver, n=6.
(D)Quantification of bands in C.

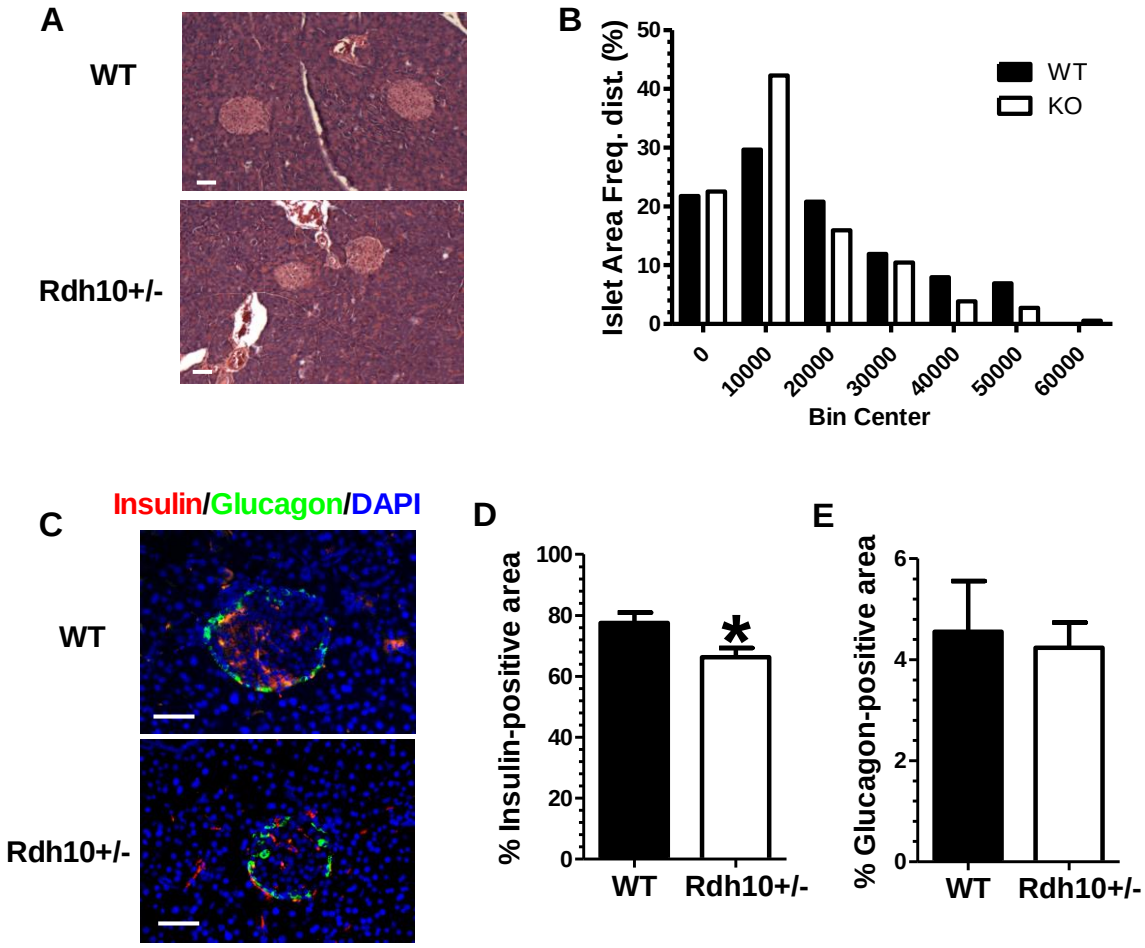

Figure 44. *Rdh10*$^{+/-}$ males have reduced islet sizes and less insulin content in islets.

(A) Representative histology picture (H and E) of pancreatic islets.

(B) Pancreatic islet size distribution in WT and *Rdh10*$^{+/-}$. Bin size= pixel number. WT n=5, *Rdh10*$^{+/-}$ n=8

(C)Representative immune florescence picture of pancreatic islets. Blue: DAPI stain for unclears. Green: glucagon staining (Primary antibody, ab10988). Red: Insulin staining (Primary antibody, ab7842).

(D) Quantification of insulin positive area

(E) Quantification of glucagon area.

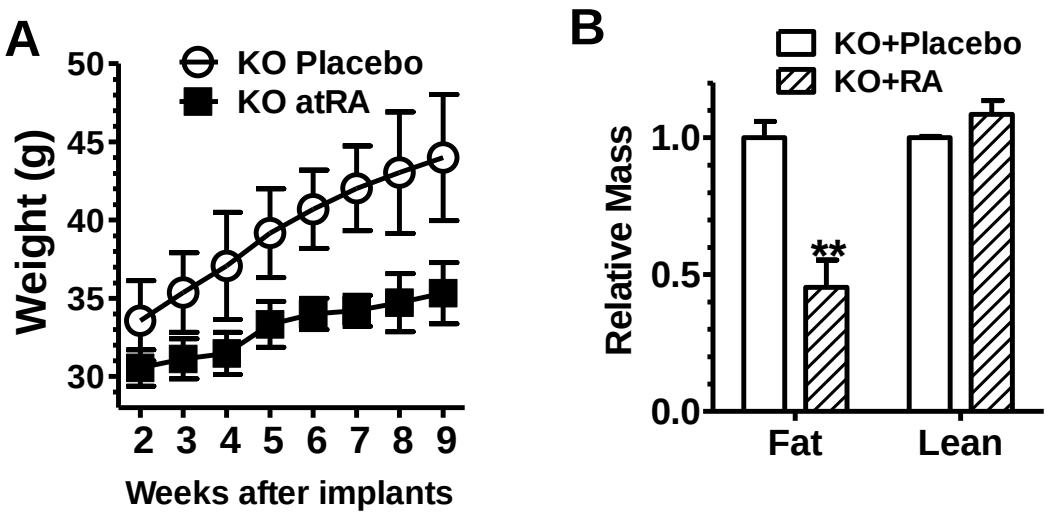

Figure. 45. atRA reduces *Rdh10*$^{+/-}$ body weight and fat weight.

(A)Body weight of mice treated with atRA or placebo. Males, fed HFD, n=3-4 each group.
(B) EchoMRI measurement of fat mass and lean mass, males fed HFD, 4 month old. n= 3-4 each group.

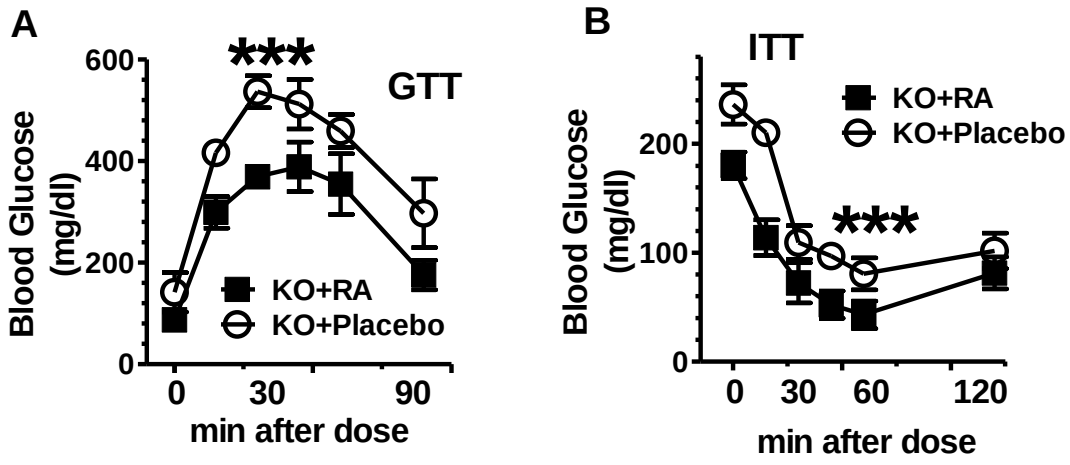

Figure. 46. atRA improves glucose tolerance and insulin sensitivity in *Rdh10*$^{+/-}$ mice.

(A)Glucose tolerance test, males fed HFD, 4 month old. n= 3-4 each group.
(B) Insulin tolerance test, males fed HFD, 4 month old. n= 3-4 each group.

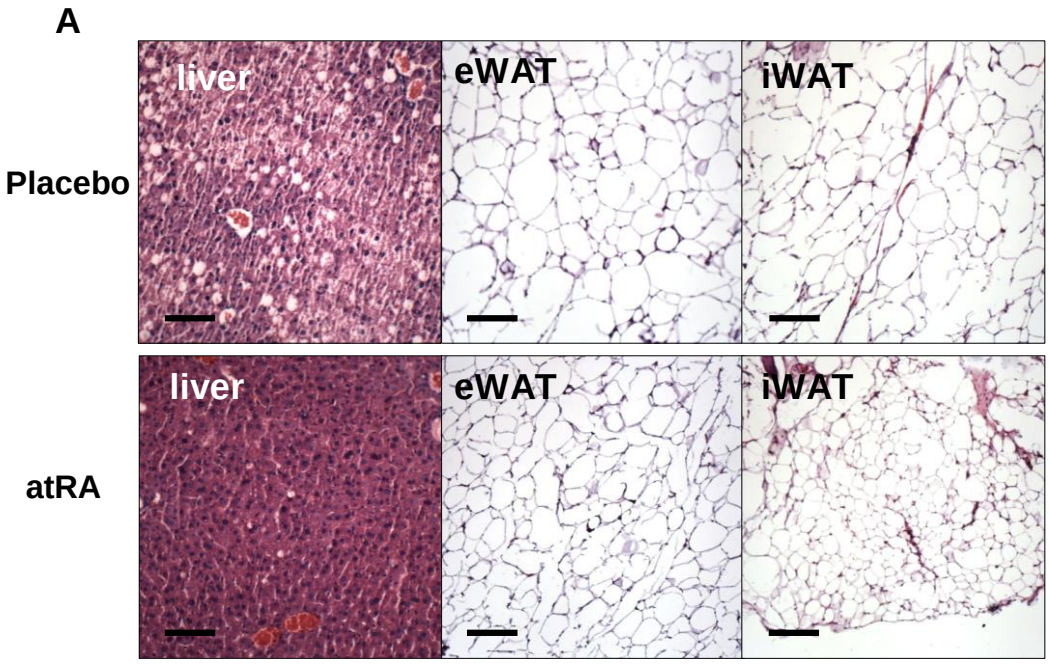

Figure 47. atRA rescues liver steatosis and white adipocyte cell size expansion.

Representative H and E staining histology pictures of liver, eWAT and iWAT. Males HFD, 4 month old. Placebo or atRA was implanted in 2 week old *Rdh10*$^{+/-}$ mice and kept till 4 month old.

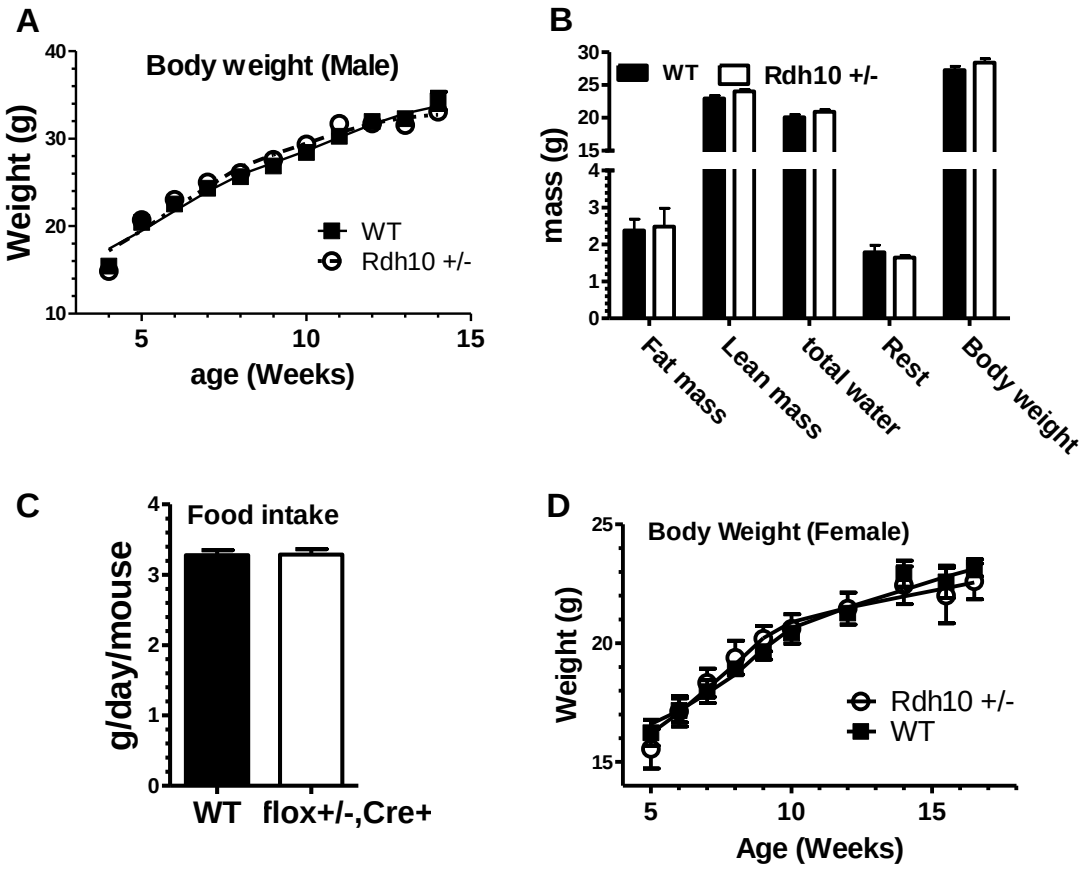

Figure 48. *Rdh10*$^{+/-}$ male mice fed a LFD showed no significant difference in body weight.

A. Body weight, males LFD, 4 IU vitamin A. WT n=30, *Rdh10*$^{+/-}$ n=23
B. EchoMRI analysis of body composition. Males, LFD. WT n=13, *Rdh10*$^{+/-}$ n=8
C. Food intake, Males fed LFD. WT n=12, *Rdh10*$^{+/-}$ n=8
D. Body weight of Female fed LFD 4IU vitamin A. WT n=10, *Rdh10*$^{+/-}$ n=9.

Discussion

The effects of atRA dosing on adipogenesis and lipid metabolism has been reported. Several studies reported weight loss in obese mice after being dosed with atRA (Bonet et al., 2012b). Schwarz. *et al* reported that atRA binds to RAR and inhibits adipogenesis (Schwarz et al., 1997b).Berry *et al* reported that atRA signals through PPARβ/δ and activates lipolysis and lipid oxidation in mature adipocytes(Berry and Noy, 2009b). However, despite the beneficial effect of atRA, high doses are toxic and teratogenic, and these experiments were done with pharmacological and sometimes toxic doses. This suggests necessity for studying retinoid metabolism in more detail before applying retinoids to treat obesity and metabolic disease. Here, we are the first to demonstrate that Rdh10 is an important retinoid metabolizing enzyme that affects adipogenesis and metabolic disease progression in adult mice. Furthermore, this study showed that a slight decrease of retinoic acid, a 20% decrease in liver and 10% decrease in white adipose, increased the susceptibility of mice to diet induced obesity and subsequent metabolic disorders. A low dose of atRA, 5 mg-pellet for 90 day release, greatly decreased mice bodyweight, fat composition, increased glucose tolerance and improved insulin resistance. This further suggests the therapeutic implication of low dose atRA to treat obesity and related metabolic disorders. We found in this study that reduced Rdh10 activity decreases atRA synthesized in MEF, and that was not compensated by other retinoid metabolizing enzymes. This decrease of atRA caused the MEF to be more sensitive to adipogenesis signals and thus increased the adipogenesis rate. In mice, the fast rate of adipogenesis surpassed the rate of angiogenesis, which potentially causes insufficient oxygen supply to the adipose tissue, which leads to inflammation and adipose tissue dysfunction. The dysfunctional adipocytes release FFA into the circulation, and for storage in other tissues such as liver.

atRA has been reported to be involved in liver lipid metabolism. atRA treatment increases fatty oxidation in human hepatoma cells (HepG2) (Amengual et al., 2012). A 4-day treatment with a pharmacological dose of atRA increases expression of genes related to fatty acid oxidation in mice liver (Amengual et al., 2010). Although these studies established a connection between atRA and liver oxidation, most focused on the effect of pharmacological doses of atRA, and did not investigate the effect of atRA reduction. Our study reports that reduced function of Rdh10 would lead to a 20% decrease of atRA in liver; this small decrease of atRA, when coupled with a HFD, has a dramatic effect on development of liver steatosis. Liver steatosis was reversed when mice were given 1.7 mg/kg of atRA, far lower than the dose that was previously reported (Amengual et al., 2010). The fact that the *Rdh10*$^{+/-}$ mice were more obese compared to their WT litter mates, and given that it was reported that obesity is another cause of liver steatosis, we hypothesize that the phenotype we observed was a result of two pathology pathways. First, FFA were released into circulation as a result of WAT damage, and were carried to the liver via portal vein, re-esterified and stored in liver. A second mechanism could be a liver autonomous effect caused by atRA deficiency.

Further study with a liver specific knockout of *Rdh10* will help to elucidate whether the phenotype is liver autonomous, or as a result of obesity. We also found that only the *Rdh10*+/- males, not the females, developed liver steatosis when fed a HFD. This suggests a sex-specific response to HFD induced liver disease.

We also observed bone marrow fat accumulation in *Rdh10*$^{+/-}$ females, but not males. More interestingly, *Rdh10*$^{+/-}$ females fed a low fat diet (LFD) showed increased bone marrow fat compare to the WT littermates, even without a difference in body weight. The function of atRA on osteoblast and osteoclast differentiation has been studied, yet results was inconclusive. There have been only rare reports on how retinoids metabolism affect bone marrow fat development. One paper reported that loss of Raldh1 protects mice against Pparγ induced bone marrow adiposity (Nallamshetty et al., 2014b). However, it's questionable whether it is the atRA generated by Raldh1 or other potential functions of Raldh1 that affect bone marrow adiposity, since we discovered that the resistance of Raldh1 KO mice to diet induced obesity is not related to its atRA generating function (Yang et al.). Our study could potentially be the first to link atRA, or *Rdh10*, to the development of bone marrow fat.

This paper also brought up interesting insights about gender specific fat accumulation in different tissues, suggesting potential interactions between retinoids and sex steroid signaling. Estrogen receptorα (ERα) was reported to affect the response of females and males to HFD exposure by differentially regulating hypothalamic inflammation (Morselli et al., 2016). It was also reported that RAR and ERα co-localize genome wide in a breast cancer model (Hua et al., 2009), suggesting potential cross talk between those two receptors.

In summary, we have identified and characterized the function of Rdh10 in regulating adipogenesis and lipid metabolism. This study is the first to provide insight on the function of Rdh10 in adult animals, further stressing the importance of vitamin A metabolism in the development of obesity and the resulting metabolic diseases, such as liver steatosis, insulin resistance and bone marrow fat accumulation. Further study is needed with tissue specific Rdh10 knockout models to understand the mechanisms of action contributing to the phenotype in different tissues. This study also demonstrated that a prolonged low dose of atRA treatment protects against diet induced obesity and metabolic disorders, suggesting application of low dose atRA for therapeutic purposes.

Chapter.3 Resistance to Diet Induced Obesity of RALDH1 KO mice is independent of retinoid function

Introduction

Diverse physiological processes during vertebrate conception, embryogenesis and postnatal development rely on retinoid signaling (Ross and Gardner, 1994; McLaren and Kraemer, 2012). Two reactions convert the parent retinoid retinol (vitamin A) into all-*trans*-retinoic acid (atRA), an activated autocoid of retinol. Retinol dehydrogenases (Rdh), of the short-chain dehydrogenase/reductase gene family, catalyze conversion of retinol into retinal, whereas retinal dehydrogenases (Raldh) of the Aldh gene family catalyze the reaction that converts retinal into RA irreversibly (Napoli, 2012b; Kedishvili, 2016). At least three isoforms of Rdh (mouse Rdh1/human Rdh16, Rdh10, Dhrs9) and Raldh (Raldh1, 2, 3) contribute to RA biosynthesis. Tissues and cells often co-express multiple isoforms of Rdh and Raldh (Wang et al., 2011; Kent et al., 2016), suggesting non-redundant functions: a premise supported by gene ablations that reveal different phenotypes for each, albeit related to RA function (Dupé et al., 2003; Jette et al., 2004; Ribes et al., 2006; Siegenthaler et al., 2009; Lin et al., 2010; Everts et al., 2013).

RA inhibits adipogenesis, while promoting energy consumption and reducing adiposity (Bonet et al., 2012c; Noy, 2013). Mice fed a high-fat diet (HFD) dosed chronically with RA resist weight gain (Mercader et al., 2006; Jeyakumar et al., 2006; Berry and Noy, 2009c). RA supplementation to HFD-fed mice restricts average weight to ~29 g relative to controls of ~42 g over 8 weeks (Berry et al., 2012). Conversely, chronically feeding a vitamin A-deficient HFD increases adiposity (Ribot et al., 2001). Extending these observations of pharmacological RA effects and vitamin A insufficiency, ablating Rdh1 allows a 33% increase in fat mass in mice fed a low-fat diet, relative to controls (Zhang et al., 2007b). In vitro, RA inhibits preadipocyte differentiation into mature adipocytes in ST13, NIH3T3-LI, 3T3-F44A and C3H10T1/2 cell lines (Sato et al., 1980; Kuri-Harcuch, 1982; Schwarz et al., 1997c; Pairault and Lasnier, 1987; Hisada et al., 2013) though activating RAR (Kamei et al., 1994; Berry et al., 2010; Green et al., 2017).

Raldh1 (aka Aldh1a1) was established as an Raldh by its ability to access Crbp1-complexed retinal, inhibition by apo-Crbp1, an intracellular indicator of retinoid status, and a decrease in liver RA upon inhibition (Posch et al., 1992; Penzes et al., 1997; Arnold et al., 2015). Unexpectedly, ablation of Raldh1 caused resistance to diet-induced obesity (DIO) from impaired adipogenesis, by proposing retinal as an autocoid that activates RAR and/or proposing RA as an inducer of adipogenesis (Ziouzenkova et al., 2007b; Reichert et al., 2011). Raldh1 “moonlights” extensively, however. Raldh1 has been identified as an androgen binding-protein (Pereira et al., 1991; Yoshida et al., 1993; McCammon et al., 1993), and functions in the cornea and lens of mammalian eyes as crystallin (Bateman et al., 2003). Raldh1 recognizes multiple substrates, including oxazaphosphoranes (Sládek, 1999) and aldehyde lipid peroxidation products,

such as malondialdehyde and nonenal (Grünblatt and Riederer, 2016). Raldh1 also contributes to γ-aminobutyric acid biosynthesis in dopaminergic neurons (Kim et al., 2015). Thus, Raldh1 has multiple functions independent of retinoid metabolism.

We studied the *Raldh1*-null mouse (KO) and mouse embryonic fibroblasts (MEF) derived from KO to determine the impact of Raldh1 ablation on retinoid concentrations, metabolism and function. The data indicate that retinoid metabolism or activation/inhibition of RAR in pre-adipocytes do not underlie the KO phenotype.

Material and Methods

Animals-Animal studies were done in accordance with the guidelines issued by the UC-Berkeley Animal Use and Care Committee. *Raldh1*$^{+/-}$ mice were purchased from Jackson Laboratory (Stock #012247). Upon arrival, mice were fed a vitamin A-sufficient purified diet (VAS), with 4 IU vitamin A/g as retinol (AIN-93G diet) as recommended by the National Research Council (Reeves, 1997). Heterozygotes were interbred, yielding homozygous null mice (KO) that were interbred and maintained on the VAS. C57Bl/6J mice were used as controls. Mice were fed the VAS at least 2 generations to allow adaptation. When noted, some mice were fed a VAS modified to contain 50% fat-derived calories (VAS-HFD).

Retinoid Quantification-Tissue and cellular atRA was quantified by LC-MS/MS as in (Kane and Napoli, 2010) with some modification. In the LC, chromatography was done using a Suplex pkb-100 column (Supelco, 2.1 x 250 mm, 5 µm particles) with 3 min of 80% acetonitrile/20% water/0.1% formic acid, followed by a linear gradient to 95% acetonitrile/5% water/0.1% formic acid over 9 min, held for 4 min, returned by linear gradient to 80/20/0.1 over 1 min, and held 8 min, all at 0.4 mL/min. Tissue and cellular retinal was measured using LC-MS/MS as in (Wang et al., 2015). Cellular retinol was measured as in (Kane et al., 2008b).

MEF isolation and differentiation- *Raldh1* WT and KO MEFs were isolated from e13.5-e14 embryos, then cultured in UV irradiated growth media (DMEM+10% BCS + penstrip). MEFs were induced to differentiation with growth medium and 1uM Dexamethasone, 500uM Isobutylmethylaxanthine (IBMX), 0.85uM insulin and 100nM Rosiglitizone for 3 days, then cultured in growth medium with 0.85uM insulin and 100nM Rosiglitizone for another 4 days.

Cellular retinoid assays- On differentiation day 0 or 7, WT and KO MEFs were dosed with 250 nM retinol (HPLC purified) for 2 hours hidden from light or under yellow light. Cells were collected and flash frozen, then analyzed for retinoids.

Oil Red O quantification- on dd7, wells were washed with PBS and fixed with 10% formalin overnignt. Cells were then stained with ORO working solution for 30mins, then washed with distilled water for 5 times and visualized by inverted microscope.

Gene Expression-Total RNA was extracted by TRIzol (Sigma Aldrich). 1ug total RNA was used for reverse transcription (iscript biorad). RT-qPCR was preformed with Bio-RAD CFX Connect Real-Time Detection System to quantify the relative expression of genes. Expression of each gene is normalized to the geometric mean of Gusb and Tbp (endogenous controls) and then WT MEF expression on differentiation day 0. qPCR Primers were Life Technologies. *Rdh10* (Mm00467150_m1), *Dhrs9* (Mm00615706_m1), *Dhrs3*(Mm00488080_m1). *Aldh1a1* (Mm00657317_m1), *Aldh1a2* (Mm00501306_m1), *Aldh1a3* (Mm00474049_m1), *Cyp26B1* (Mm00558507_m1), *Rarb* (Mm01319677_m1), *Pparg* (Mm00440940_m1), *Fabp4* (Mm00445878_m1), *Zfp423* (Mm00677660_m1).

RAR/PPARd ant/agonists- MEFs were cultured in adipogenic medium as indicated above and treated with vehicle (DMSO) , RAR pan-antagonist (AGN 193109, 200 nM), RAR agonist (TTNPB, 100 nM), PPARδ agonist (GW 0742, 100 nM), and PPARδ antagonist (PT-S58, 1 µM) from dd0 to dd7.

Results

Male and female KO mice respond differently to the amount of dietary fat

If fed for more than one generation, a vitamin A-sufficient diet (VAS) normalizes endogenous retinoid levels from the unusually high levels associated with chow diets, which provide copious vitamin A (Obrochta et al., 2014). To avoid confounding effects of copious retinoids, *Raldh1*-null mice (KO) were fed a purified VAS for at least two generations after purchase from Jackson Labs. Mice were then fed a VAS with high fat (HFD) beginning at weaning (3-weeks-old). Both male and female KO mice gained less weight when fed a HFD, relative to WT, but the effect was more pronounced in females (Figure 49A, D). The most resistance to weight gain occurred in females between 5 and 10 weeks old, and in males from 3 to 10 weeks old. Thereafter weight differences were maintained without further increases incremental differences (Figure 49B, E). Because the weight differences from 10 to 33 weeks old were maintained, data were averaged to obtain a value for the steady-state differences in weight between WT and KO of both sexes to reveal a 10.7 ± 0.6 g difference between female WT and KO and a 7.1 ± 0.6 g difference between male WT and KO (Figure 49C, F). Exchanging the VAS for an HFD at 13 weeks old and maintaining the diets for a further 13 weeks induced a difference in weight gain in both male and females of ~7 and 8 g, respectively (Figure 49G). Male KO, however, resisted weight gain even when fed a VAS, with ~6 g difference between WT and KO. Female mice fed a VAS weighed the same regardless of genotype. These data suggest that both male and female Raldh1 KO mice are resistant to DIO, while the phenotype is more pronounced in females.

Changes in retinal and atRA with genotype, diet and sex do not support a retinoid-dependent *Raldh1*-null phenotype

We quantified retinal and atRA in tissues of male and female mice fed either a VAS or a HFD to gain insight into the effects of *Raldh1* ablation, dietary fat, and sex on tissue retinoid concentrations (Figure 50-52). Because fasting vs re-feeding affects tissue atRA levels (Obrochta et al., 2015), mice were fasted 16 hr and then refed 4 to 4.5 hr before tissue collection. We quantified retinal and atRA in subcutaneous (femoral) WAT (fWAT), visceral (epididymal or perimetrial) WAT (eWAT/pWAT), and liver.

Differences between WT and KO should be primary drivers of the phenotype. Liver atRA decreased by 22-38% in KO relative to WT in both sexes and regardless of diet. No significant and/or marked changes occurred relative to WT in adipose atRA concentrations regardless of diet in either sex, with the exception of a 12% decrease ($P<0.05$) in male KO eWAT fed the VAS. Relative to WT, KO showed no significant differences in retinal concentrations in males or females regardless of diet, with three exceptions. In males, retinal in VAS-fed KO increased 40% in fWAT ($P<0.04$), and retinal in livers of KO fed the VAS-HFD doubled ($P<0.03$) relative to WT. In females, only pWAT fed a VAS-HFD showed increased retinal (60%, $P<0.04$) relative to WT.

Dietary fat also affects retinoid concentrations. The VAS-HFD resulted in statistically significant atRA decreases in the three KO female tissues assayed relative to the VAS (10-40%, $P<0.02$), and also caused a 40% decrease ($P<0.002$) in fWAT of female WT. atRA values in male KO were not affected by diet. atRA of WT males changed significantly in fWAT (25% decrease, $P<0.04$) and liver (22% increase, $P<0.02$) as a result of the VAS-HFD. Retinal in adipose of female KO did not respond to diet, but liver retinal decreased 30% ($P<0.05$) with a VAS-HFD. Liver retinal in female WT decreased by 60% ($P<0.009$) with the VAS-HFD, as did pWAT by 30%.

Finally, we considered sex differences. The sex of WT mice fed a VAS had no statistically significant impact on atRA, but KO females had increased atRA in both WAT depots (~60% increases, $P<0.0001$) and a 15% decrease ($P<0.007$) in liver, relative to males. In the VAS-HFD mice, sex differences occurred in livers of both WT and KO (20 to 30% decreases in females, $P<0.008$), but not in adipose. The sex of mice fed a VAS had a limited effect on retinal levels, with only liver of female KO mice increasing relative to males (100% increase, $P<0.0001$). The VAS-HFD affected only WT mice with a 34% decrease ($P<0.02$) in female subcutaneous WAT, and a 70% increase in retinal in female liver .

The decreases in liver atRA in the KO relative to WT in both sexes and with both diets is consistent with Raldh1 contributing to endogenous liver atRA under physiological conditions. The data, however, do not support a conclusion that increased retinal contributes to the phenotype, because the KO phenotype is strongest in females fed a HFD. Although the retinal concentration increased in pWAT of KO relative to WT,

there was no significant difference in pWAT retinal between VAS and VAS-HFD, and no significant sex difference in pWAT vs. eWAT of mice fed a VAS-HFD.

KO phenotypic effects are cell autonomous

We sought to determine whether the phenotype was cell-autonomous with respect to mesenchymal stem cell differentiation into adipocytes. Mouse embryonic fibroblasts (MEF) derived from KO failed to differentiate into adipocytes as efficiently as WT MEF. Oil red O staining of MEF after differentiation day 7 (dd7) revealed 6.5-fold lower ability to accumulate lipids (Figure 53A, B). Reduction of *Ppar*γ and *Fabp4* (AP2) mRNA expression in KO confirms an underlying deficiency in adipogenesis (Figure 53C, D). Expression of *Zfp423*, however, remained similar between WT and KO throughout adipogenesis, but tended to statistical significance.

atRA arrests MEF adipogenesis in a dose-dependent manner

To further characterize MEF as a model of retinoid effects on adipogenesis, we determined atRA dose-response effects on differentiation of WT MEF into adipocytes. MEF were treated continuously from dd0 through dd7 with fresh atRA included in each daily medium change. Consistent with results from adipogenesis models in established cell lines, atRA inhibited adipogenesis of MEF. atRA had an IC_{50} of 4.6 nM with *PPAR*γ and 2.6 nM with *Fabp4* mRNA (Figlure 2A) and 26 nM for oil red O staining (Figure 2B). As low as 1 nM atRA caused a 28-37% decrease in *PPAR*γ and *Fabp4* mRNA. Increasing doses increased the mRNA of the atRA target gene *Rarβ*, as expected (de The et al., 1990), with induction observed at 1 nM (Figure 2C). The results suggest that atRA has a inhibitory effect on adipogenesis, even at dose as low as 1nM.

Effects of differentiation on retinoid metabolism

We tested the effects of expression changes in retinoid metabolon genes on retinoid metabolism in MEF. Two hr incubation with 100 nM retinal increased intracellular retinol modestly in WT MEF, but increased retinyl esters ~3-fold during the course of differentiation and decreased atRA levels by around 70% (Figure 54A). Retinal ester and retinol level was also around 40% higher in WT compared to Raldh1 KO on dd7(Figure 54A). Two hour incubation of MEF with 250 nM retinol on either dd0 or dd7 resulted in uptake of the same amounts of retinol, regardless of dd or genotype (Figure 54B, left). Retinal concentrations were not impacted by genotype, but decreased ~50% on dd7 (Figure 54B, middle) when compared to dd0. atRA synthesis changes due to both differentiation and genotype (Figure 54B, right). Differentiation reduced atRA synthesis 56% in WT and 64% in KO. KO also showed a 45 to 32% decrease in atRA synthesis on dd0 and dd7, respectively, relative to WT. These data suggest that there was no net increase of retinaldehyde synthesized in Raldh1 KO MEFs no matter before or after adipogenesis, so it is not likely the increase of retinaldehyde is the cause of the phenotype as claim by previous publications. However, atRA was level was around 50% lower in dd0 Raldh1 KO, but this can hardly explain the phenotype. As it was showed by dose response curve result, atRA has an inhibitory effect on adipogenesis even at low

dose. In other words, lower atRA level could increase adipogenesis but not inhibit adipogenesis.

An RAR pan-antagonist does not reverse the KO phenotype

The decrease in retinal and atRA during MEF differentiation exclude retinoids as driving the KO phenotype. To confirm whether the retinoic acid nuclear receptors mediate the KO phenotype, we treated MEFs from dd0 until dd7 with antagonists and agonists of RAR. 200nM RAR pan-antagonist AGN193109 did not alter differentiation of WT or KO MEFs or the difference in the degree of differentiation between WT and KO MEFs, as assayed by oil red O and gene expression(Figure 55A-C). KO MEFs maintained a 44% decrease in ability to differentiate in the presence of the RAR antagonist. 100nM RAR pan-agonist TTNPB further suppressed both lipid accumulation (Figure 56A and B) and adipogenic gene expression (Figure 56C), showing that both WT and KO remained sensitive to RAR induction. The PPARδ agonist GW0742 increased adipogenesis to the same extent in both genotypes (~30%), whereas the PPARδ antagonist PT-S58 had no effect in either phenotype. These results suggest that the resistance to adipogenic induction of Raldh1 KO MEF cannot be related to atRA related pathway. Since treating cells with neither of the two nuclear receptors that atRA binds to rescues the phenotype.

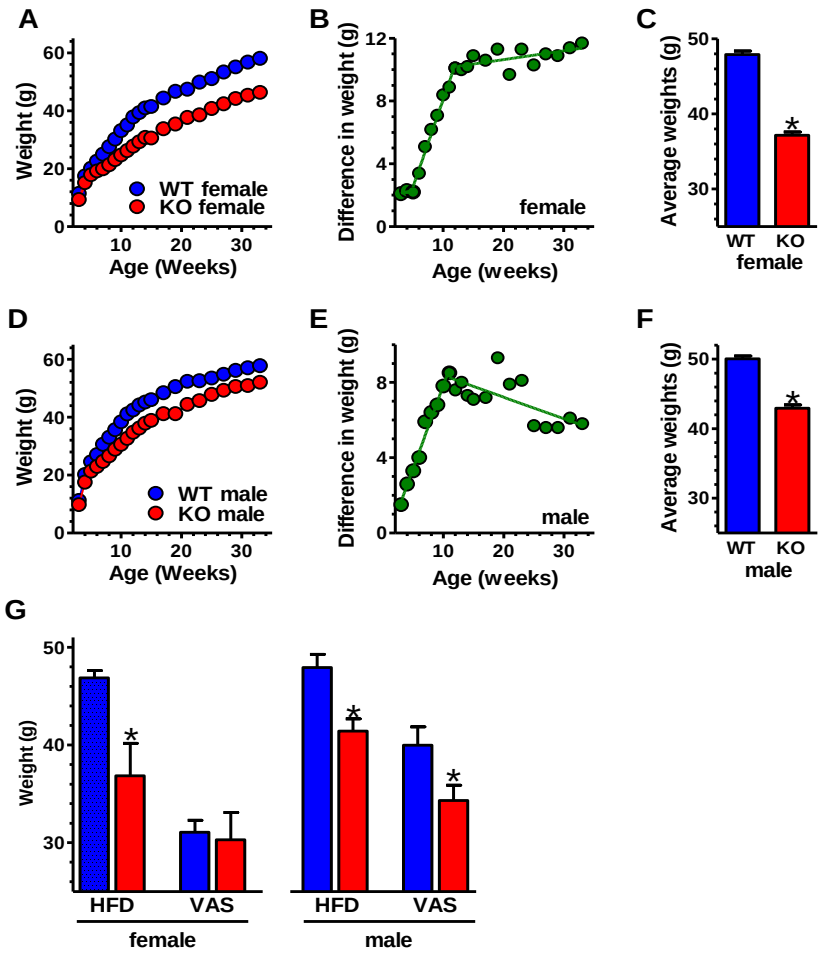

Figure 49. M**ale and female mice respond differently to VAS vs HFD**
(A) Weights of female mice fed a HFD beginning at weaning (n = 23 WT, 25 KO). Values at each age: p<0.001.
(B) Differences in weights between female WT and KO with age.
(C) Average weight difference of all female WT and KO mice in ages 12-33 wks old: *p<0.001 (n = 286 WT, 324 KO).
(D) Weights of male mice fed a HFD beginning at weaning (n = 16 WT, 20 KO). Values at each age: p<0.003.
(E) Differences in weights between male WT and KO with age.
(F) Average weight difference of all male WT and KO mice in ages 11-33 wks old: *p<0.001 (n = 221 WT, 223 KO.
(G) Weights of 26-week-old mice fed either a HFD beginning at 13-wk-old or continued with a VAS: *p<0.05 compared to WT (n = 7-10 per group).

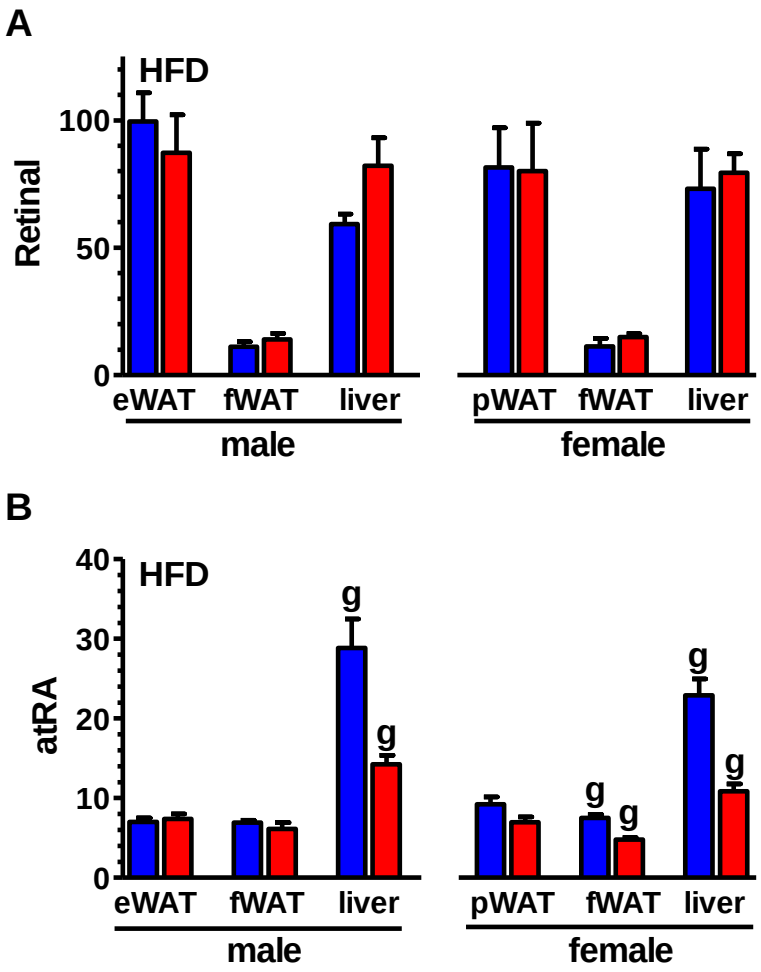

Figure 50. Tissue retinoid concentrations in HFD young mice.
Mice were fasted overnight then refed 4-4.5 hr: WT, blue bars; KO, red. Units are pmol/g tissue.

(A) Retinal in 6 to 7-wk-old fed a HFD for 2 weeks.
(B) atRA in the same mice as in A.
[g]Significant difference between genotypes in the same tissue, sex and diet.
[g, d, s]$p < 0.05$.

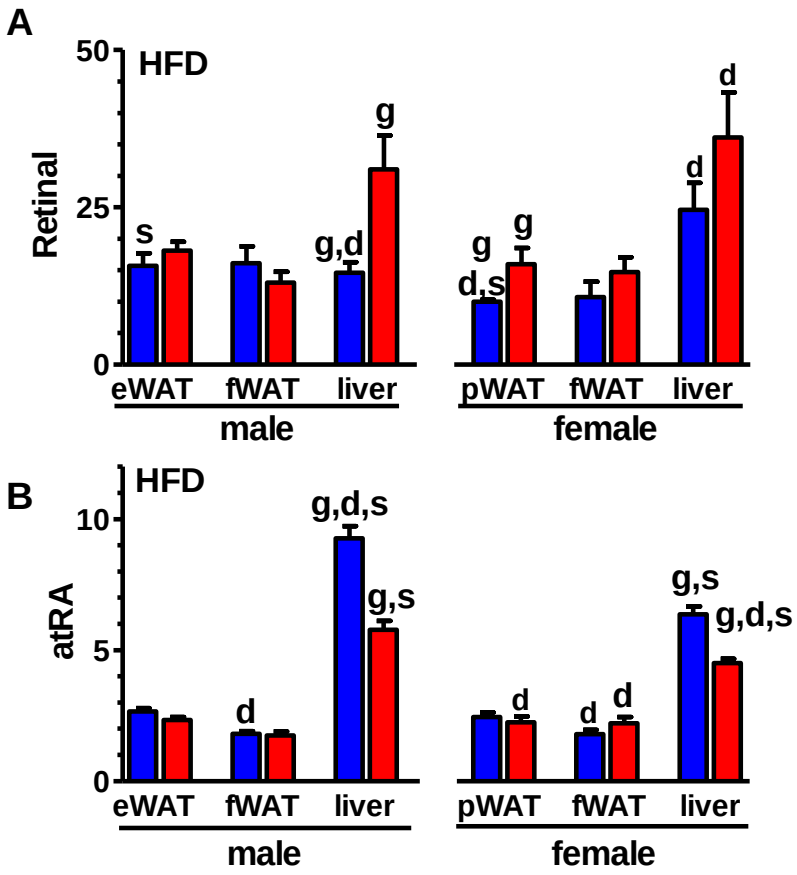

Figure 51. Tissue retinoid concentrations in HFD old mice.

Mice were fasted overnight then refed 4-4.5 hr: WT, blue bars; KO, red. Units are pmol/g tissue.

(A) Retinal in 26-wk-old mice fed a HFD beginning at 13 wk old.
(B) atRA in the same mice as in A.
[g]Significant difference between genotypes in the same tissue, sex and diet.
[d]Significant difference between diets (VAS vs. HFD) in the same tissue, sex and genotype.
[s]Significant difference between sexes in the same tissue, genotype and diet.
[g, d, s]$p < 0.05$.

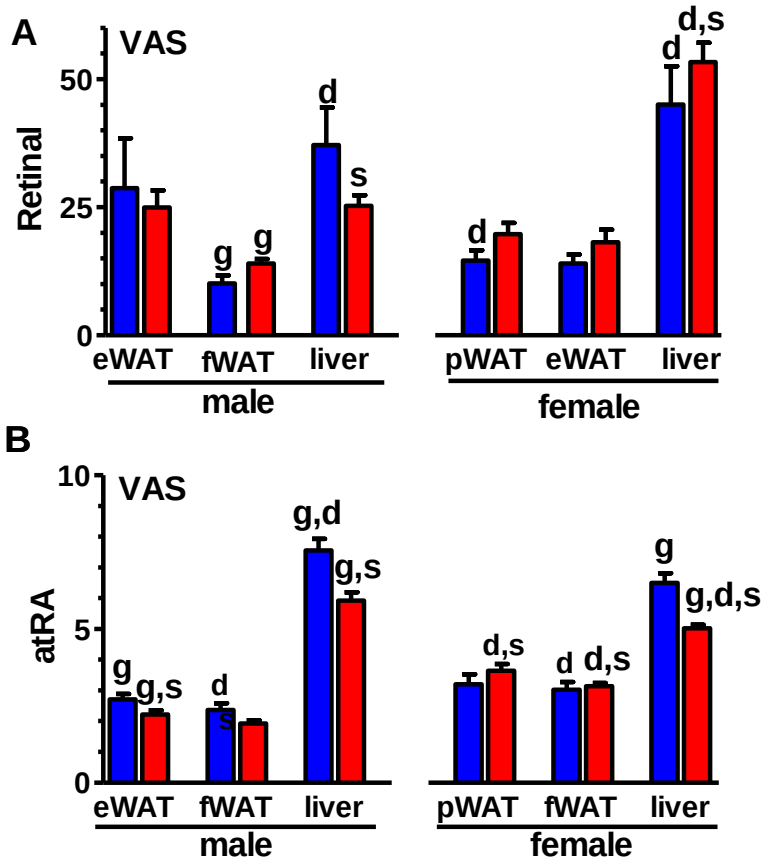

Figure 52. Tissue retinoid concentrations in VAS old mice.
Mice were fasted overnight then refed 4-4.5 hr: WT, blue bars; KO, red. Units are pmol/g tissue.
(A) Retinal in 26-wk-old mice fed a VAS beginning at 13 wk old.
(B) atRA in same mice as in A.
[g]Significant difference between genotypes in the same tissue, sex and diet.
[d]Significant difference between diets (VAS vs. HFD) in the same tissue, sex and genotype.
[s]Significant difference between sexes in the same tissue, genotype and diet.
[g, d, s]$p < 0.05$.

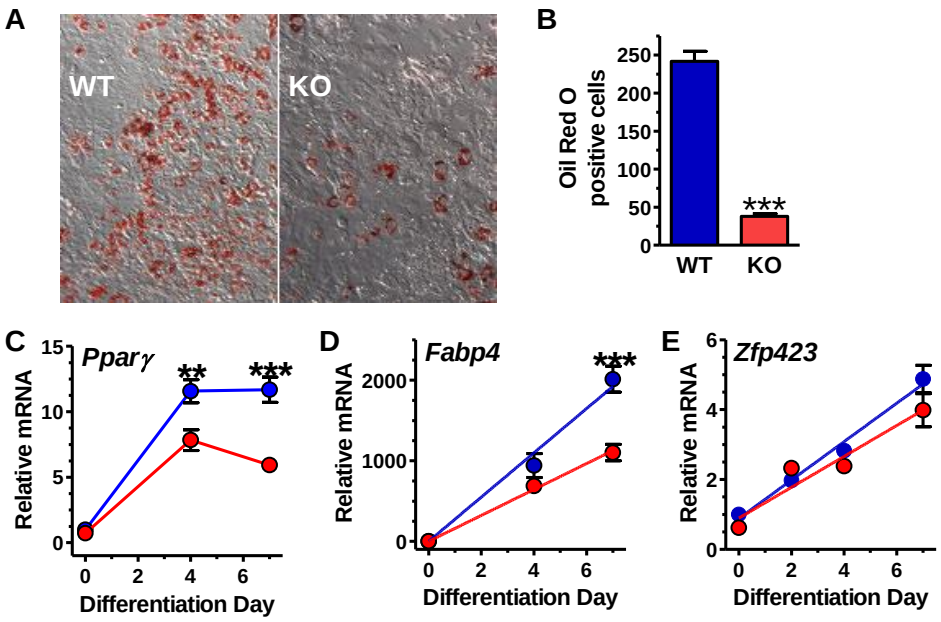

Figure 53. Raldh1 ablation causes cell-autonomous impairment in adipogenesis
(A) MEF differentiation into adipocytes. Representative images of cells stained with oil red O on dd7.
(B) Quantification of oil red O staining of cells illustrated in A: n = 4 **p<0.01.
(C) *Pparg* mRNA expression during adipogenesis. Two-way ANOVA: genotype p<0.0001; dd p<0.001. Bonferroni post-tests of dd (WT vs. KO): **p<0.01, ***p<0.001.
(D) *Fabp4* (*Ap2*) mRNA expression during adipogenesis. Two-way ANOVA, genotype p<0.0002; dd p<0.0001. Bonferroni post-test of dd (WT vs KO): ***p<0.001.
(E) *Zfp423* mRNA expression during adipogenesis. Two-way ANOVA. genotype p=0.054; dd p<0.0001.

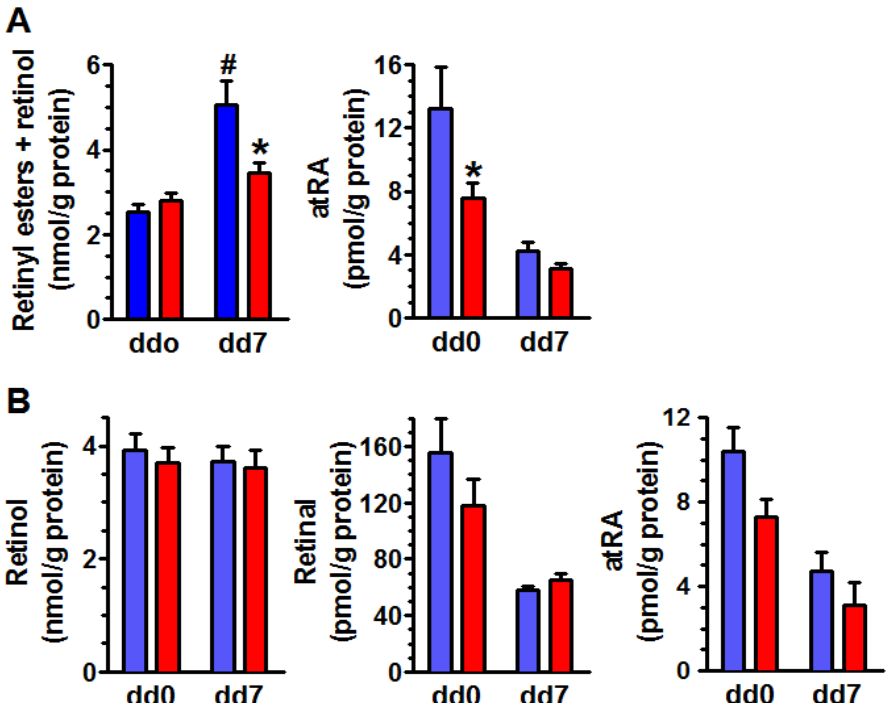

Figure 54. Retinoid metabolism during MEF differentiation into adipocytes

(A) Retinal conversion into RE plus retinol vs atRA before (dd0) and after (dd7) MEF differentiation into adipocytes. Cells were incubated 2 hr with 100 nM retinal, n = 9-10 wells. Two-way ANOVA: RE + retinol genotype $p=0.06$, dd $p<0.0001$; atRA genotype $p<0.03$, dd $p<0.0001$. Bonferroni posttest *$p<0.05$ relative to WT. #$p<0.0008$ WT dd0 vs dd7.
(B) Retinol conversion into retinal and atRA. Cells were incubated 2 hr with 250 nM retinol, n = 8 wells. Left panel, retinol recovered. Two-way ANOVA: retinal genotype $p>0.3$, dd $p<0.0001$; atRA genotype $p<0.03$, dd $p<0.0001$.

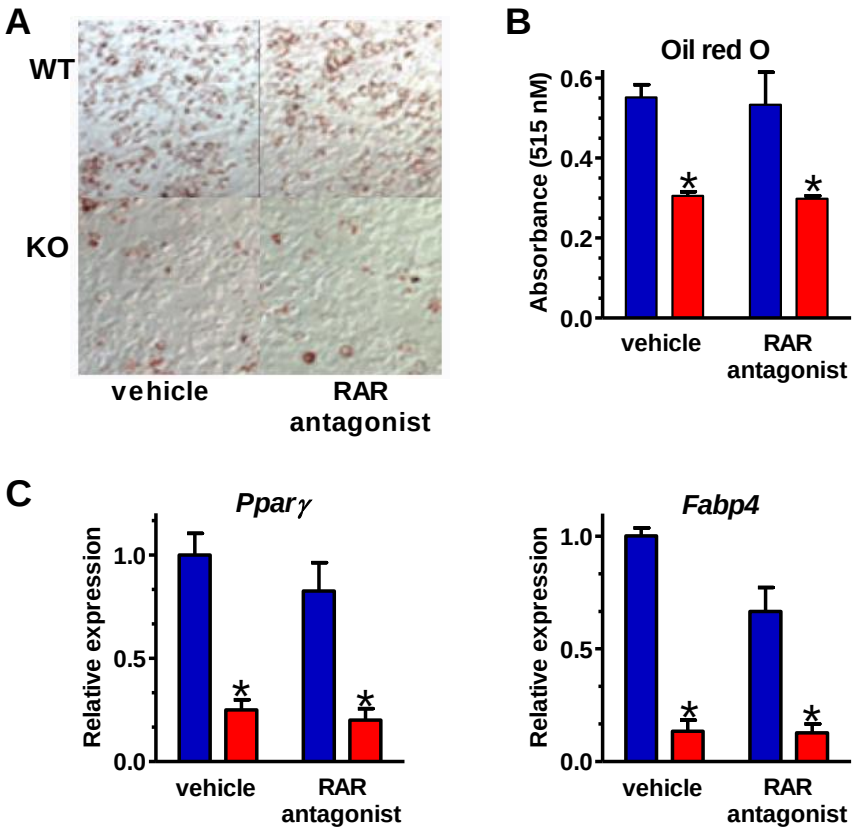

Figure 55. Antagonism of RAR does not reverse the *Raldh1*-null (KO) phenotype
(A) Effects of an RAR pan-antagonist on MEF differentiation. MEF were treated with vehicle or antagonist (200 nM AGN193109) from dd0 through dd7 and were stained with oil red O at the end of dd7. B, C, E, F: WT (blue), KO (red).
(B) Quantification of RAR pan-antagonist treatment in A: Two-way ANOVA: genotype *p<0.0006, n= 3 plates. *Bonferroni posttests p<0.05 WT vs KO.
(C) Expression of adipocyte marker genes in MEF treated with the RAR pan-antagonist in A. Two-way ANOVA: genotype *p<0.0001, n= 3 plates. *Bonferroni posttests p<0.05, WT vs KO, except for RAR agonist.

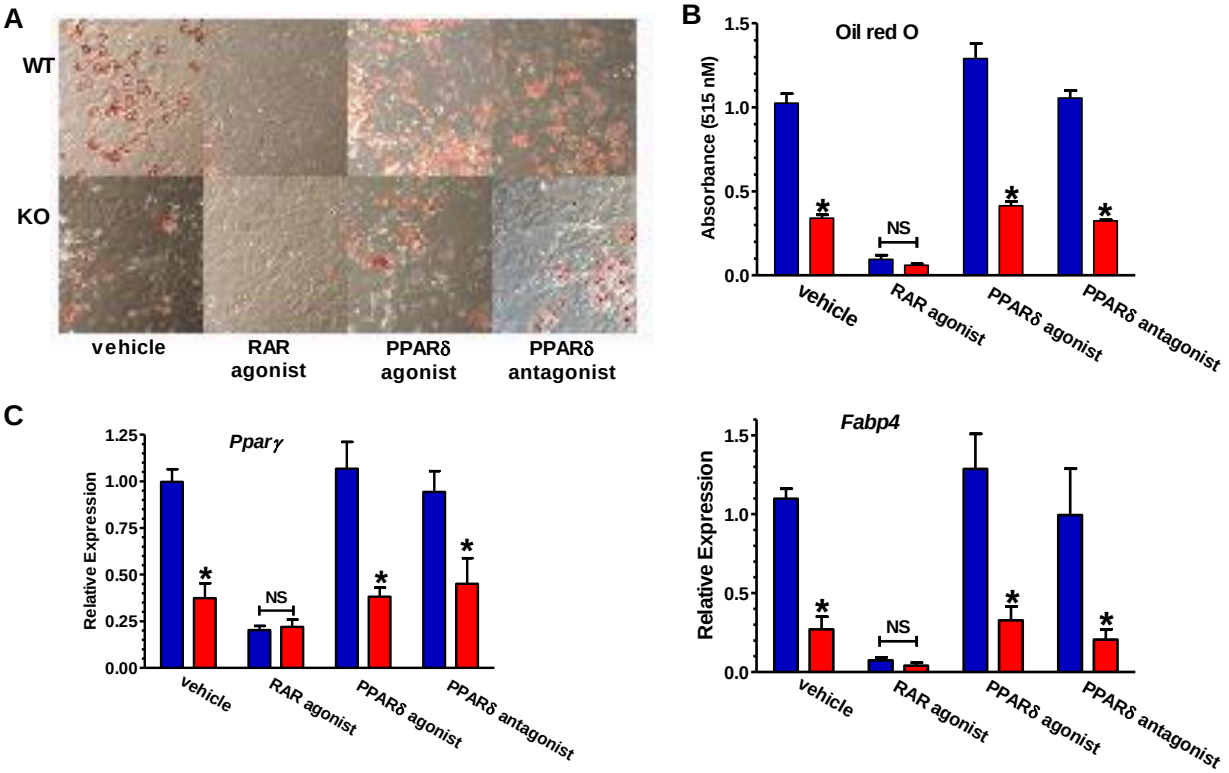

Figure 56. Neither activation nor antagonism of RAR and PPARδ reverses the *Raldh1*-null (KO) phenotype

(A) Effects of an RAR agonist (100 nM TTNPB), PPARδ agonist (100 nM GW0742), or PPARδ antagonist (1 μM GSK3787) on MEF differentiation. Cells were treated from dd0 through dd7, and were oil red O stained at the end of dd7.

(B) Quantification of results in D. Two-way ANOVA, genotype differences between WT and KO for all treatments, $p<0.0004$; impact of dose for RAR agonist, $p<0.0001$. Bonferroni posttests: vehicle WT vs KO, *$p<0.001$.

(C) Expression of adipocyte marker genes in MEF treated as described in D. Two-way ANOVA, genotype differences between WT and KO for all treatments, $p\leq0.002$, n = 3; impact of dose for RAR agonist, $p<0.001$. Bonferroni posttests: vehicle WT vs KO, *$p<0.05$ WT vs KO, except for RAR agonist.

Discussion

The data reveal that mice with an Raldh1-ablation do not resist diet induced weight gain by altering retinal or atRA metabolism or function. This work also shows that Raldh1 ablation allows males to resist weight gain regardless of dietary fat content and manifests mostly during adolescence in both sexes fed a HFD, which suggests that the effect of RALDH1 could be early during development or during adolescence, when mice start to gain weight fast. No difference was detected in liver or adipose retinal during development of the phenotype, and only decreases in RA occurred. In other words, neither retinal nor atRA changes could be considered initiator of the phenotype, since low atRA would cause weight gain. Tissue and condition restricted increases in retinal that occurred after the phenotype emerged did not correlate with weight gain based on genotype, diet or sex, and decreases in RA should have exacerbated weight gain. Upon HFD feeding, the increase of retinal and decrease of atRA in mice tissue could potentially be the result of the phenotype rather than the initiator of the phenotype, since differences of retinal was only detected after the onset of but not before the phenotype started. Raldh1 ablation did not decrease RA biosynthesis by MEF from retinol, the parent retinoid. Nor did compensation occur in expression of other retinoid metabolon enzymes. KO MEFs remain responsive to the anti-adipogenic properties of RA. Neither RAR nor PPARδ antagonism prevented the phenotype. Thus, rationale does not exist for postulating involvement of retinal, RA and RAR in driving the KO phenotype. This evidence should direct attention from retinoids concerning the mechanism of Raldh1 in weight gain and prompt study of its retinoid-independent functions during adolescence.

Akune, T., Ohba, S., Kamekura, S., Yamaguchi, M., Chung, U., Kubota, N., Terauchi, Y., Harada, Y., Azuma, Y., Nakamura, K., et al. (2004). PPAR γ insufficiency enhances osteogenesis through osteoblast formation from bone marrow progenitors. J. Clin. Invest. *113*, 846–855.

Alberti, K.G.M., Zimmet, P., and Shaw, J. (2005). The metabolic syndrome—a new worldwide definition. The Lancet *366*, 1059–1062.

Amengual, J., Ribot, J., Bonet, M.L., and Palou, A. (2010). Retinoic Acid Treatment Enhances Lipid Oxidation and Inhibits Lipid Biosynthesis Capacities in the Liver of Mice. Cell. Physiol. Biochem. *25*, 657–666.

Amengual, J., Petrov, P., Bonet, M.L., Ribot, J., and Palou, A. (2012). Induction of carnitine palmitoyl transferase 1 and fatty acid oxidation by retinoic acid in HepG2 cells. Int. J. Biochem. Cell Biol. *44*, 2019–2027.

Andrei, A.M., Berbecaru-Iovan, A., Din-Anghel, F.R.I., Stanciulescu, C.E., Berbecaru-Iovan, S., Banita, I.M., and Pisoschi, C.G. (2017). Interplay between Hypoxia, Inflammation and Adipocyte Remodeling in the Metabolic Syndrome. In Hypoxia and Human Diseases, J. Zheng, and C. Zhou, eds. (InTech), p.

Arnold, S.L.M., Kent, T., Hogarth, C.A., Griswold, M.D., Amory, J.K., and Isoherranen, N. (2015). Pharmacological inhibition of ALDH1A in mice decreases all-trans retinoic acid concentrations in a tissue specific manner. Biochem. Pharmacol. *95*, 177–192.

Ashique, A.M., May, S.R., Kane, M.A., Folias, A.E., Phamluong, K., Choe, Y., Napoli, J.L., and Peterson, A.S. (2012). Morphological defects in a novel Rdh10 mutant that has reduced retinoic acid biosynthesis and signaling. Genesis *50*, 415–423.

Auguet, T., Berlanga, A., Guiu-Jurado, E., and Porras, J.A. (2014). Molecular pathways in non-alcoholic fatty liver disease. Clin. Exp. Gastroenterol. 221.

Balmer, J.E., and Blomhoff, R. (2002). Gene expression regulation by retinoic acid. J. Lipid Res. *43*, 1773–1808.

Bateman, O.A., Purkiss, A.G., van Montfort, R., Slingsby, C., Graham, C., and Wistow, G. (2003). Crystal structure of eta-crystallin: adaptation of a class 1 aldehyde dehydrogenase for a new role in the eye lens. Biochemistry (Mosc.) *42*, 4349–4356.

Bergman, R.N., Kim, S.P., Catalano, K.J., Hsu, I.R., Chiu, J.D., Kabir, M., Hucking, K., and Ader, M. (2006). Why Visceral Fat is Bad: Mechanisms of the Metabolic Syndrome. Obesity *14*, 16S–19S.

Berry, D.C., and Noy, N. (2009a). All-trans-Retinoic Acid Represses Obesity and Insulin Resistance by Activating both Peroxisome Proliferation-Activated Receptor ?/? and Retinoic Acid Receptor. Mol. Cell. Biol. *29*, 3286–3296.

Berry, D.C., and Noy, N. (2009b). All-trans-Retinoic Acid Represses Obesity and Insulin Resistance by Activating both Peroxisome Proliferation-Activated Receptor ?/? and Retinoic Acid Receptor. Mol. Cell. Biol. *29*, 3286–3296.

Berry, D.C., and Noy, N. (2009c). All-trans-retinoic acid represses obesity and insulin resistance by activating both peroxisome proliferation-activated receptor beta/delta and retinoic acid receptor. Mol. Cell. Biol. *29*, 3286–3296.

Berry, D.C., Soltanian, H., and Noy, N. (2010). Repression of cellular retinoic acid-binding protein II during adipocyte differentiation. J. Biol. Chem. *285*, 15324–15332.

Berry, D.C., DeSantis, D., Soltanian, H., Croniger, C.M., and Noy, N. (2012). Retinoic acid upregulates preadipocyte genes to block adipogenesis and suppress diet-induced obesity. Diabetes *61*, 1112–1121.

Björntorp, P. (1990). “Portal” adipose tissue as a generator of risk factors for cardiovascular disease and diabetes. Arterioscler. Dallas Tex *10*, 493–496.

Bonet, M.L., Ribot, J., and Palou, A. (2012a). Lipid metabolism in mammalian tissues and its control by retinoic acid. Biochim. Biophys. Acta BBA - Mol. Cell Biol. Lipids *1821*, 177–189.

Bonet, M.L., Ribot, J., and Palou, A. (2012b). Lipid metabolism in mammalian tissues and its control by retinoic acid. Biochim. Biophys. Acta BBA - Mol. Cell Biol. Lipids *1821*, 177–189.

Bonet, M.L., Ribot, J., and Palou, A. (2012c). Lipid metabolism in mammalian tissues and its control by retinoic acid. Biochim. Biophys. Acta *1821*, 177–189.

Cali, A.M.G., and Caprio, S. (2009). Ectopic Fat Deposition and the Metabolic Syndrome in Obese Children and Adolescents. Horm. Res. Paediatr. *71*, 2–7.

Cao, Y. (2007). Angiogenesis modulates adipogenesis and obesity. J. Clin. Invest. *117*, 2362–2368.

Cristancho, A.G., and Lazar, M.A. (2011). Forming functional fat: a growing understanding of adipocyte differentiation. Nat. Rev. Mol. Cell Biol. *12*, 722–734.

Duester, G. (2008). Retinoic Acid Synthesis and Signaling during Early Organogenesis. Cell *134*, 921–931.

Dupé, V., Matt, N., Garnier, J.-M., Chambon, P., Mark, M., and Ghyselinck, N.B. (2003). A newborn lethal defect due to inactivation of retinaldehyde dehydrogenase type 3 is prevented by maternal retinoic acid treatment. Proc. Natl. Acad. Sci. U. S. A. *100*, 14036–14041.

Enomoto, H. (2003). Runx2 deficiency in chondrocytes causes adipogenic changes in vitro. J. Cell Sci. *117*, 417–425.

Everts, H.B., Silva, K.A., Montgomery, S., Suo, L., Menser, M., Valet, A.S., King, L.E., Ong, D.E., and Sundberg, J.P. (2013). Retinoid metabolism is altered in human and mouse cicatricial alopecia. J. Invest. Dermatol. *133*, 325–333.

Green, A.C., Kocovski, P., Jovic, T., Walia, M.K., Chandraratna, R. a. S., Martin, T.J., Baker, E.K., and Purton, L.E. (2017). Retinoic acid receptor signalling directly regulates osteoblast and adipocyte differentiation from mesenchymal progenitor cells. Exp. Cell Res. *350*, 284–297.

Grünblatt, E., and Riederer, P. (2016). Aldehyde dehydrogenase (ALDH) in Alzheimer's and Parkinson's disease. J. Neural Transm. Vienna Austria 1996 *123*, 83–90.

Harms, M., and Seale, P. (2013). Brown and beige fat: development, function and therapeutic potential. Nat. Med. *19*, 1252–1263.

Hartmann, C. (2009). Transcriptional networks controlling skeletal development. Curr. Opin. Genet. Dev. *19*, 437–443.

Hayes, D.P. (2008). Adverse effects of nutritional inadequacy and excess: a hormetic model. Am. J. Clin. Nutr. *88*, 578S–581S.

Hisada, K., Hata, K., Ichida, F., Matsubara, T., Orimo, H., Nakano, T., Yatani, H., Nishimura, R., and Yoneda, T. (2013). Retinoic acid regulates commitment of undifferentiated mesenchymal stem cells into osteoblasts and adipocytes. J. Bone Miner. Metab. *31*, 53–63.

Hua, S., Kittler, R., and White, K.P. (2009). Genomic Antagonism between Retinoic Acid and Estrogen Signaling in Breast Cancer. Cell *137*, 1259–1271.

Jette, C., Peterson, P.W., Sandoval, I.T., Manos, E.J., Hadley, E., Ireland, C.M., and Jones, D.A. (2004). The tumor suppressor adenomatous polyposis coli and caudal related homeodomain protein regulate expression of retinol dehydrogenase L. J. Biol. Chem. *279*, 34397–34405.

Jeyakumar, S.M., Vajreswari, A., and Giridharan, N.V. (2006). Chronic dietary vitamin A supplementation regulates obesity in an obese mutant WNIN/Ob rat model. Obes. Silver Spring Md *14*, 52–59.

Jiang, W., and Napoli, J.L. (2012). Reorganization of cellular retinol-binding protein type 1 and lecithin:retinol acyltransferase during retinyl ester biosynthesis. Biochim. Biophys. Acta BBA - Gen. Subj. *1820*, 859–869.

Jiang, W., and Napoli, J.L. (2013). The Retinol Dehydrogenase Rdh10 Localizes to Lipid Droplets during Acyl Ester Biosynthesis. J. Biol. Chem. *288*, 589–597.

Johnson, P.R., and Hirsch, J. (1972). Cellularity of adipose depots in six strains of genetically obese mice. J. Lipid Res. *13*, 2–11.

Kamei, Y., Kawada, T., Mizukami, J., and Sugimoto, E. (1994). The prevention of adipose differentiation of 3T3-L1 cells caused by retinoic acid is elicited through retinoic acid receptor alpha. Life Sci. *55*, PL307-312.

Kane, M.A., and Napoli, J.L. (2010). Quantification of endogenous retinoids. Methods Mol. Biol. Clifton NJ *652*, 1–54.

Kane, M.A., Chen, N., Sparks, S., and Napoli, J.L. (2005). Quantification of endogenous retinoic acid in limited biological samples by LC/MS/MS. Biochem. J. *388*, 363–369.

Kane, M.A., Folias, A.E., Wang, C., and Napoli, J.L. (2008a). Quantitative profiling of endogenous retinoic acid in vivo and in vitro by tandem mass spectrometry. Anal. Chem. *80*, 1702–1708.

Kane, M.A., Folias, A.E., and Napoli, J.L. (2008b). HPLC/UV quantitation of retinal, retinol, and retinyl esters in serum and tissues. Anal. Biochem. *378*, 71–79.

Kedishvili, N.Y. (2016). Retinoic Acid Synthesis and Degradation. Subcell. Biochem. *81*, 127–161.

Kelly, N.H., Schimenti, J.C., Patrick Ross, F., and van der Meulen, M.C.H. (2014). A method for isolating high quality RNA from mouse cortical and cancellous bone. Bone *68*, 1–5.

Kent, T., Arnold, S.L., Fasnacht, R., Rowsey, R., Mitchell, D., Hogarth, C.A., Isoherranen, N., and Griswold, M.D. (2016). ALDH Enzyme Expression Is Independent of the Spermatogenic Cycle, and Their Inhibition Causes Misregulation of Murine Spermatogenic Processes. Biol. Reprod. *94*, 12.

Kim, J.-I., Ganesan, S., Luo, S.X., Wu, Y.-W., Park, E., Huang, E.J., Chen, L., and Ding, J.B. (2015). Aldehyde dehydrogenase 1a1 mediates a GABA synthesis pathway in midbrain dopaminergic neurons. Science *350*, 102–106.

Korner, J., and Aronne, L.J. (2003). The emerging science of body weight regulation and its impact on obesity treatment. J. Clin. Invest. *111*, 565–570.

Kuri-Harcuch, W. (1982). Differentiation of 3T3-F442A cells into adipocytes is inhibited by retinoic acid. Differ. Res. Biol. Divers. *23*, 164–169.

Lawler, H.M., Underkofler, C.M., Kern, P.A., Erickson, C., Bredbeck, B., and Rasouli, N. (2016). Adipose Tissue Hypoxia, Inflammation, and Fibrosis in Obese Insulin-Sensitive and Obese Insulin-Resistant Subjects. J. Clin. Endocrinol. Metab. *101*, 1422–1428.

Lin, S.-C., Dollé, P., Ryckebüsch, L., Noseda, M., Zaffran, S., Schneider, M.D., and Niederreither, K. (2010). Endogenous retinoic acid regulates cardiac progenitor differentiation. Proc. Natl. Acad. Sci. U. S. A. *107*, 9234–9239.

McCammon, D.K., Zhou, P., Turney, M.K., McPhaul, M.J., and Kovacs, W.J. (1993). An androgenic affinity ligand covalently binds to cytosolic aldehyde dehydrogenase from human genital skin fibroblasts. Mol. Cell. Endocrinol. *91*, 177–183.

McLaren, D.S., and Kraemer, K. (2012). Vitamin A in health. World Rev. Nutr. Diet. *103*, 33–51.

Mercader, J., Ribot, J., Murano, I., Felipe, F., Cinti, S., Bonet, M.L., and Palou, A. (2006). Remodeling of white adipose tissue after retinoic acid administration in mice. Endocrinology *147*, 5325–5332.

Mercader, J., Madsen, L., Felipe, F., Palou, A., Kristiansen, K., and Bonet, L. (2007). All-Trans Retinoic Acid Increases Oxidative Metabolism in Mature Adipocytes. Cell. Physiol. Biochem. *20*, 1061–1072.

Mercader, J., Palou, A., and Luisa Bonet, M. (2010). Induction of Uncoupling Protein-1 in Mouse Embryonic Fibroblast-derived Adipocytes by Retinoic Acid. Obesity *18*, 655–662.

Morselli, E., Frank, A.P., Palmer, B.F., Rodriguez-Navas, C., Criollo, A., and Clegg, D.J. (2016). A sexually dimorphic hypothalamic response to chronic high-fat diet consumption. Int. J. Obes. *40*, 206–209.

Nallamshetty, S., Le, P.T., Wang, H., Issacsohn, M.J., Reeder, D.J., Rhee, E.-J., Kiefer, F.W., Brown, J.D., Rosen, C.J., and Plutzky, J. (2014a). Retinaldehyde dehydrogenase 1 deficiency inhibits PPARγ-mediated bone loss and marrow adiposity. Bone *67*, 281–291.

Nallamshetty, S., Le, P.T., Wang, H., Issacsohn, M.J., Reeder, D.J., Rhee, E.-J., Kiefer, F.W., Brown, J.D., Rosen, C.J., and Plutzky, J. (2014b). Retinaldehyde dehydrogenase 1 deficiency inhibits PPAR?-mediated bone loss and marrow adiposity. Bone *67*, 281–291.

Napoli, J.L. (2012a). Physiological insights into all-trans-retinoic acid biosynthesis. Biochim. Biophys. Acta BBA - Mol. Cell Biol. Lipids *1821*, 152–167.

Napoli, J.L. (2012b). Physiological insights into all-trans-retinoic acid biosynthesis. Biochim. Biophys. Acta *1821*, 152–167.

Noy, N. (2013). The one-two punch: Retinoic acid suppresses obesity both by promoting energy expenditure and by inhibiting adipogenesis. Adipocyte *2*, 184–187.

Obrochta, K.M., Kane, M.A., and Napoli, J.L. (2014). Effects of diet and strain on mouse serum and tissue retinoid concentrations. PloS One *9*, e99435.

Obrochta, K.M., Krois, C.R., Campos, B., and Napoli, J.L. (2015). Insulin Regulates Retinol Dehydrogenase Expression and all-trans-Retinoic Acid Biosynthesis through FoxO1. J. Biol. Chem.

Otto, T.C., and Lane, M.D. (2005). Adipose Development: From Stem Cell to Adipocyte. Crit. Rev. Biochem. Mol. Biol. *40*, 229–242.

Pairault, J., and Lasnier, F. (1987). Control of the adipogenic differentiation of 3T3-F442A cells by retinoic acid, dexamethasone, and insulin: a topographic analysis. J. Cell. Physiol. *132*, 279–286.

Patel, J.J., Butters, O.R., and Arnett, T.R. (2014). PPAR agonists stimulate adipogenesis at the expense of osteoblast differentiation while inhibiting osteoclast formation and activity: PPAR AGONISTS INHIBIT BONE CELL FUNCTION. Cell Biochem. Funct. *32*, 368–377.

Pei, L., and Tontonoz, P. (2004). Fat's loss is bone's gain. J. Clin. Invest. *113*, 805–806.

Penzes, P., Wang, X., and Napoli, J.L. (1997). Enzymatic characteristics of retinal dehydrogenase type I expressed in Escherichia coli. Biochim. Biophys. Acta *1342*, 175–181.

Pereira, F., Rosenmann, E., Nylen, E., Kaufman, M., Pinsky, L., and Wrogemann, K. (1991). The 56 kDa androgen binding protein is an aldehyde dehydrogenase. Biochem. Biophys. Res. Commun. *175*, 831–838.

Persaud, S.D., Lin, Y.-W., Wu, C.-Y., Kagechika, H., and Wei, L.-N. (2013). Cellular retinoic acid binding protein I mediates rapid non-canonical activation of ERK1/2 by all-trans retinoic acid. Cell. Signal. *25*, 19–25.

Pino, A.M., Rosen, C.J., and Rodríguez, J.P. (2012). In Osteoporosis, differentiation of mesenchymal stem cells (MSCs) improves bone marrow adipogenesis. Biol. Res. *45*, 279–287.

Pittenger, M.F., Mackay, A.M., Beck, S.C., Jaiswal, R.K., Douglas, R., Mosca, J.D., Moorman, M.A., Simonetti, D.W., Craig, S., and Marshak, D.R. (1999). Multilineage potential of adult human mesenchymal stem cells. Science *284*, 143–147.

Posch, K.C., Burns, R.D., and Napoli, J.L. (1992). Biosynthesis of all-trans-retinoic acid from retinal. Recognition of retinal bound to cellular retinol binding protein (type I) as substrate by a purified cytosolic dehydrogenase. J. Biol. Chem. *267*, 19676–19682.

Ran, F.A., Hsu, P.D., Wright, J., Agarwala, V., Scott, D.A., and Zhang, F. (2013). Genome engineering using the CRISPR-Cas9 system. Nat. Protoc. *8*, 2281–2308.

Reeves, P.G. (1997). Components of the AIN-93 diets as improvements in the AIN-76A diet. J. Nutr. *127*, 838S–841S.

Reichert, B., Yasmeen, R., Jeyakumar, S.M., Yang, F., Thomou, T., Alder, H., Duester, G., Maiseyeu, A., Mihai, G., Harrison, E.H., et al. (2011). Concerted action of aldehyde dehydrogenases influences depot-specific fat formation. Mol. Endocrinol. Baltim. Md *25*, 799–809.

Rhinn, M., Schuhbaur, B., Niederreither, K., and Dolle, P. (2011). Involvement of retinol dehydrogenase 10 in embryonic patterning and rescue of its loss of function by maternal retinaldehyde treatment. Proc. Natl. Acad. Sci. *108*, 16687–16692.

Ribes, V., Wang, Z., Dollé, P., and Niederreither, K. (2006). Retinaldehyde dehydrogenase 2 (RALDH2)-mediated retinoic acid synthesis regulates early mouse embryonic forebrain development by controlling FGF and sonic hedgehog signaling. Dev. Camb. Engl. *133*, 351–361.

Ribot, J., Felipe, F., Bonet, M.L., and Palou, A. (2001). Changes of adiposity in response to vitamin A status correlate with changes of PPAR gamma 2 expression. Obes. Res. *9*, 500–509.

Ross, A.C., and Gardner, E.M. (1994). The function of vitamin A in cellular growth and differentiation, and its roles during pregnancy and lactation. Adv. Exp. Med. Biol. *352*, 187–200.

Saeed, H., Taipaleenmäki, H., Aldahmash, A.M., Abdallah, B.M., and Kassem, M. (2012). Mouse Embryonic Fibroblasts (MEF) Exhibit a Similar but not Identical Phenotype to Bone Marrow Stromal Stem Cells (BMSC). Stem Cell Rev. Rep. *8*, 318–328.

Sato, M., Hiragun, A., and Mitsui, H. (1980). Preadipocytes possess cellular retinoid binding proteins and their differentiation is inhibited by retinoids. Biochem. Biophys. Res. Commun. *95*, 1839–1845.

Schwarz, E.J., Reginato, M.J., Shao, D., Krakow, S.L., and Lazar, M.A. (1997a). Retinoic acid blocks adipogenesis by inhibiting C/EBPbeta-mediated transcription. Mol. Cell. Biol. *17*, 1552–1561.

Schwarz, E.J., Reginato, M.J., Shao, D., Krakow, S.L., and Lazar, M.A. (1997b). Retinoic acid blocks adipogenesis by inhibiting C/EBPbeta-mediated transcription. Mol. Cell. Biol. *17*, 1552–1561.

Schwarz, E.J., Reginato, M.J., Shao, D., Krakow, S.L., and Lazar, M.A. (1997c). Retinoic acid blocks adipogenesis by inhibiting C/EBPbeta-mediated transcription. Mol. Cell. Biol. *17*, 1552–1561.

Siegenthaler, J.A., Ashique, A.M., Zarbalis, K., Patterson, K.P., Hecht, J.H., Kane, M.A., Folias, A.E., Choe, Y., May, S.R., Kume, T., et al. (2009). Retinoic acid from the meninges regulates cortical neuron generation. Cell *139*, 597–609.

Sládek, N.E. (1999). Aldehyde dehydrogenase-mediated cellular relative insensitivity to the oxazaphosphorines. Curr. Pharm. Des. *5*, 607–625.

Stephens, J.M. (2012). The Fat Controller: Adipocyte Development. PLoS Biol. *10*, e1001436.

Sun, F., Pan, Q., Wang, J., Liu, S., Li, Z., and Yu, Y. (2009). Contrary Effects of BMP-2 and ATRA on Adipogenesis in Mouse Mesenchymal Fibroblasts. Biochem. Genet. *47*, 789–801.

de The, H., del Mar Vivanco-Ruiz, M., Tiollais, P., Stunnenberg, H., and Dejean, A. (1990). Identification of a retinoic acid responsive element in the retinoic acid receptor & beta;gene. Nature *343*, 177–180.

Trayhurn, P. (2013). Hypoxia and Adipose Tissue Function and Dysfunction in Obesity. Physiol. Rev. *93*, 1–21.

Trayhurn, P., and Wood, I.S. (2004). Adipokines: inflammation and the pleiotropic role of white adipose tissue. Br. J. Nutr. *92*, 347.

Viccica, G., Francucci, C.M., and Marcocci, C. (2010). The role of PPARγ for the osteoblastic differentiation. J. Endocrinol. Invest. *33*, 9–12.

Wang, A., Ding, X., Sheng, S., and Yao, Z. (2008). Retinoic acid inhibits osteogenic differentiation of rat bone marrow stromal cells. Biochem. Biophys. Res. Commun. *375*, 435–439.

Wang, C., Kane, M.A., and Napoli, J.L. (2011). Multiple retinol and retinal dehydrogenases catalyze all-trans-retinoic acid biosynthesis in astrocytes. J. Biol. Chem. *286*, 6542–6553.

Wang, J., Yoo, H.S., Obrochta, K.M., Huang, P., and Napoli, J.L. (2015). Quantitation of retinaldehyde in small biological samples using ultrahigh-performance liquid chromatography MS/MS. Anal. Biochem.

Williams, A.R., and Hare, J.M. (2011). Mesenchymal Stem Cells: Biology, Pathophysiology, Translational Findings, and Therapeutic Implications for Cardiac Disease. Circ. Res. *109*, 923–940.

Yan, T., Wergedal, J., Zhou, Y., Mohan, S., Baylink, D.J., and Strong, D.D. (2001). Inhibition of human osteoblast marker gene expression by retinoids is mediated in part by insulin-like growth factor binding protein-6. Growth Horm. IGF Res. *11*, 368–377.

Yoshida, A., Hsu, L.C., and Yanagawa, Y. (1993). Biological role of human cytosolic aldehyde dehydrogenase 1: hormonal response, retinal oxidation and implication in testicular feminization. Adv. Exp. Med. Biol. *328*, 37–44.

Zhang, M., Hu, P., Krois, C.R., Kane, M.A., and Napoli, J.L. (2007a). Altered vitamin A homeostasis and increased size and adiposity in the rdh1-null mouse. FASEB J. *21*, 2886–2896.

Zhang, M., Hu, P., Krois, C.R., Kane, M.A., and Napoli, J.L. (2007b). Altered vitamin A homeostasis and increased size and adiposity in the rdh1-null mouse. FASEB J. Off. Publ. Fed. Am. Soc. Exp. Biol. *21*, 2886–2896.

Zhang, W., Deng, Z.-L., Chen, L., Zuo, G.-W., Luo, Q., Shi, Q., Zhang, B.-Q., Wagner, E.R., Rastegar, F., Kim, S.H., et al. (2010). Retinoic Acids Potentiate BMP9-Induced Osteogenic Differentiation of Mesenchymal Progenitor Cells. PLoS ONE *5*, e11917.

Zhang, Y., Li, X., Qian, S., Guo, L., Huang, H., He, Q., Liu, Y., Ma, C., and Tang, Q.-Q. (2012). Down-Regulation of Type I Runx2 Mediated by Dexamethasone Is Required for 3T3-L1 Adipogenesis. Mol. Endocrinol. *26*, 798–808.

Ziouzenkova, O., Orasanu, G., Sharlach, M., Akiyama, T.E., Berger, J.P., Viereck, J., Hamilton, J.A., Tang, G., Dolnikowski, G.G., Vogel, S., et al. (2007a). Retinaldehyde represses adipogenesis and diet-induced obesity. Nat. Med. *13*, 695–702.

Ziouzenkova, O., Orasanu, G., Sharlach, M., Akiyama, T.E., Berger, J.P., Viereck, J., Hamilton, J.A., Tang, G., Dolnikowski, G.G., Vogel, S., et al. (2007b). Retinaldehyde represses adipogenesis and diet-induced obesity. Nat. Med. *13*, 695–702.